Fabrication and Optimization of Dp44mT-loaded Polymeric Nanoparticles for Treatment of Malignant Cells

by
Claire Katherine Holley

A dissertation submitted to the Department of Biomedical Engineering,
Cullen College of Engineering
in partial fulfillment of the requirements for the degree of

Doctor of Philosophy

in Biomedical Engineering

Chair of Committee: Sheereen Majd, Ph.D.

Committee Member: Mohammad Reza Abidian, Ph.D.

Committee Member: T. Randall Lee, Ph.D.

Committee Member: Xinli Liu, Ph.D.

Committee Member: Chandra Mohan, M.D., Ph.D.

University of Houston
May 2020

DEDICATION

I dedicate this work to my parents who, throughout the course of this research, experienced their own battles with cancer. Thankfully, they are both in remission. Their experiences during treatment inspired this work and have made be proud to be a biomedical engineer.

ACKNOWLEDGMENTS

No one is an island unto themselves, which is especially true when completing a doctoral degree. I would like to take a moment to express my gratitude to the following people who have been particularly important during this experience.

First, I would like to thank Dr. Majd for all of the advice and training gained as her doctoral student. She took a chance on me, as I had no prior biomedical engineering training. While it has not been an easy journey, she has been supportive of my ongoing growth throughout my time in her lab. I have become a more analytical and inquiring scientist, as well as a better writer and presenter, under her tutelage. I wish her all the best for the future of her lab and ongoing research.

Second, I would like to thank the members of my dissertation committee for the time, advice, and support they have given my research. Many thanks to Dr. Abidian for his support and shared facilities, which has been vital for the progress of my research. Dr. Abidian also taught the first materials-based class I attended at the University of Houston, the knowledge of which has been used for many aspects of my doctoral research. I would also like to thank both Dr. Lee and Dr. Mohan for their advice and collaboration. Dr. Lee has generously allowed us the continued use of his equipment and chemicals. We never would have gotten our nanoparticle experiments started without him. Later, his expert advice helped to propel my project forward through the last portion of my dissertation. Similarly, Dr. Mohan has been an invaluable resource, especially with our cellular and animal-based experiments. I am particularly thankful for his collaboration with our breast and colorectal cancer cell experiments, which really

broadened the impact of my research. I would also like to thank Dr. Liu for her time and guidance. Our interaction has been brief, but I appreciate all of her advice and offers of support with our animal experiments.

I would also like to acknowledge all of the members of the Majd Lab, current and past, who assisted me with this research. While we met under stressful circumstances, I am very grateful to both Dr. Soo Hyun Park and Dr. You Jung Kang, for taking the time to train me in essential nanomaterial fabrication protocols, even though you were both busy writing your own dissertations. As for the current members of the Majd Lab, including Chung-Fan (Joseph) Kuo, Fereshteh Mirab, and Yifei Wang, thank you so much for your collaboration with many of my experiments. There were also several undergrads with whom I worked closely during my tenure in the lab; many thanks to Sukaina Alkhalifah, Dang Dang, Joshua Lewis, Ramsha Navaid, and Bridgett Sinquefield. I hope you have learned as much from me as I have learned from you.

Last but not least, there are many friends and family to which I owe my gratitude, especially my parents, Dr. Samantha Stanley, Dr. Martin & Mrs. Emma Antensteiner, Anthony Kisucky, and Kerry Swift. These people have kept me going through the roughest of times, both personal and professional. The smallest action or word is sometimes all it takes to keep someone on the right track. I really cannot emphasize it enough – your support has been everything! Thank you all so much.

ABSTRACT

Cancer is the second leading cause of mortality worldwide, resulting in over eight million deaths per year. In the fight against cancer, traditional chemotherapeutics are not very effective due to poor delivery, toxicity to healthy tissues, and ever-increasing cancer resistance. Since neoplastic cells require increased levels of iron (Fe) to proliferate, a promising strategy for cancer treatment is Fe deprivation using metal chelators. One such chelator, Di-2-pyridylketone-4,4-dimethyl-3-thiosemicarbazone (Dp44mT), has been shown to be extremely toxic towards many types of cancer in its free form (IC_{50} of 4 - 500 nM), due to its ability to chelate both Fe and copper (Cu), produce reactive oxygen species (ROS) through redox cycling, and overcome multi-drug resistance in malignant cells. Therefore, Dp44mT presents a promising candidate for the treatment of highly aggressive tumors. However, due to the hydrophobicity and toxicity of this compound, encapsulating Dp44mT into a nano-carrier will enhance its therapeutic effectiveness, while also preventing premature drug degradation, improving biodistribution and drug release to the tumor, and mitigating negative side effects to healthy tissues. The objective of this project was the development of a new anti-cancer nano-formulation based on Dp44mT and the *in vitro* evaluation of this formulation against malignant cells.

To this end, we first utilized two distinct techniques, nanoprecipitation and single emulsion, to fabricate nanoparticle of poly(lactic-co-glycolic acid)(PLGA) loaded with Dp44mT (referred to as "Dp44mT-NPs"). During fabrication, Dp44mT encapsulation efficiency and NP size was optimized through the

adjustment of the polymer, drug, and surfactant concentrations, as well as injection rate. The resultant Dp44mT-NPs were also characterized for shape, surface potential, colloidal stability and drug release. Next, we assessed, for the first time, the therapeutic effectiveness of both free and encapsulated Dp44mT in glioma (U251, U87) cells, as compared to healthy astrocytes. We further applied our Dp44mT-NPs to other malignant cells, namely breast (MCF7) and colorectal (HT29) cancer cells, to evaluate this nano-formulation as a universal anti-cancer platform. Finally, we modified this nano-formulation, via surface PEGylation and conjugation of a cancer-specific targeting ligand, to improve nanoparticle stability, biodistribution, and delivery for future *in vivo* applications. We then re-evaluated the efficacy of our PEGylated Dp44mT-NPs against malignant cells, both with and without targeting. Lastly, we assessed the ability of these PEGylated NPs to bypass the endothelial layer of an *in vitro* Blood-Brain Barrier model. In summary, this dissertation presents the fabrication, optimization, and assessment of a novel nano-formulation, containing anti-cancer chelator Dp44mT, for future application as a chemotherapeutic against malignant cells.

TABLE OF CONTENTS

LIST OF TABLES

LIST OF FIGURES

LIST OF FORMULAS

CHAPTER I

INTRODUCTION

1.1. Societal Impact of Cancer

One of the greatest health issues in our society to date is cancer. Cancer causes approximately 22% of all deaths annually [1-3], ranking it as the second highest cause of mortality worldwide, surpassed only by cardiovascular disease (**Figure 1.1**). In 2012, over 14 million cases of cancer were diagnosed globally, of which over 57% of those cases resulted in death [4]. This translates to approximately 21,000 deaths per day worldwide. While cancer has an impact worldwide, its influence is most apparent in wealthy and industrialized (first-world) countries [4], where infectious diseases, nutrient-deprivation, and sanitation-related diseases are less problematic. In the United States alone, cancer kills over 600,000 people per year, which is a daily mortality rate of 1,600 people [1]. These rates are further influenced by social behaviors (e.g., diet, exercise, drinking, smoking), life expectancy, race and genetics, as well as environmental exposure [1].

Cancer also has an enormous and ever increasing financial burden on society; it is estimated that over $80 million was spent on cancer-related medical costs, including pharmaceuticals, surgery, and doctor's visits, the United States in 2015 [1, 4]. However, cost of treatment is not the only impact of cancer on the economy. When combined with secondary costs, including travel, loss of income, reduced productivity, and end-of-life expenses, it was estimated that the total annual economic cost of cancer was over one

trillion dollars in 2010. As costs of medical care and rates of cancer occurrence increase, this cost will only continue to rise. Together, cancer is a huge burden on society, both socially and financially. As such, we need more effective methods of treating these deadly diseases. Given that, this study will focus on breast cancer, colorectal cancer, and glioblastoma (brain cancer), as representative models, more details on these cancers are discussed below.

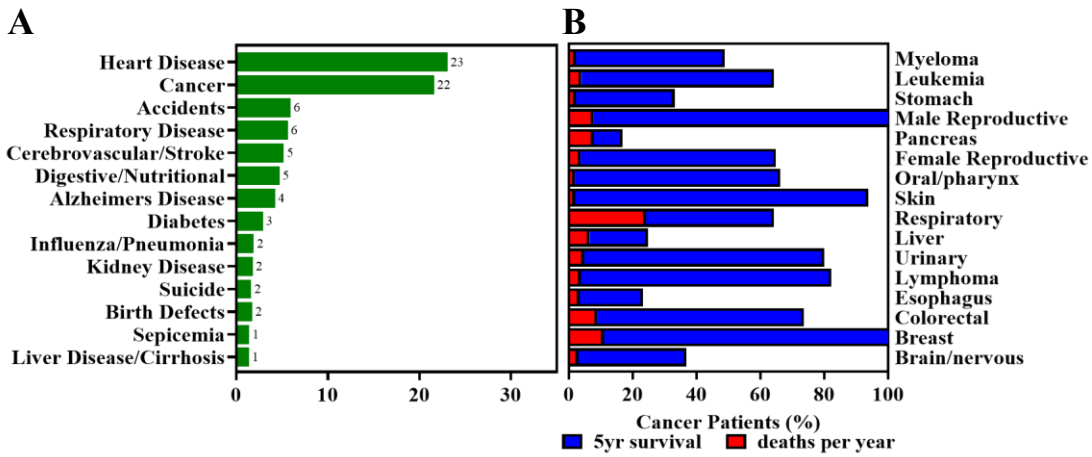

Figure 1.1 Societal Impact of Cancer. (A) Leading causes of death worldwide and (B) Rates of mortality and five-year survival in common cancers [1-4].

1.1.1. Breast Cancer

Globally, breast cancer is the second most common type of cancer worldwide, with over 1.6 million cases, or an incidence 11.9%, diagnosed in 2012 [4]. While both men and women are affected by this type of cancer, it is heavily weighted towards women, and is the primary cause of cancer death in women [1, 4-6], due genetic and hormonal influences [5, 7]. The majority (50 - 80%) of breast cancer patients are diagnosed with invasive ductal carcinoma [6], cancerous epithelium of the milk duct that has invaded the surrounding fibrous tissue, when they are between 50 - 65 years of age. If detected

early via mammography [1, 5], the mortality rate is relatively low at 6.4% (or 5.2/100,000) [4] and the five year survival rate is quite high at > 85% [5, 7]. However, the main cause of death for breast cancer patients is not the primary tumor but instead metastasis to other sights [6], which commonly targets the lymph nodes, bone, lung, and liver [6]. Hence, the first line of treatment is chemotherapy, followed by surgery and/or radiation [6]. Even with treatment, If the tumor becomes metastatic, metastasis reduces 5 year survival drastically to ~ 30% [5, 6] and recurrence after surgery occurs in 40% of cases [6].

1.1.2. Colorectal Cancer

Colorectal cancer is the third most common type of cancer, with over 1.3 million cases diagnosed globally, or an incidence of 9.7%, in 2012 [4]. Colorectal adenocarcinoma, cancer of the mucus-producing glandular cells of the colon/rectum, is the most common form of colorectal cancer (> 95%). is most commonly diagnosed in patients of 70 years median age [7], the majority of which are men [4, 5]. Other than family history, risk factors are mostly related to age and lifestyle choices (e.g., diet, alcohol consumption, and weight) [5]. The result is the second leading cause of cancer-related mortality [8] of 8.5% (or 7/100,000) in 2012 [4]. While early diagnosis, via colonoscopy, and treatment can result in very high long-term survival of 90% [5], the average five year survival rate is currently only a moderate 65% [7], as most adults tend to avoid proper screening procedures. Metastasis, usually to the lung or liver, severally reduces long-term survival to < 10% [5], therefore the current median survival is 24 months even with aggressive combinatorial therapy [8].

1.1.3. Glioblastoma Multiforme (GBM)

Glioblastoma/GBM, cancerous non-neuronal (glial) support cells of the brain, is the most common and aggressive primary brain tumor in humans. With a 3% incidence [1, 9], GBM is not nearly as common as breast cancer (11.9%) or colorectal cancer (9.7%), as described above [4]. In fact, brain/nervous cancers do not even rank within the top ten cancers affecting the global population. Even so, GBM accounts for approximately 14,000 new diagnoses per year in the United States [9], which is 15 - 20% of total brain tumors diagnosed annually [9-13]. Similar to the other two cancers discussed above, GBM is predominantly observed in older patients (> 50 years) [14]. However, unlike the other cancers, the five-year survival is very poor, at less than 16% [10, 15]. As such, aggressive treatment typically only extends life by additional 12 - 16 months [10, 16]. GBM also causes a huge social burden; with the cost of initial care reaching over $150,000, it has the highest per-patient cost of any cancer group.

1.2. Current Cancer Treatments

Regardless of the type of cancer, the traditional modes of treatment usually involve a combination of surgery, radiation, and chemotherapy. (**Figure 1.2**) The combination of therapies prescribed to a patient is dependent upon the stage, grade, and location of the cancer, as well as patient comorbidity, age, and personal preferences [7].

The most aggressive cancer therapy is surgery. When applicable, resection of the cancerous tumor and nearby lymph nodes is the quickest way to reduce cancer burden and increase the chance of patient survival [17]. However, surgery is not always

applicable, perhaps due to the location or size of the tumor. To preserve the quality of life of a colorectal patient, for instance, surgery might instead be replaced with a regimen of aggressive chemotherapy and/or radiation [7]. Another disadvantage to surgery is incomplete tumor resection and recurrence, which is quite common for diffuse and/or metastatic cancers, like glioblastoma, where it is difficult to locate and remove all cancerous tissue. Therefore, surgery is usually followed by aggressive regimens of radiation and chemotherapy.

Radiation therapy is used to kill cancer cells through the application of ionizing radiation, which damages cellular DNA beyond repair. While radiation can be applied by external or internal (implantable) means depending on the cancer being treated [18], external exposure is by far the most common technique. The limitations of this technique are penetration depth and accuracy. For deeply located tumors like glioblastoma, radiation must bypass the skull and healthy brain/nervous tissues in order to effectively localize to the cancerous tissue. However, this can damage the surround healthy tissues since radiation is not cell-specific [19]. It has also been reported that hypoxic tumor regions have reduced sensitivity to radiation, which predisposes the cancer to metastasize [19]. As such, radiation is typically used in conjunction with surgery and chemotherapy [18].

Chemotherapy utilizes biological/chemical agents to kill rapidly-dividing cells remaining in the primary tissue or that might have spread to other parts of the body [19, 20]. As such, this type of therapy includes the application of small-molecule anti-neoplastic drugs, gene-modifying drugs or nucleic acids, and even modified immune or stem cells. The efficacy of a chemotherapeutic regimen depends on the type, stage,

location, and size of the cancer being treated. Its effectiveness is often limited by the drug's high toxicity, issues with tumor-specific delivery, and multi-drug resistance. While some chemotherapeutic agents can be administered directly to the tumor site, through ointments (skin), meshes (uterine, bladder), inserted chips/pumps (brain), oral inhalants (lung), etc. [20, 21], many cancers are located in deeper or more fragile organs for which direct application is too invasive. Treatment in these organs relies on vascular application, which has been reported to be very effective for systemic cancers, like leukemia, or cancers involving filtration organs (e.g., liver or kidney cancer). For other cancers, however, vascular drug delivery relies upon the enhanced permeability and retention (EPR) effect [19] to bypass biological barriers and access the tumor. While this may be beneficial for controlled-delivery platforms like nanoparticles, this "leaky vasculature" can also cause drug delivery problems due to irregular flow, occlusions and high interstitial pressure [19]. To overcome ineffective delivery, short drug half-life and poor drug solubility [22], while maintaining therapeutic drug levels in the tumor tissue, chemotherapeutics are applied in large, repetitive doses. Since chemotherapy drugs are often not cell-specific, general drug application results in off-target toxicity in healthy tissues and the formation of multi-drug resistance (MDR). MDR is an ever increasing complication against successful chemotherapy as it negates the effectiveness of the applied chemotherapeutic and often leads to metastasis [23]. Together, these issues emphasize the need for more effective and targeted therapies.

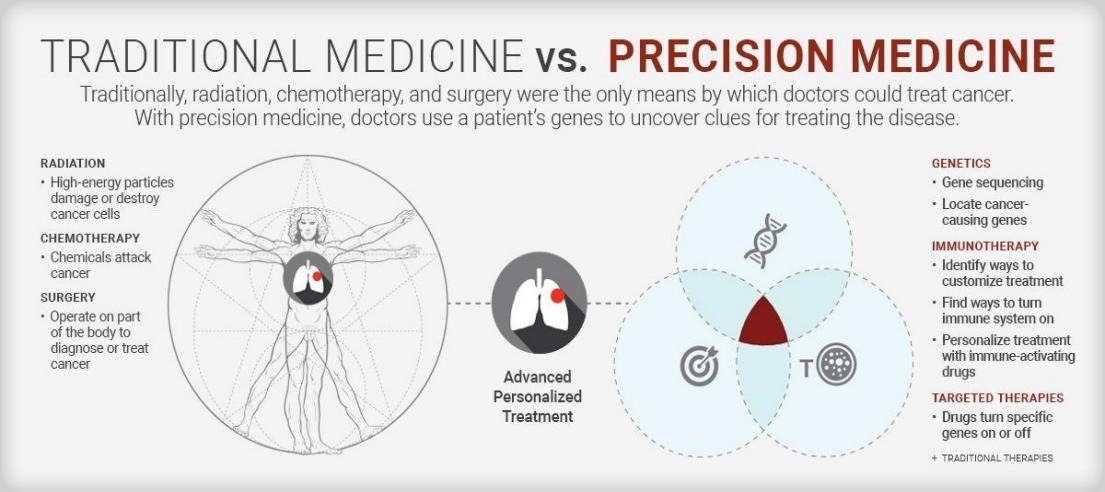

Figure 1.2. The Many Sides of Cancer Therapy. A comprehensive summary of traditional cancer treatment regimens as compared to new precision medicine regimens being applied for personalized therapy [24].

1.3. Iron Chelation in Cancer

Due to the need for more effective therapies for the treatment of malignant cells, a recent trend in the field is focused on pursuing more generalized cellular targets which are common to multiple cancer cell types. In this vein, the use of metal chelators, specifically iron (Fe) chelators, has become of particular interest, as Fe is essential for the proper functioning of all cells [25, 26] and it has been observed that altered Fe metabolism is a key hallmark in many cancers [25].

Intracellular Fe is involved in many major cellular functions including: proper heme functionalization during hemostasis, DNA synthesis, cell cycle regulation and division, and the proper function of proteins containing Fe-Sulphur (S) clusters, which contribute to genomic stability and respiratory function [25, 27]. One of the most important Fe-containing metalloenzymes is ribonucleotide reductase, which converts ribonucleotides into deoxyribonucleotides for DNA synthesis [27]. To maintain these essential cellular

functions, intracellular Fe levels are normally tightly regulated through a combination of iron storage, transport, distribution, and the production of reactive oxygen species (ROS). ROS production, which results from the controlled redox cycling of Fe and copper (Cu), is also important several cellular processes including lipid peroxidation, protein oxidation, and nucleic acid degradation [26].

In disease states, this normal regulation of Fe can be disrupted by the presence of either too much iron, due to excessive environmental absorption, or too little iron, due to the influence of iron chelators [25]. Due to the rapid growth rate of cancer cells and their increased need for Fe uptake compared to healthy cells (**Figure 1.3**), cancer cells reprogram cellular Fe metabolism in their favor. They upregulate proteins that are involved in Fe uptake (e.g., transferrin receptor-1 (TfR1), 6-transmembrane epithelial antigen of prostate (STEAP) metalloreductase proteins, and lipocalin-2 (LCN2)), downregulate the expression of Fe storage and efflux proteins (e.g., ferritin, ferroportin) [25], and interrupt the translation of iron-regulatory proteins (IRP1/2) [28]. The overall result is an unregulated net influx of Fe contributing to uncontrolled cellular growth and division. Thus, one method of killing cancer cells that is currently being explored is the use of Fe chelators to deprive cancer cells of essential Fe.

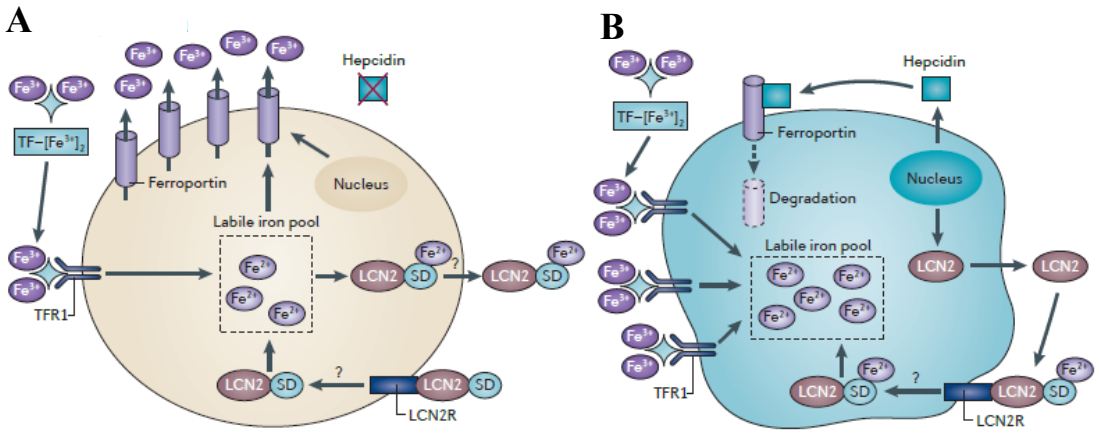

Figure 1.3. The Uptake and Intracellular Impact of Iron. Iron influx and efflux in (A) healthy vs. (B) malignant cells [25].

Fe chelators are small molecules that utilize the movement of donor and acceptor electrons to form stable complexes with transition metal ions [29-31]. Traditionally, Fe chelators such as Deferoxamine (DFO) were used in hematology cases as a treatment for iron overdoses; now they are being developed to target the proteins essential for Fe influx, efflux, and regulation for use in cancer treatments [32, 33]. The majority of chelators can readily bypass cellular membranes due to their small size and lipophilicity. However, there are a few exceptions, like DFO, that have been found to trigger cancer cell apoptosis but are not very effective as chemotherapeutics due to their hydrophilic nature, resulting in poor membrane permeability and uptake [34-37].

Once in the cytosol, these molecules work through two main strategies: (1) cellular deprivation of Fe to prevent essential cellular growth and division and (2) redox cycling leading to the production of toxic ROS [25, 26, 34]. These toxic free radicals are capable of permeabilizing endosomal membranes and triggering the intracellular caspase-3/9 apoptotic pathway via cytochrome-c activation [38]. By binding up essential transition metals, chelators also trigger the inhibitory function of iron-containing metalloenzymes

[26]. Chelator toxicity is, therefore, a function of its ability to bind multiple transition metal conformations (low metal selectivity) [26] and inhibit multiple essential cellular pathways, as is summarized in **Figure 1.4**. Other chelators have been found to modulate the expression of cell cycle regulatory proteins, which are commonly altered in cancer cells. Iron chelation has been reported to reduce the activity of cyclin-dependent kinases-2 (CDK-2), which normally promotes cell cycle progression, thereby inducing apoptosis [28]. Other chelators have been found to up-regulate N-myc downstream regulated gene 1 (NDRG1), which has been shown to inhibit the invasion and metastasis of some cancers [39, 40]. Although chelators have been shown to be effective at killing cancer cells, their efficiency is either limited by their chemical characteristics or cancer-developed resistance.

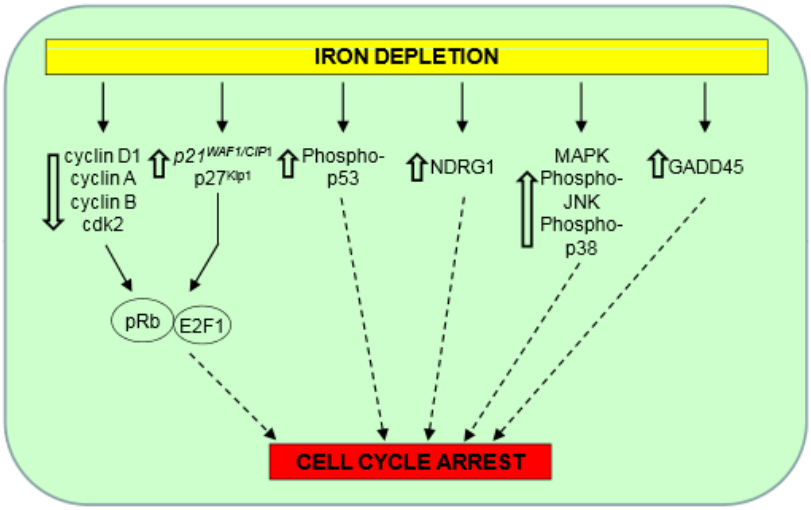

Figure 1.4. The Downstream Effects of Iron Depletion. Iron Depletion leads to a change in intracellular regulation pathways resulting in cell cycle arrest and apoptosis [41].

1.4. A Family of Chelators with Excellent Anti-tumor Activity:

Thiosemicarbazones

The thiosemicarbazone (TSC) family of chelators was designed to address the lipophilicity and permeability issues experienced with other chelators. Reported as early as the 1960s [42, 43], the ability of TSCs to form stable complexes with multiple transition metal ions, including Cu(I/II) and Fe(II/III), and perform redox cycling with both complexes plays a significant role in their biological activity and makes them versatile pharmacophores [29-31, 44]. TSCs have also been reported to markedly upregulate NDRG1 [45, 46]. One such TSC, Triapine (3-aminopyridine-2-carboxaldehyde thiosemicarbazone, (3-AP)), has made it successfully to Phase II clinical trials [47, 48]. This tridentate Fe chelator acts mainly as a ribonucleotide reductase inhibitor to prevent DNA repair and synthesis, but it has also been reported to form redox complexes and produce ROS in renal cell carcinoma [49]. Unfortunately, Triapine has not been found to be very effective in clinical trials and comes with very significant side effects [27, 50].

Another more active TSC, however, shows much more promise. Di-2-pyridylketone-4,4-dimethyl-3-thiosemicarbazone (Dp44mT) is a small, hydrophobic chelator that has been tested against over 30 cancer cell lines, with an average $IC_{50} \sim 30$ nM (IC_{50} ranges from 5 - 400 nM depending on the cell line) [45], which is more effective than other TSCs like Triapine ($IC_{50} = 1$ - 3 μM), other chelators including DFO ($IC_{50} = 3$ - 25 μM), and even other common chemotherapeutics such as DOX ($IC_{50} =$ 0.3 - 1 μM) [38, 45, 46, 51-53]. As summarized in **Figure 1.5**, Dp44mT's enhanced cytotoxicity can be attributed to three main functions: (1) high Fe and Cu chelation

efficacy due to its ability to inhibit Fe uptake from TFR1 and increase Fe release from cells [51, 54]; (2) production of ROS via Fe and Cu-redox complexes resulting in apoptosis [51]; and (3) utilization of the NDRG1 pathway to block cellular proliferation, overcome cancer metastasis, and bypass p53-induced MDR [45, 51, 55]. While Dp44mT has an apparent selectivity towards neoplastic tumor cells rather than normal cells (IC_{50} > 25 μM in fibroblasts) [51], suggesting that it should have reduced side effects on healthy tissues, it should be noted that large doses of 0.75 mg/kg of free Dp44mT, administrated in free form [45], have been found to cause myocardial lesions in mice [45, 46, 56]. Therefore, to enhance its therapeutic effectiveness to target cancer cells while reducing off-target toxicity to healthy cells, Dp44mT should be encapsulated into an effective carrier/delivery system.

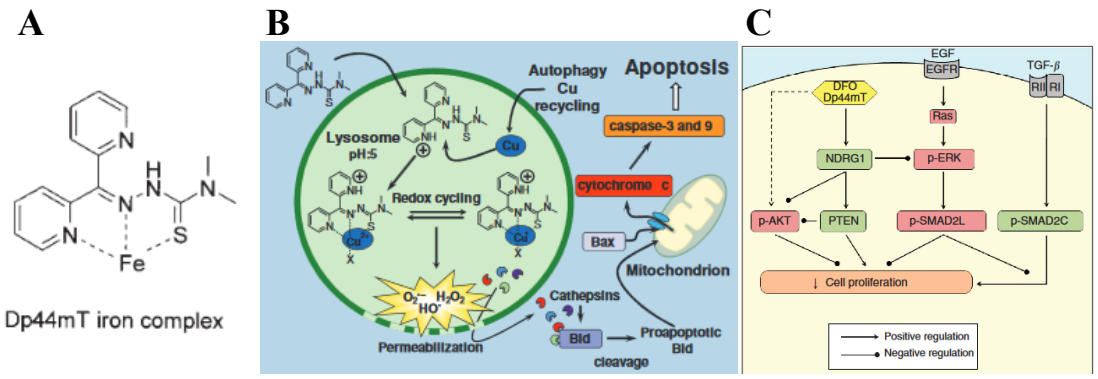

Figure 1.5. Dp44mT and Its Mechanism of Action. Dp44mT toxicity occurs by (A) chelating iron and copper [54], (B) producing of reactive oxygen species [38], and (C) altering intracellular signaling pathways [55].

1.5. The Use of Nano-Carriers in Cancer Therapy

Due to the toxicity, instability, and ambiguous delivery of current chemotherapeutic drugs, better platforms are required to enhance the effects and delivery of these

compounds. One option is to employ the use of nano-carriers for the delivery of these chemotherapeutics. Nanomaterials and nano-scale based platforms have become very popular for many medical applications due to the unique properties afforded by their size range and their versatility in curing diseases or repairing damaged tissues [57, 58]. Materials in this size range have an increased surface-to-volume ratio compared to larger materials, which results in changes to the material reactivity, elasticity, magnetic properties, conductivity, etc. [59]. Nanoparticles (NPs) are also able to access tiny areas of the body for better drug delivery [60] and can be easily manipulated for targeted and controlled delivery of their toxic payload, while bypassing the immune system and filtration organs, resulting in a more effective treatment regimen with reduced side effects [61]**.** In **Figure 1.6** are the major classes of NPs currently used for medical applications, which include: liposomes, nanoshells (including quantum dots), metals and metal oxides, carbon-based particles (carbon nanotubes and fullerenes), nano-emulsions, nanocrystals, and polymer-based nanomaterials (including dendrimers) [59].

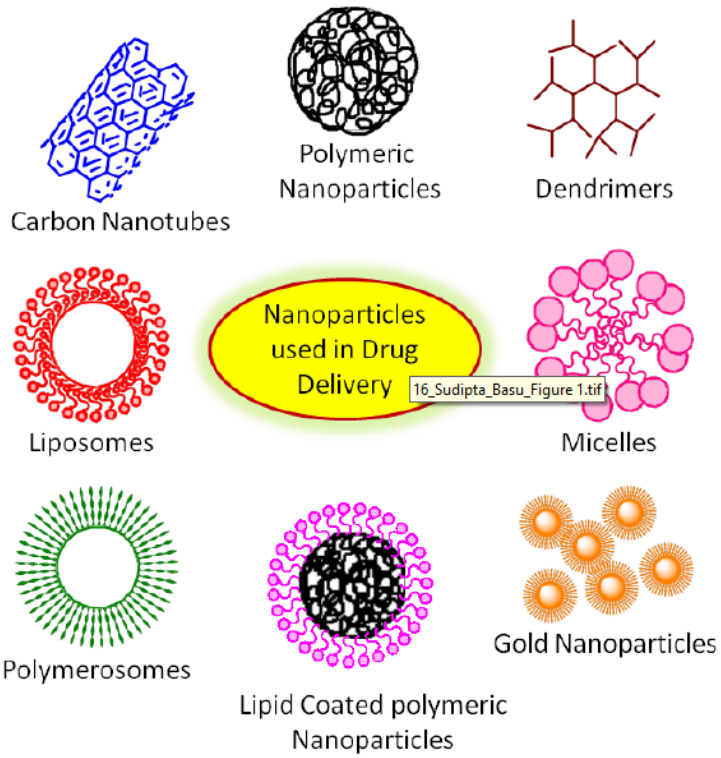

Figure 1.6. Nano-Carriers Utilized for Drug Delivery in Medicine [62].

1.5.1. The Benefits of PLGA as a Nano-Carrier

Among the multitude of available nano-scale carriers that have been explored for efficient chemotherapeutic delivery (**Figure 1.6**) [61, 63, 64], NPs composed of poly(D,L-lactic-co-glycolic acid) (PLGA) have become particularly popular for drug delivery purposes.Since PLGA was first approved for use by the Food and Drug Administration (FDA) in 1984, it has become the best defined and most commonly ised polymeric biomaterial for the fabrication of drug delivery platforms [64, 65]. PLGA is an amorphous polymeric biomaterial composed of poly lactic acid and poly glycolic acid (PGA) in a diblock formation [63]. It is very versatile because it can be dissolved in a wise range of common solvents and subsequently processed into almost any size or

shape [66, 67], including microspheres, microcapsules, nanoparticles, and implants [64]. PLGA has also become particularly popular for drug delivery due to its various physical characteristics. However, there are a series of parameters that must be considered during NP fabrication in order to achieve optimal chemotherapeutic delivery, including chemical characteristics of the encapsulated drug, NP durability and biodistribution, and the ability to overcome physical barriers within the body. Here, we examine the impact of these parameters, in lieu of naked drug administration, for improved cancer treatment efficacy.

First, NPs comprised of PLGA are very mechanically strong and stable. Compared to nano-carriers fabricated from lipids (e.g., liposomes), PLGA nano-carriers are not likely to burst or be damaged by various handling processes [63]. The mechanical strength of this polymer can be tuned through the polymer's molecular weight, lactic acid/glycolic acid ratio, swelling behavior, crystallinisty, and geometric regularity of individual chains [63, 68-70]. This is especially important for chemotherapeutic delivery via the vasculature, as any nano-platform applied in this manner will experience various changes in blood flow, pressure, and vessel size. The stability and durability of a nano-carrier can then be enhanced through the use of surfactants [71] or the covalent attachment of poly(ethylene glycol) (PEG) [72]. The addition of PEG chains creates a hydrophilic layer at the aqueous interface of the nano-carrier which increases the carrier's colloidal stability [73, 74]. The degree/density of PEGylation, PEG chain length, and molecular weight will determine the degree of steric coverge that can be achieved for a nano-carrier [61]. Improved stability results in increased circulation half-life and decreased cellular uptake, which in turn improves NP

biodistribution and half-life. Consequentially, prolonged circulation time leads to prolonged drug delivery and activity at tumor sites. At the same time, the PEG layer also prevents protein aggregation [74] to the nanoparticle surface [61, 63] thereby helping the nanoparticle escape detection and degradation by the immune system [63, 74, 75].

Second, PLGA is an excellent drug carrier due to its ability to encapsulate large quantities of drug and modulate subsequent drug release. Due to the methyl side groups present in the PLGA backbone, this polymer is hydrophobic and therefore has been shown to be an excellent material for the encapsulation of variety of drugs including small hydrophobic drugs [63, 64, 75, 76]. Since most chemotherapeutic compounds are not stable long-term, or have very low solubility in aqueous solutions, these drugs are rapidly degraded or absorbed upon application in aqueous systems, resulting in reduced drug effectiveness against cancer cells, toxic side effects to healthy tissues, and the need for greater and repeated doses. Therefore, non-covalent entrapment (encapsulation) of unstable or toxic drugs inside a PLGA NP core can protect the drug from direct exposure to the aqueous environment thereby preventing degradation, improving delivery to the target tissue in a controlled manner, and preventing toxicity to healthy tissues [22, 77-79]. Inevitable drug release from PLGA is then controlled through a combination of drug diffusion and polymeric matrix degradation, the rate of which can be tuned through the lactic acid/glycolic acid ratio, molecular weight, polymeric end groups, pH, temperature, amount and type of encapsulated drug, as well as NP size and shape (surface area ratio) [63, 64, 75].

Third, unlike metallic or silica-based NPs, PLGA-based nano-carriers do not require removal or excretion after delivering their chemotherapeutic payload as PLGA is a biodegradable material. PLGA hydrolysis at its ester linkages [63, 64] produces lactic acid and glycolic acid monomers (**Figure 1.7)**, both of which are natural compounds that participate in a number of physiological and biochemical pathways [64, 80]. Therefore, there is minimal toxicity associated with the use of this biocompatible material for drug delivery or other biomaterial applications [80].

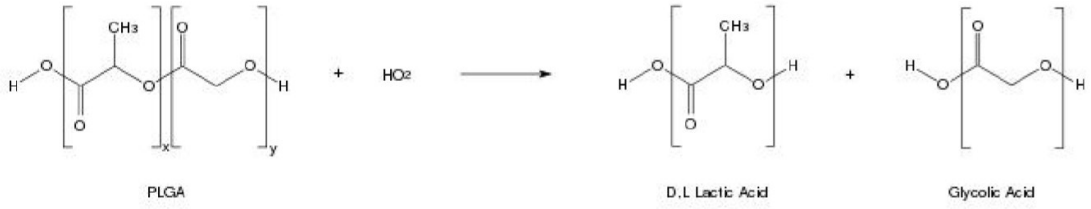

Figure 1.7. The Structure and Degradation of PLGA [63].

Lastly, while traditional chemotherapeutic drugs are dependent upon their chemical properties (polarity, charge, size, etc.) for delivery and are not cell specific [80], PLGA NPs can be easily modified, as represented in **Figure 1.8**, to take advantage of passive or active targeting techniques [60], which will enable them to bypass biological barriers for more effective drug delivery to tumors.

Passive targeting simply relies on the basic characteristics of the NPs (size, shape, and surface potential) to take advantage of the enhanced permeability and retention (EPR) effect, the “leakiness” of the vasculature around a tumor due to tumor growth and corresponding inflammation [59, 80]. One such characteristic, PLGA NP size, can

be adapted for improved biodistribution and delivery. It has been observed that larger particles (> 200 nm) tend to trigger humoral responses and get engulfed by immune cells. They also have a tendency to be filtered out of the blood by the liver and spleen [22, 78]. On the other hand, studies have shown that very small (< 50 nm) particles are likely to be filtered out of the blood by the kidneys [78]. Therefore, NPs ranging from 50 - 200 nm, which have been found to accumulate in tumor tissues, are much better at evading the immune system and avoiding filtration [61, 75, 78]. The shape of a NP can also be adjusted to optimize biodistribution and delivery. Previous research has shown that spherical polymeric nanoparticles are internalized faster and to a greater extent compared to their non-spherical counterparts [50, 79]. This is due to the fact that non-spherical polymeric nanoparticles have a predominance of low curvature regions which results in reduced cellular attachment and internalization, as well as prolonged survival in circulation [79]. Similarly, due to their hydrophobicity [63], PLGA NPs have a negative surface potential, which has been found to be less cytotoxic than particles with positive surface potentials and also allows them to maintain appropriate colloidal stability [61].

Active targeting, on the other hand, involves the modification of the NP surface, through the attachment of biochemical moieties ("targeting ligands"), to facilitate precise delivery and uptake by cancerous cells. These biochemical targeting moieties, which include small molecules, antibodies, membrane receptors, peptides, and nucleic acids [59, 60], can help nano-carriers bypass endothelial barriers, like the Blood-Brain Barrier (BBB), in order to reach the tumor site. Polysorbate 80/LDL, OX26 TfR antibody, lactoferrin, etc. have all been shown to improve delivery of large molecule

drugs into the brain via receptor-mediated transcytosis [80]. Tissue targeting also ensures that the NPs only deliver their drug payload once they are uptaken by the appropriate target cells. Together, this increases the effectiveness of the chemotherapy while also reducing toxic side effects to off-target tissues. Therefore, the most successful nano-formulations combine features of passive and active targeting to maximize NP delivery to cancer cells [80].

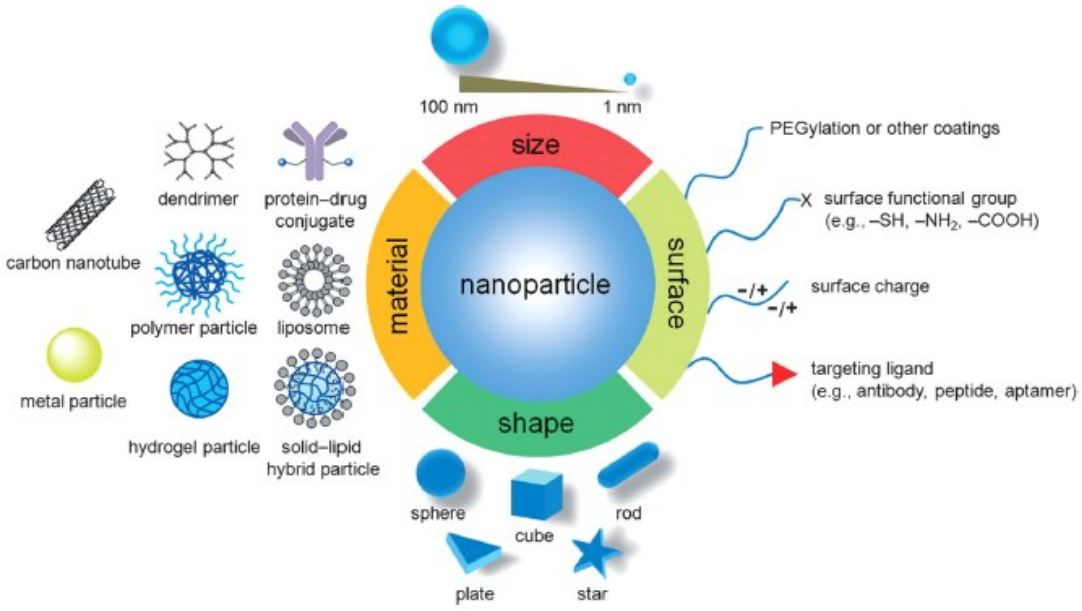

Figure 1.8. Nanoparticle Properties for Optimal Drug Delivery. Surface properties can be optimized for increased nanoparticle stability, prolonged biodistribution, and cell-specific delivery [71].

1.6. Research Objectives

The goal of this dissertation is to develop the first nano-scale carrier for the encapsulation and delivery of iron chelator, Dp44mT, and evaluate the effectiveness of this therapeutic formulation against malignant cells. In **Chapter 2**, we apply two distinct methods of nanoprecipitation and single emulsion to fabricate PLGA nanoparticles

loaded with iron chelator Dp44mT. This chapter focuses on the optimization of each technique required to produce our ideal nanoparticles. Characterization of the resultant nanoparticles allows for comprehensive comparison of these techniques for future nanoparticle fabrication. In **Chapter 3**, we provide a preliminary assessment of the therapeutic potential of our Dp44mT-loaded nano-formulation in brain, breast, and colorectal cancer cells *in vitro*. This chapter focuses on the cytotoxicity and exposure time required for sufficient cancer cell apoptosis, in comparison to the application of free Dp44mT. We then report the efficacy of this platform for drug delivery to a variety of malignant cells. In **Chapter 4**, we modify our Dp44mT-loaded nano-formulation for future *in vivo* application. This chapter focuses on improving the stability and biodistribution of our nano-formulation through the attachment of PEG and targeting ligands to the surface of the nanoparticles. We further evaluate and optimize the effectiveness of this new nano-formulation against cancer cells *in vitro*. Finally, in **Chapter 5**, we discuss the implications of this new nanoparticulate platform for future delivery of Dp44mT to cancer cells *in vivo*, along with some of future directions of this research.

CHAPTER II
FABRICATION AND OPTIMIZATION OF DP44MT-LOADED NANOPARTICLES

2.1. Abstract

This chapter describes the preparation of poly(lactic-co-glycolic acid) (PLGA) nanoparticles (NPs) loaded with iron chelator Dp44mT, using two common techniques of nanoprecipitation and single emulsion. Using nanoprecipitation, we examined the impact of polymer type and amount, drug-to-polymer ratio, and surfactant concentration in the aqueous phase on the formation of our Dp44mT-loaded NPs (referred to as Dp44mT-NPs), which were characterized for shape, size, surface potential, colloidal stability, encapsulation efficiency, loading capacity, and drug release. Similarly, we produced Dp44mT-NPs using single emulsion and optimized polymer concentration, surfactant concentration, injection rate, and drug-to-polymer ratio. These NPs were also characterized for shape, size, surface potential, colloidal stability, encapsulation efficiency, and loading capacity. We then preformed a comprehensive comparison of the NPs produced by each of these techniques, to determine the optimal method for the fabrication of our Dp44mT-loaded nano-carrier. Overall, this chapter establishes the parameters necessary to produce our ideal nano-formulation, for future drug delivery to malignant cells.

2.2. Introduction

PLGA NPs have been widely applied in drug delivery systems [81-84]. These NPs can be produced through a number of techniques such as nanoprecipitation as well as single – and double–emulsions [60, 85]. However, it has been shown that the results of these techniques for encapsulation of pharmaceutical cargos into PLGA NPs can vary significantly, depending on the properties of the cargo. Since Dp44mT and PLGA are both hydrophobic, these compounds require the use of an organic solvent (or "oil" phase) for dissolution. Therefore, the fabrication techniques most commonly used to produce such NPs are nanoprecipitation or single emulsion. In this study, for the first time, we employ both of these techniques for the fabrication of Dp44mT-loaded PLGA NPs (Dp44mT-NPs).

Nanoprecipitation has been reported to be particularly efficient for encapsulation of hydrophobic compounds [65]. It requires a water-miscible organic solvent (e.g., acetone), as the NPs are formed from organic phase diffusion out of the out of the micro-droplets and into the surrounding aqueous phase. To this end, Dp44mT-NPs were prepared by nanoprecipitation and then we studied the effect of modulating polymer type (lactic acid (LA)-to-glycolic acid (GA) ratio), amount of poly(vinyl alcohol) (PVA) surfactant in the aqueous phase, and drug-to-polymer ratio. The resultant NPs were characterized for size, surface potential, morphology, and colloidal stability. We further examined the encapsulation efficiency, loading capacity, and release of Dp44mT from PLGA NPs.

However, it has been noted that there is the potential for poor drug encapsulation if the drug in question is partially soluble in the aqueous phase at low concentrations (i.e., appreciable solubility). As this is the case with Dp44mT, this drug will have a tendency to dissipate into the continuous aqueous phase, resulting in drug lost from the system [65]. Single emulsion (oil-in-water emulsion/solvent evaporation) is another common technique for encapsulating hydrophilic or hydrophobic compounds into micro- and nano-scale particles [60, 65, 85]. This technique uses a water-immiscible solvent (e.g., dichloromethane, DCM), which is then removed by vacuum evaporation, to prevent the flux of drug into the aqueous phase after injection [65]. The size of NPs can then be tuned by type and concentration of stabilizer, polymer concentration, and homogenization speed [60]. In order to examine the potential of the single emulsion technique for loading Dp44mT into NPs of PLGA with a size range proper for cancer therapy (i.e., 80 - 120 nm) [22] and high encapsulation efficiencies (> 60%), we studied the effect of modulating the method and rate of organic phase injection, amount of PVA in the aqueous phase, and PLGA concentration in the organic phase. We then characterized the resultant NPs for size, zeta potential, colloidal stability, encapsulation efficiency, and loading capacity. Comparison of the NPs produced by these two techniques will reveal the optimal NP formulation as a vehicle for Dp44mT delivery in future cancer treatment.

2.3. Experimental Methods

2.3.1. Materials

Dichloromethane (DCM) was purchased from Acros Organics (New Jersey, USA). Centrifuge filter tubes (50,000 MWCO) were from Millipore Sigma (Burlington, MA). 50:50 poly(lactic-co-glycolic acid) (PLGA) (10,000 - 15,000 MW), 75:25 PLGA (10,000 - 15,000 MW), methoxy poly(ethylene glycol)-b-poly(lactic-co-glycolic acid) (mPEG-PLGA; 2,000 - 15,000 MW), and maleimide poly(ethylene glycol)-b-poly(lactic-co-glycolic acid) (mal-PEG-PLGA; 5,000 - 20,000 MW) were from PolySciTech (West Lafayette, IN). Di-2-pyridylketone-4,4-dimethyl-3-thiosemicarbazone (Dp44mT), acetone, ethanol, and polyvinyl alcohol (PVA) (31,000 - 50,000 MW) were from Sigma-Aldrich (St. Louis, MO). Biotech CE dialysis membrane (3,500 - 5,000 Da MWCO) was from Spectrum Labs (Rancho Dominguez, CA). Silicon wafer was purchased from UniversityWafer (Boston, MA).

2.3.2. Fabrication of Dp44mT-loaded Nanoparticles via Nanoprecipitation

We applied a modified nanoprecipitation method for the preparation of Dp44mT-loaded PLGA NPs [86, 87]. Briefly, for the 0.15 mg/mL Dp44mT-NPs, 1 mg of PLGA and 0.15 mg of Dp44mT were co-dissolved in 1 mL of acetone, and this organic phase solution was injected into 3 mL of deionized (D.I.) water containing 1% (w/v) PVA at a flow rate of 60 mL/hr under magnetic stirring. The solution was gently stirred for about 45 - 60 min at room temperature in a fume hood to evaporate the organic solvent. The resultant NPs **(Figure 2.1)** were concentrated via centrifugation (4,700 rpm for 30

min) and then washed two-to-three times by addition of 1 mL of D.I. water followed by centrifugal filtration to remove unloaded drug. Lastly the NPs were resuspended to a final concentration of 1 mg/mL PLGA and 0.15 mg/mL of Dp44mT (referred to as 0.15 mg/mL Dp44mT-NPs) in water. These NPs were stored in 4°C until usage.

For variation of the drug: polymer ratio, the amount of Dp44mT co-dissolved with PLGA was changed to either 0.0375 mg or 0.3 mg. All other steps remained the same as mentioned above. To vary PVA percentage in aqueous phase, the amount of PVA was adjusted to either 0.5% or 4% and the mixture was filtered with a 0.2 μm filter before use. All other steps remained the same as mentioned above. The other NP formulations used for this study are summarized in **Table 2.1.**

2.3.3. Fabrication of Dp44mT-loaded Nanoparticles via Single Emulsion

We applied a modified single emulsion method [85] for the preparation of Dp44mT-loaded PLGA NPs. Briefly, for the 0.15 mg/mL Dp44mT-NPs, 1 mg of PLGA and 0.15 mg of Dp44mT were co-dissolved in 1 mL of dichloromethane (DCM), and this organic phase solution was injected onto the surface of 2 mL of deionized (D.I.) water containing 1% (w/v) PVA at a flow rate of 90 mL/hr under magnetic stirring. The solution was then stirred for 15 seconds (sec) after which the emulsified solution was homogenized for 30 sec using a Q55 tip sonicator (QSonica LLC, Newton, CT) at an amplitude of 35%. The emulsified solution was then placed under vacuum for 2 hrs using a rotary evaporator (Heidolph International, Schwabach, Germany) to allow for the evaporation of the DCM. The resultant NPs (**Figure 2.7**) were then concentrated and washed four times with D.I water via ultracentrifugation (Optima Max 130,000

ultracentrifuge, Beckman Coulter, Palo Alto, CA) at 13,000 rpm for 15 min each to remove unloaded drug and residual polymer and emulsifier. Lastly the NPs were re-suspended in water to a final concentration of 1 mg/mL PLGA and 0.15 mg/mL of Dp44mT. These NPs were stored at 4°C until usage.

For studying the effect of the injection rate on NP formation, the injection method was changed from dropwise manual addition to continuous injection with flow rates of 22.5 - 90 mL/hr using a syringe pump. All other steps remained the same as mentioned above. To vary PVA concentration in aqueous phase, the amount of PVA was adjusted to either 1% or 5% and the mixture was filtered with a 0.2 μm filter before use while all other steps remained the same as above. To vary PLGA concentration in the organic phase, the amount of PLGA was adjusted to 1, 10, or 100 mg/mL while keeping other steps the same as mentioned above.

2.3.4. Imaging

For scanning electron microscopy (SEM), a small droplet of diluted NP solution was placed on a clean piece of silicon wafer or glass, dried using vacuum pump, and coated with a thin (10 - 20 nm) layer of gold. The coated sample was then secured to a stand via carbon tape before SEM imaging was performed using a FEI 235 Dual-Beam Focused Ion-Beam System (FEI, Hillsboro, OR).

2.3.5. Size Distribution and Surface Potential

Particle size distribution was measured by dynamic light scattering (DLS) using a Malvern Nano ZS (Malvern Instruments, Malvern, UK) at room temperature. This

instrument was also used for zeta potential measurements. For each measurement, at least three replicates were used to calculate the average and standard deviation (SD).

2.3.6. Colloidal Stability

For colloidal stability studies, a solution of 1 mg/mL PLGA NPs was diluted in an equal volume of either water or 1X PBS, pH 7.4 and incubated at 37°C. Size distribution and zeta potential of NPs were monitored over the course of a week. Resulting data is represented by the mean ± SD, n > 3.

2.3.7. Encapsulation Efficiency and Loading Capacity

To assess the encapsulation efficiency of Dp44mT in PLGA NPs, we measured the amount of drug that was not encapsulated in NPs and used this value to calculate the encapsulation efficiency. Upon the fabrication of NPs, the centrifugal waste solution from the wash steps was collected and used to determine the amount of free (i.e., unencapsulated) Dp44mT using UV/vis spectrophotometry (SpectraMax M5 Molecular Devices, Molecular Devices, Sunnyvale, CA) at 329 nm wavelength since the aromatic rings in Dp44mT have maximum light absorption at this wavelength [87-89]. A standard curve was produced using a set of samples with known Dp44mT concentrations. This standard curve was used to convert the measured absorbance value into Dp44mT concentration, which was then used for encapsulation efficiency calculation using **Equation (2.1):**

$$Encapsulation\ Efficiency\ (\%) = 100 - (\frac{Df}{Di} \times\ 100). \qquad \textbf{(2.1)}$$

In this equation, D_f represents the amount of Dp44mT that was not encapsulated in the NPs (from spectrophotometry measurements of the centrifugal waste), and D_i represents the initial amount of Dp44mT used in the organic phase (i.e., "Drug fed").

Based on the obtained encapsulation efficiency for Dp44mT, we determined the mass of encapsulated drug and then calculated the loading capacity of NPs using **Equation (2.2)**:

$$Loading\ Capacity\ (\%) = (\frac{Dm}{Mt}) \times\ 100. \qquad \textbf{(2.2)}$$

In this equation, D_m represents the mass of Dp44mT encapsulated in NPs and M_t represents the total mass of NPs (i.e., mass of PLGA in organic phase plus the mass of encapsulated Dp44mT). Resulting data is represented by mean ± SD, n > 3.

2.3.8. Drug Release

For Dp44mT release studies, concentrated Dp44mT-NPs were diluted in 2X PBS to produce a solution with a final concentration of 1 mg/mL PLGA and 0.15 mg/mL of Dp44mT (referred to as 0.15 mg/mL Dp44mT-NPs) in 1X PBS. The NP solution was then placed in dialysis tubes (1 mL per tube) and the tubes were immersed in 1 L of 1X PBS solution at 37°C under magnetic stirring. At each time point, one dialysis tube was removed, the NP sample inside was collected, and the amount of drug remaining within the NPs was measured. For these measurements, the NP samples were diluted with acetone (ratio of 1:1) to release the encapsulated Dp44mT from NPs thereby allowing the amount of Dp44mT

remaining in each sample to be measured by UV/vis spectrophotometry at 329 nm. Note that the standard curve for this experiment was based on known dilutions of Dp44mT dissolved in a 1:1 acetone: 1X PBS solution. The release percentage was then calculated using **Equation (2.3)**:

$$Drug\ Release\ (\%) = 100 - \left(\frac{Dt}{D0} \times\ 100\right). \quad \textbf{(2.3)}$$

In this equation, D_t represents the amount of encapsulated Dp44mT remaining in NPs at each time point and D_0 represents the initial amount of Dp44mT encapsulated in NPs (measured at time = 0 min). Resulting data is represented by mean ± SD, n > 3.

2.3.9. Statistical Analysis

GraphPad Prism 8 was used to perform student's t-tests to compare experimental groups and to evaluate statistical significance. For all collected data, statistical significance is represented by $*p < 0.05$, $**p < 0.01$, $***p < 0.001$.

2.4. Results and Discussion for Nanoprecipitation

2.4.1 Preparation and Characterization of Dp44mT-loaded Nanoparticles

Among different techniques developed for the preparation of nano-scale PLGA particles, nanoprecipitation has proven to be particularly suitable for encapsulation of small hydrophobic agents [63, 64, 75]. The nanoprecipitation technique utilizes a water-miscible solvent (e.g., acetone) as its organic phase. After injection into the aqueous phase, the solvent diffuses out of the injected micro-droplets and into the aqueous phase,

thereby solidifying the hydrophobic components (polymer and drug) into the finalized nanoparticle. The NPs are then easily collected and purified via centrifugation [90]. Here, we applied this technique and injected a solution of PLGA and hydrophobic drug, Dp44mT, dissolved in acetone into an aqueous solution containing a 1% PVA as a stabilizer, which resulted in the formation of Dp44mT-NPs via rapid solvent displacement [86] (**Figure 2.1**).

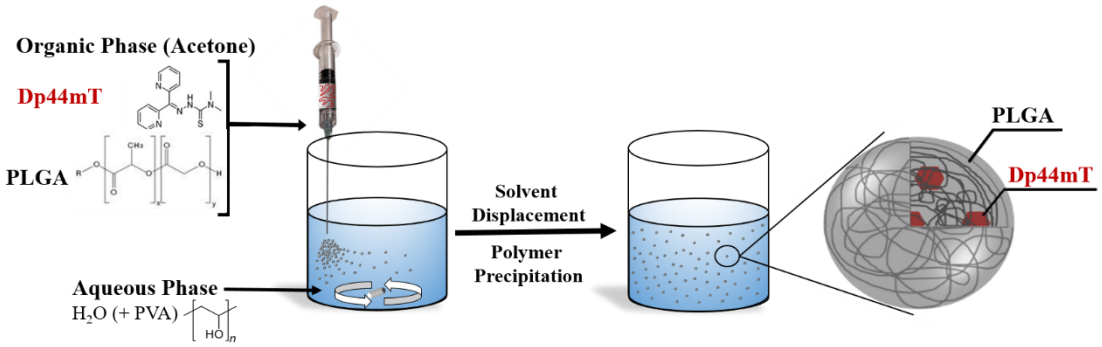

Figure 2.1. Schematic of Dp44mT-loaded PLGA NP fabrication via nanoprecipitation.

Using this approach, a number of NPs with slight variations in their formulation, such as drug to PLGA ratio, PLGA monomer (i.e., LA:GA) ratio, and encapsulated cargo were fabricated and characterized for size, morphology, surface potential, encapsulation efficiency, and loading capacity as summarized in **Table 2.1**.

Table 2.1. NP formulations, formed via nanoprecipitation, examined in this study with their corresponding size distribution, polydispersity index (PDI), zeta potential, drug encapsulation efficiency, and drug loading capacity.

	Organic Phase		Particle		Zeta	Encapsulation	Loading
	Drug:PLGA [mg/mL]	PLGA* [LA:GA]	Size [nm]	PDI	Potential [mV]	Efficiency [%]	Capacity [%]
PLGA-NP	-	50:50	85±15	0.28±0.05	-17±9	-	-
+Dp44mT-NP	0.15:1	50:50	92±19	0.23±0.04	-14±10	57±7	7.8±0.9
Dp44mT-NP	0.0375:1	50:50	100±12	0.12±0.03	-7±3	74±16	2.7±0.6
Dp44mT-NP	0.15:1	75:25	60±22	0.26±0.02	-17±7	86±3	9.1±1.6
C6-NP	0.01:1	50:50	99±18	0.28±0.06	-9±6	95±5	0.9±0.1

* PLGA type based on the ratio of lactic acid (LA) to glycolic acid (GA).
+ The NP formulation used for the cytotoxicity experiments.

We assessed the morphology of the produced NPs using SEM imaging and found these NPs were spherical in shape and relatively homogenous as depicted in **Figure 2.2A**. As represented in **Figure 2.2B**, further evaluation of size distribution using dynamic light scattering (DLS) confirmed the production of PLGA NPs with a size distribution of 85 ± 15 nm, and also revealed that inclusion of Dp44mT in PLGA NPs led to a slight increase in the average size of NPs, to 100 ± 12 nm with a polydispersity index (PDI) of < 0.25. Interestingly, we observed a drop in NP size when the monomer ratio in PLGA was switched from 50:50 to 75:25, which corresponded to a more hydrophobic polymer matrix. We attributed this result to the stronger interactions between PLGA chains and the hydrophobic molecule Dp44mT and presumably, a more compact drug-polymer matrix in the resultant NPs. Nevertheless, all the produced NPs remained close to the optimal size range of 50 - 200 nm, which avoids the mononuclear phagocyte system and renal filtration while also escaping hepatic and splenic filtration, for therapeutic delivery in cancer [22, 78, 79].

Measurements of zeta potential revealed that all the examined NP formulations were negatively charged, suggesting a good colloidal stability for these particles. We further evaluated the colloidal stability of these NPs under physiological conditions, at 37°C under gentle agitation, over the course of several days. As illustrated in **Figure 2.2C,** with slight fluctuations, the size of Dp44mT-NPs incubated in water remained close to their original size, showing the stability of these NPs. In PBS, however, the NP average size and its variation had an increasing trend. Although this size change was not statistically significant, it suggested that the long-term storage of these NPs could benefit

from further modification. Together, these data demonstrate that nanoprecipitation can produce Dp44mT-encapsulating PLGA NPs with relatively homogenous size and shape and with a good level of colloidal stability, potentially suitable for cancer therapy.

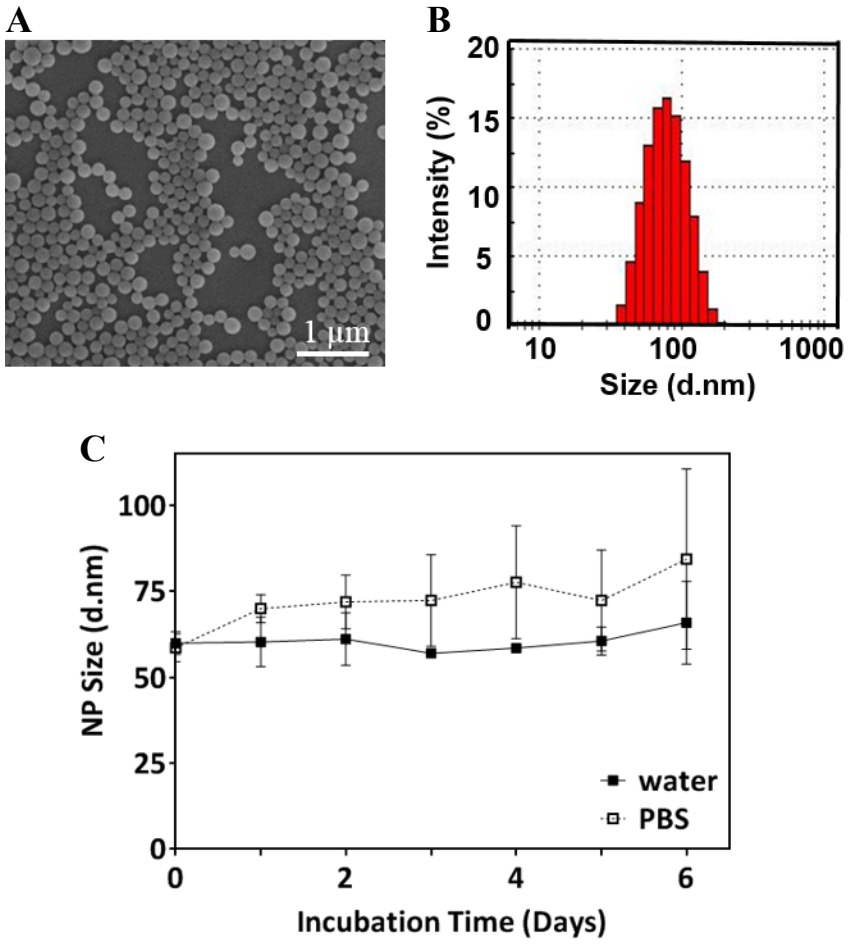

Figure 2.2. Characterization of Dp44mT-NPs, prepared by nanoprecipitation, through (A) SEM, (B) representative DLS size distribution, and (C) colloidal stability of Dp44mT-NPs in solution over time.

2.4.2. Encapsulation Efficiency and Loading Capacity

Encapsulation efficiency, which represents the percentage of drug entrapped in NP relative to the total amount of drug used for the formulation, is an important parameter

for evaluating the capacity of nano-carriers and should ideally be high [75]. While we previously demonstrated that PLGA NPs can incorporate Dp44mT with high encapsulation efficiency (~ 81%) compared to another commonly used carrier nanoliposomes (~ 4%) [87], here we aimed to further investigate the effect of PVA percentage, PLGA type, and drug-to-polymer ratio on this parameter. To evaluate the capacity of PLGA NPs for encapsulation of Dp44mT, we measured the encapsulated amount of this chelator in PLGA NPs by UV/vis spectrophotometry and calculated the encapsulation efficiency as described in the methods section.

Our results showed that encapsulation efficiency was significantly improved by: (1) increasing the amount of PVA in aqueous phase (0.5 - 4% w/v) where encapsulation increased from ~ 43% to ~ 82% (**Figure 2.3A**), (2) increasing the polymer's lactic acid to glycolic acid monomer ratio (50:50, 75:25, and 90:10) resulting in encapsulation efficiencies of ~ 60% to ~ 89% (**Figure 2.3B**), or (3) by decreasing the drug-to-polymer ratio (0.0375 - 0.3: 1 mg/mL) leading to encapsulation of ~ 35% increasing to ~ 75% (**Figure 2.3C**).

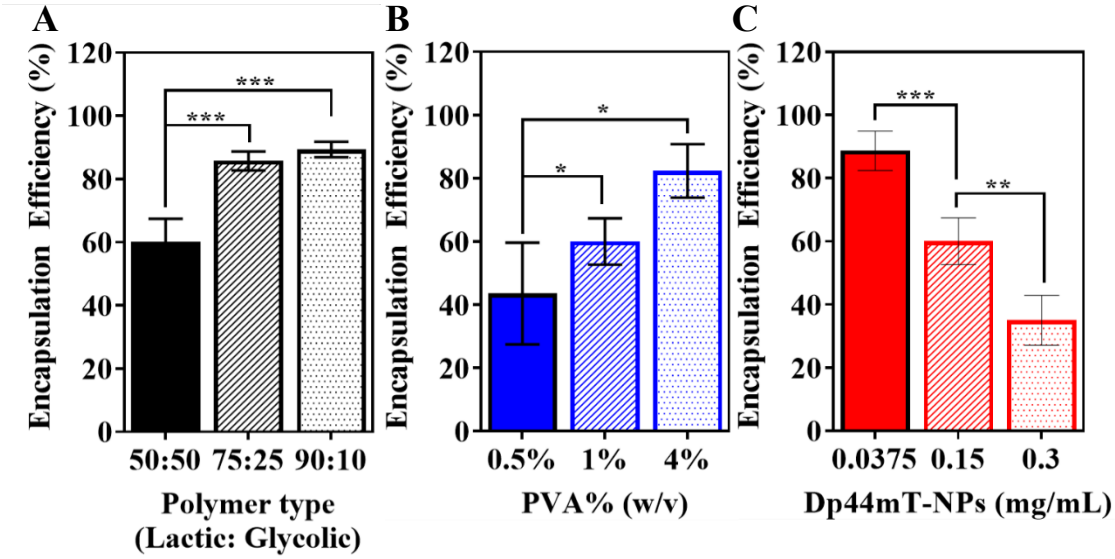

Figure 2.3. Optimization of Dp44mT encapsulation efficiency in PLGA NPs, prepared by nanoprecipitation, influenced by (A) PLGA type, (B) PVA %, and (C) Dp44mT-to-PLGA ratio.

Overall, the average encapsulation efficiency of Dp44mT in PLGA NPs varied within a relatively high range of 57 - 86% for different formulations, indicating the appropriateness of PLGA NPs for encapsulation of this chelator (see **Table 2.1**). This range is indeed comparable to the previously reported values for encapsulation of other hydrophobic compounds such as docetaxel (~ 75%) and coumarin (~ 88%) in nanoprecipitated PLGA particles [91, 92]. Notably, encapsulation of Dp44mT in these PLGA NPs clearly improved the solubility of this hydrophobic agent in aqueous solution (**Figure 2.4**) similar to previously reported results for other hydrophobic compounds such as docetaxel and coumarin [91, 92].

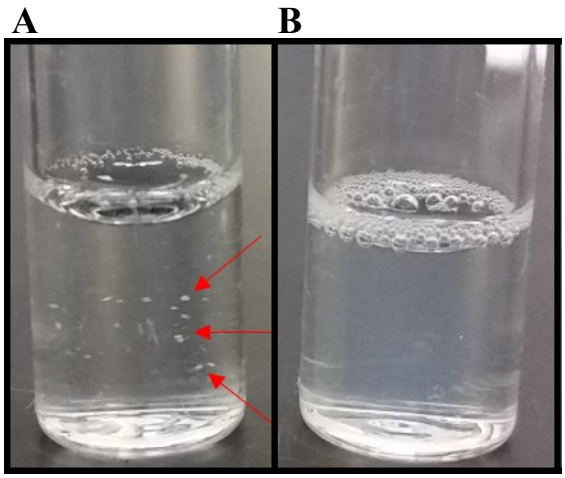

Figure 2.4. Solubility of free Dp44mT and Dp44mT-loaded PLGA NPs. (A) 500 µM free Dp44mT in water (red arrows mark precipitated Dp44mT) compared to (B) 500 µM free drug loaded in PLGA NPs.

Another significant parameter for evaluation of nano-formulations is the drug loading capacity, which represents the ratio of drug mass in NP to the total NP mass and is thus, essential for dosing calculations particularly for *in vivo* studies. Calculated as described in the methods section, the loading capacity of the examined Dp44mT-NP formulations here varied between 2.7% and 9.1%. Unlike the encapsulation efficiency, the average loading capacity of Dp44mT-NPs decreased from 7.8% to 2.7% when the drug to PLGA ratio was reduced (**Figure 2.5**). However, increasing the hydrophobicity of PLGA (75:25) enhanced the average loading capacity to 9.1%. Both 7.8% and 9.1% for loading capacity of Dp44mT-NPs are considered relatively high values for this parameter [77, 91]. These findings confirm that PLGA NPs can serve as an effective carrier for the chelator Dp44mT and slight variations in Dp44mT-NP formulation can be utilized to fine-tune their encapsulation and loading efficiencies.

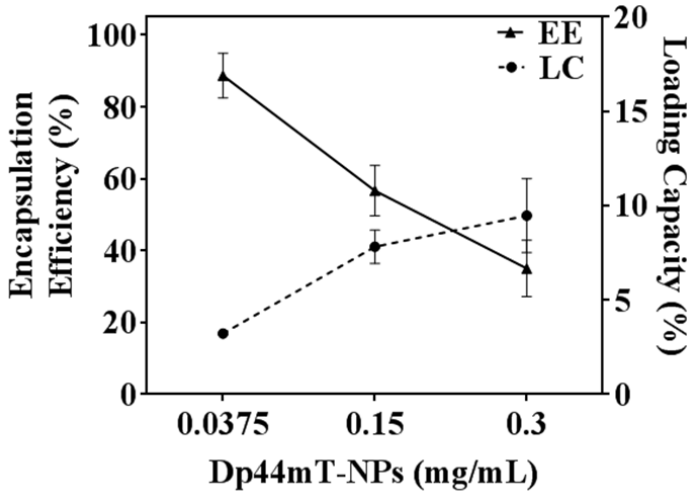

Figure 2.5. Relationship between encapsulation efficiency and loading capacity of Dp44mT in PLGA NPs, due to change in Dp44mT: PLGA ratio in the organic phase.

2.4.3. Drug Release Studies

Release kinetics of a cargo from a particular carrier is essential for the cargo's biodistribution and efficacy [63, 64, 75, 76, 78]. It thus, deserves careful consideration during the development and assessment of a nano-formulation. To investigate the release of Dp44mT from PLGA NPs, here we incubated Dp44mT-NPs in PBS (pH 7.4) at body temperature (i.e., 37°C) under gentle agitation and monitored the fractional release of Dp44mT over time. As depicted in graphs in **Figure 2.6**, Dp44mT release showed a relatively fast phase (i.e., burst release) that was followed by a slower phase over time (i.e., sustained release). Interestingly, nearly half of the encapsulated Dp44mT was released from these particles within the first few hours. Since the kinetics of drug release from PLGA particles is the collective result of bulk diffusion and bulk degradation of PLGA matrix [93, 94], the drug release profile depends on both the cargo properties and

the properties of PLGA, such as molecular weight and monomer ratio (i.e., LA:GA) [63, 64]. While 50:50 PLGA is known to have the fastest degradation among different PLGAs, its degradation typically occurs within weeks [63, 64]. In agreement with these findings, here we observed no detectable degradation of these particles in water or PBS within a one-week period (**Figure 2.2C**). The initial fast release of Dp44mT from the NPs was hence, attributed to a non-homogenous dispersion of the drug within the polymer matrix with its highest concentrations near the surface of NPs [95]. In order to reduce the initial rate of Dp44mT release from PLGA NPs, we examined some of the parameters that are known to influence the cargo's release kinetics including increased PLGA hydrophobicity (i.e., increasing LA:GA ratio that reduces the degradation of PLGA) and reduced drug to polymer ratio [63, 64]. In fact, both of these parameters enhanced the entrapment of Dp44mT within the PLGA NPs (**Table 2.1**) and presumably affected the dispersion of this chelator in NPs. As anticipated, both increasing the LA:GA ratio and lowering Dp44mT to PLGA ratio effectively reduced the release rate of Dp44mT from the NPs (**Figure 2.6A-B**). This trend was, however, more pronounced in **Figure 2.6B** that depicts the effect of drug to polymer ratio. These data demonstrate that the release of Dp44mT from these PLGA NPs can be effectively tuned to reach a desired profile for the application of these Dp44mT-NPs *in vivo*.

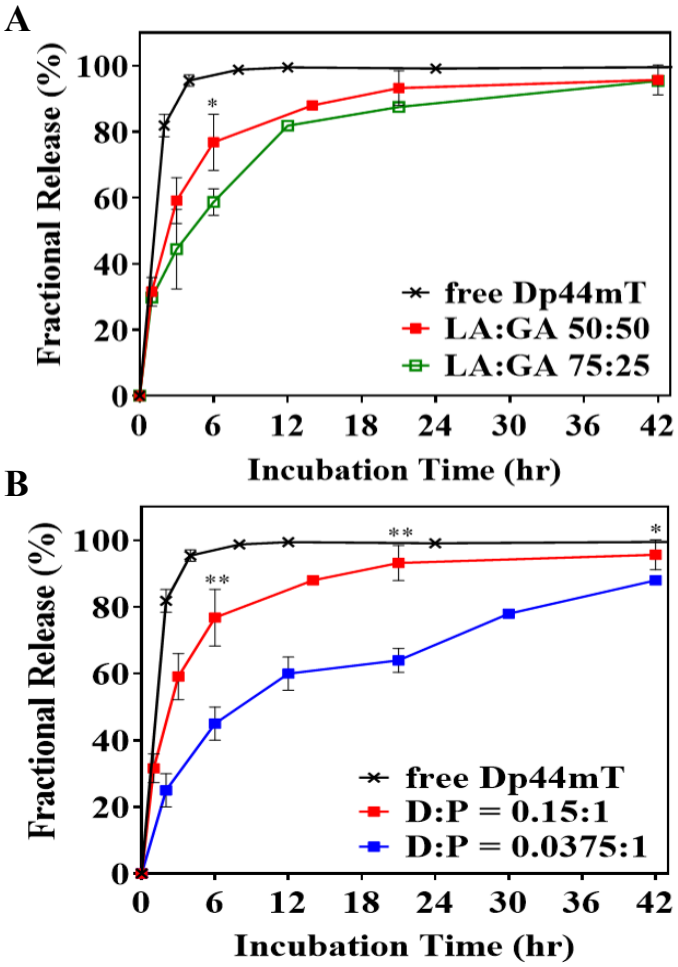

Figure 2.6. Profile of release of Dp44mT from PLGA NPs. (A) Time-dependent fractional release of Dp44mT from NPs with (A) different PLGA types or (B) different Dp44mT-to-PLGA ratios.

2.5. Results and Discussion for Single Emulsion

2.5.1. Preparation and Characterization of Dp44mT-loaded Nanoparticles

NPs used for delivery of therapeutics should ideally be in the size range of 10 - 200 nm to avoid filtration by either the renal, hepatic, or immune systems [22, 96]. This optimal size range can be further reduced to 80 - 120 nm by the need to utilize vascular diffusion for delivery to tumors while still avoiding aggregation due to protein adsorption at the NP surface [22, 96]. Size distribution of NPs produced by single

emulsion is affected by different fabrication parameters, including injection rate of the organic phase, surfactant concentration, and polymer concentration [85]. We hence, first focused on optimizing the size of Dp44mT-NPs for the future delivery applications through adjustment of these fabrication parameters. Here, we applied the single emulsion technique and injected a solution of PLGA and Dp44mT, dissolved in DCM, into an aqueous solution containing a 1% PVA as a stabilizer, which resulted in the formation of Dp44mT-NPs (**Figure 2.7**).

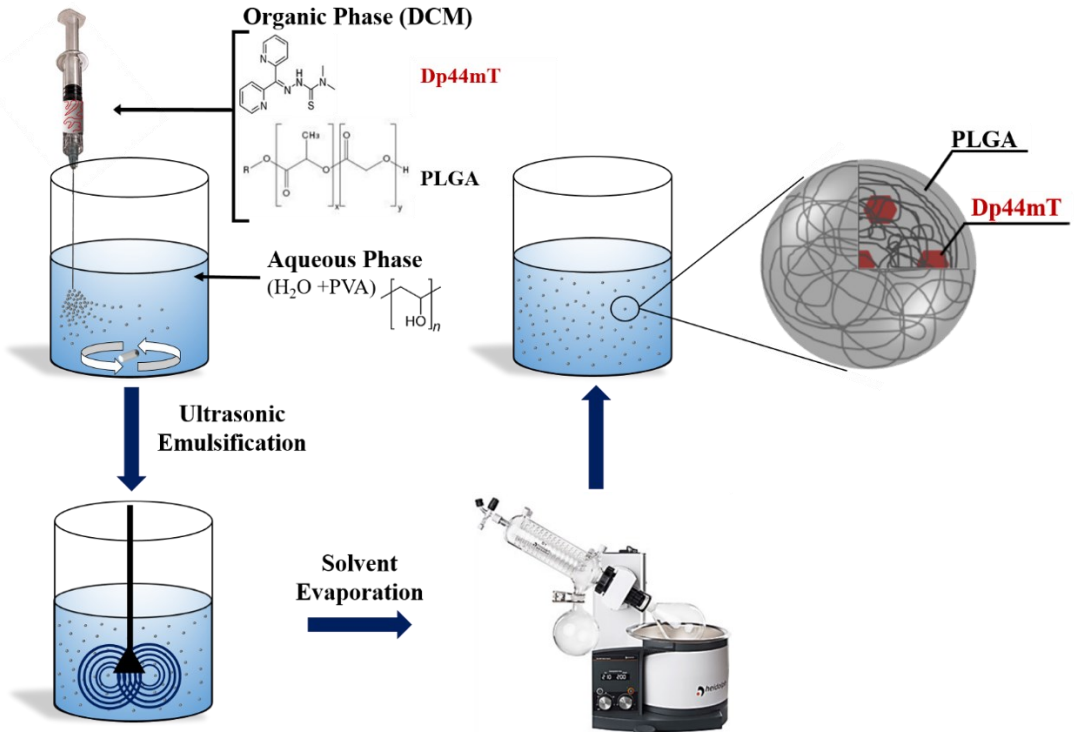

Figure 2.7. Schematic of PLGA NPs encapsulating Dp44mT fabricated by single emulsion technique.

Using a previously published single emulsion protocol [85], we initially used a 100 mg/mL concentration of PLGA in the organic phase, which was added dropwise

(manually) to an aqueous phase containing 5% PVA (w/v). The produced NPs had an average diameter of 647 nm with a large polydispersity index (PDI), suggesting a wide size distribution. We attributed this large variation in NP size to the slow and uncontrolled method of injection of organic phase to the aqueous phase. Given that a faster injection rate has been reported to reduce the size of NPs [85], we next switched from dropwise addition to continuous and controlled injection using a syringe pump. For these experiments, we examined the injection rates of 22.5, 45, and 90 mL/hr during fabrication. As depicted in **Figure 2.8A**, a faster and steadier injection indeed led to a decrease in NP size. While the average size of NPs was 439 nm for the 22.5 mL/hr injection rate, this value reduced to 266 nm for the 45 mL/hr injection rate and 339 nm for the 90 mL/hr injection rate. Although the differences in NP size among these flow rates were not statistically significant, the trend in this data suggested that increasing the flow rate results in smaller NP size. We thus, used the injection rate of 90 mL/hr for the next steps.

This increase in the injection rate of the organic phase also resulted in a significant reduction in the surface potential of the resultant particles (**Figure 2.9A).** All tested, NP formulations, however, retained a negative surface potential, ranging from -48 to -1.2 mV, suggesting that these NPs would be colloidally stable in solution.

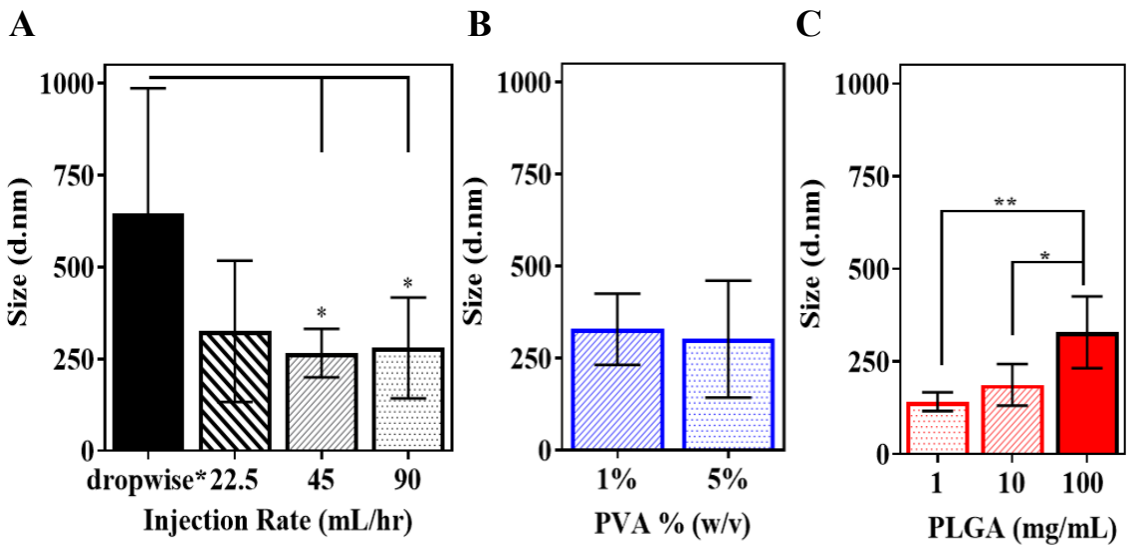

Figure 2.8. Optimization of size distribution of Dp44mT-loaded NPs, prepared by single emulsion, by modulating (A) injection rate, (B) PVA %, and (C) PLGA concentration.

Next, we examined the effect of aqueous phase surfactant concentration on particle size. As previously reported, in the single emulsion technique high concentrations of PVA can impede the complete separation of nascent droplets and result in a larger number of aggregated particles during solidification [65]. Thus, while maintaining the 100 mg/mL PLGA concentration and 90 mL/hr injection rate, we reduced the amount of PVA in the aqueous phase from 5% to 1% w/v. We anticipated that lowering the PVA amount would not only reduce the NP size but would also decrease the sample viscosity during the washing/processing steps, thereby resulting in smaller PDIs. The results, shown in **Figure 2.8B**, revealed that decreasing the amount of PVA resulted in a decrease in NP size by 32%, from 485 nm to 329 nm. Based on these results, we focused on the lower PVA percentage for the next steps of this study.

Interestingly, as presented in **Figure 2.9B,** while the surface potential of the produced NPs remained negative in these experiments, those fabricated with lower PVA

amount had a more negative surface potential (-21.8 mV) compared to those fabricated with higher amounts of PVA (-1.2 mV). This change in NP surface potential may be attributed to the reduced amount of the inherently positive PVA molecules on NPs [65]. As anticipated, reducing the PVA concentration also helped to make NP processing/washing easier and reduced the final NP solution's viscosity and opaqueness.

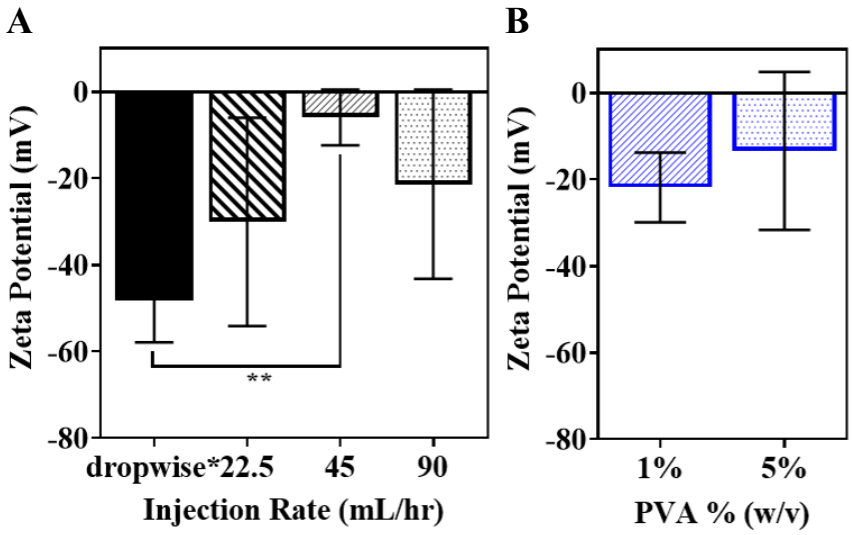

Figure 2.9. Surface potential of Dp44mT-loaded NPs prepared by single emulsion, as a result of modulating (A) injection rate of organic phase injection and (B) PVA % in the aqueous phase.

Lastly, we studied the effect of varying the concentration of PLGA on final size of NPs. For these experiments, we reduced the PLGA concentration in the organic phase from 100 mg/mL to 10 mg/mL or 1 mg/mL while maintaining the injection rate at 90 mL/hr and the PVA concentration at 1%. As illustrated in **Figure 2.8C**, decreasing the concentration of PLGA led to a decrease in the average NP size, from 329 nm to 187

nm and 136 nm, respectively. This finding is in agreement with prior reports that reducing the solvent-to-polymer ratio leads to a decrease in the size of particles [85, 89].

Together, these results demonstrated that Dp44mT-loaded particles can be produced by the single emulsion method and that through the adjustment of organic phase injection rate, surfactant amount, and PLGA concentration, the size of these NPs can be tuned to an average diameter of 136 nm with a negative surface potential, which makes them suitable for the future use in cancer therapy.

2.5.2. Encapsulation Efficiency and Loading Capacity

High drug encapsulation efficiency –the mass of drug entrapped within the particles relative to the total mass of drug added– is an important indicator of suitability of a nano-scale delivery system. We have previously demonstrated that PLGA NPs fabricated with the nanoprecipitation technique can incorporate Dp44mT with high encapsulation efficiencies (> 80%) compared to another commonly used liposomal nano-carrier (< 7%) [87]. Here, to further assess the potential of single emulsion technique for the fabrication of Dp44mT-loaded NPs, we examined the Dp44mT encapsulation efficiency in the produced NPs.

To this end, we employed the above-mentioned optimal fabrication parameters of 1% PVA in aqueous phase, 90 mL/hr injection rate of organic phase, and lower PLGA concentrations (1 and 10 mg/mL) in the organic phase to produce Dp44mT-loaded NPs. The amount of Dp44mT encapsulated in the particles was then determined by UV/vis spectrophotometry, as described in the methods section. As demonstrated in **Figure 2.10**, these results revealed a Dp44mT encapsulation efficiency of 78 ± 12% in NPs

fabricated with 10 mg/mL PLGA, and 74 ± 14% in NPs fabricated with 1 mg/mL PLGA. Others and we have previously reported that reducing the amount of polymer in the organic phase, which results in an increased drug-to-polymer ratio, lowers the cargo's encapsulation efficiency as there is physically less polymer available to entrap the free drug [87, 96]. Overall, this high encapsulation efficiency is a promising result and suggests that the single emulsion method is capable of producing PLGA NPs as an effective carrier for the hydrophobic drug Dp44mT.

Furthermore, we calculated the loading capacities –the mass of drug entrapped in NPs relative to the total mass of the entire particle formulation– of these optimal formulations as this parameter is of high importance for dosing in clinical applications. The loading capacity of NPs with 1 mg/mL PLGA was ~ 9.5% compared to the ~ 1.2% for those with 10 mg/mL PLGA. Therefore, while the lower drug-to-polymer (i.e., 10 mg/mL PLGA) formulation had a slightly higher encapsulation efficiency compared to the higher drug-to-polymer (i.e., 1 mg/mL PLGA) formulation, its loading capacity was much lower than the latter. We have previously observed a similar trend with the nanoprecipitation protocol. For therapeutic purposes, the loading capacity and encapsulation efficiency should therefore, be balanced to determine the best formulation [89].

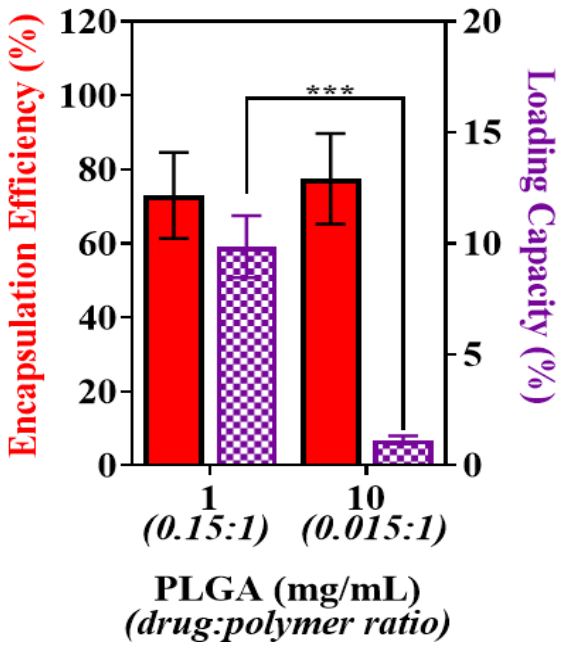

Figure 2.10. Drug carrying capacity of Dp44mT-loaded NPs prepared by single emulsion (formed using 1% PVA and 90 mL/hr injection rate), as a result of varying Dp44mT:PLGA ratio.

2.6. Comparison of Nanoprecipitation and Single Emulsion for Dp44mT-loaded Nanoparticle Fabrication

Using nanoprecipitation, we optimized the encapsulation of Dp44mT in PLGA nanoparticles by varying the polymer type, surfactant concentration, and drug-to-polymer ratio. Depending on the formulation, the highest encapsulation efficiency was found to be ~ 89%, which corresponded to a loading capacity of ~ 10% [89]. However, these NPs were fabricated from 75:25 PLGA which was found to have a slower drug release profile as compared to 50:50 PLGA. Therefore, our optimal 50:50 PLGA nano-formulation (labeled $^{+}$Dp44mT-NP in **Table 2.1**) had a moderate encapsulation efficiency of ~ 57% balanced with a loading capacity of 7.8%. We then evaluated the shape, size, and surface poatential of the NPs, all of which were found to be relatively

similar to those reported for our optimal nano-formulation: spherical, with an average size of 92 nm, and a surface potential of -14 mV [89]. The NPs were also found to be colloidally stable in water for one week at 37ºC.

Comparatively, using injection rate, polymer concentration, and surfactant concentration, we optimized PLGA NP size produced by single emulsion. Using identical fabrication parameters as the optimal $^{+}$Dp44mT-NP formulation identified for nanoprecipitation, we produced Dp44mT-NPs with an average size of 136 nm and negative surface potential of ~ -20 mV indicating colloidal stability in water at 37ºC. Based on the similarity in size to our nanoprecipitated NPs, we then evaluated the encapsulation and loading capacity of these Dp44mT-NPs, which was 77% (encapsulation efficiency) and ~ 10% (loading capacity) for the 0.15:1 drug-to-polymer ratio formulation, mirroring the Dp44mT-NPs made via nanoprecipitation. This increased drug encapsulation and loading can be attributed to the slightly larger NPs produced through this technique.

Together, these results demonstrate that, when using identical parameters of 1 mg/mL 50:50 PLGA and 0.15 mg Dp44mT in the organic phase injected into an aqueous phase containing 1% PVA, both techniques employed here are capable of producing our optimal negatively charged, spherical, Dp44mT-loaded nano-formulation of approximately 50 - 200 nm in size, with a moderate encapsulation efficiency, balanced with high loading capacity. While these two methods are comparable, it should be noted that nanoprecipitation does not require any specialized equipment, while single emulsion must be performed under vacuum, using special glassware, to remove the non-miscible organic

solvent. This specialized equipment also makes single emulsion slightly more difficult to scale up for production of larger batches of NPs. For our purposes, these two limiting factors made nanoprecipitation the more attractive method for the production of our Dp44mT-NPs.

2.7. Conclusions

This study presents the preparation and initial characterization of PLGA NPs encapsulating Dp44mT, a metal chelator with outstanding anti-tumor activity, as a new strategy for the application of this chelator for cancer treatment. We tested two different fabrication techniques, nanoprecipitation and single emulsion, and optimized the parameters of each technique to determine which technique would be optimal for Dp44mT-NP fabrication.

Using these two common techniques, we investigated the effect of polymer type and concentration, surfactant concentration, drug-to-polymer ratio, and injection rate on NP fabrication. We characterized the resultant Dp44mT-NPs for shape, size, surface potential, colloidal stability, encapsulation efficiency, loading capacity, and drug release. Together, our results demonstrate that Dp44mT-NPs can be produced by either the nanoprecipitation or single emulsion technique. The resultant PLGA NPs provide a suitable carrier for the encapsulation of Dp44mT for the future application against cancer cells. In addition, the present nano-formulation may be further optimized for targeting tumor cells through attachment of ligands.

CHAPTER III
ASSESSMENT OF DP44MT-LOADED NANOPARTICLE THERAPEUTIC EFFECTIVENSS *IN VITRO*

3.1. Abstract

In this chapter, we test the efficacy of our new anti-cancer formulation, loaded with iron chelator Dp44mT, against malignant cells *in vitro*. The outstanding anti-tumor activity of this chelator has previously been assessed in its free form in > 30 other cancer cell lines. Here, for the first time, we assessed the cytotoxicity of free Dp44mT in malignant glioma cells, specifically U251 and U87, in comparison to healthy astrocytes. Using nanoprecipitation, we then fabricated Dp44mT-loaded NPs (called Dp44mT-NPs) and assessed the efficacy of this nano-formulation against glioma (U251, U87), breast (MCF7), and colorectal (HT29) cancer cells *in vitro*. Further, we evaluated the impact of enhanced incubation time on NP cyotoxicity, as compared to prolonged exposure to free Dp44mT. Finally, we measured the uptake rate and localization of our particles, labeled with fluorescent dye coumarin-6 (C6), to evaluate the performance of PLGA NPs as an efficient delivery vehicle for Dp44mT. Overall, this chapter demonstrates the great potential of this novel Dp44mT-based nano-formulation for the use in cancer therapy.

3.2. Introduction

Fe chelator Dp44mT has shown remarkable anti-proliferative activity in over 30 cancer cell types [45, 51] since proliferative neoplastic cells, like cancer, are

known to have higher sensitivity to Fe deprivation compared to their normal counterparts [25]. However, to the best of our knowledge, its anti-cancer activity has never been assessed in glioma cells or their healthy astrocyte counterparts, which will be the focus of the first part of this study.

As we have now developed an appropriate PLGA nano-carrier for effective encapsulation and delivery of anti-tumor Dp44mT, the second part of this study will demonstrate the potential of this formulation to defeat neoplastic cells *in vitro.* To this end, we applied Dp44mT-NPs, fabricated via nanoprecipitation as optimized in **Chapter 2**, against malignant cells *in vitro*. First, the cytotoxicity of Dp44mT and Dp44mT-NPs was carefully evaluated in U87 and U251 glioma cells, as a cancer model, as well as normal astrocytes, as a healthy control. Next, we observed the cellular uptake of Dp44mT-NPs in both glioma cell lines and astrocytes to determine the mechanism and time frame for nanoparticle internalization. Lastly, to explore the versatility of this formulation as a general cancer chemotherapeutic platform, we further assessed the cytotoxicity of these NPs in other malignant cells, namely MCF7 breast cancer and HT29 colorectal cancer cells.

3.3. Experimental Methods

3.3.1. Materials

Glioma cell lines (U251, U87) were a gift from Dr. James Connor's Lab (Department of Neurosurgery, Penn State University). The breast cancer cell line (MCF7) and colorectal cancer cell line (HT29) were a gift from Dr. Chandra

Mohan's Lab (Department of Biomedical Engineering, University of Houston). MTT Cell Viability kit was from Biotium (Fremont, CA). Human Astrocytes, Astrocyte Growth Medium, Bovine Brain Microvascular Endothelial Cells (BBMVECs), and BBMVEC media, were from Cell Applications (San Diego, CA). Dulbecco's modified Eagle's medium (DMEM), Dulbecco's phosphate buffered saline (DPBS), fetal bovine serum (FBS), trypsin, and Antibiotic/Antimycotic solution were from Gibco® BRL (Carlsbad, CA). DiI (1,1-dioctadecyl 3'3, 3,3-tetramethylindo-carboxycyanate perchlorate) was from Invitrogen (Waltham, MA). Centrifuge filter tubes (10,000 and 50,000 MWCO) were from Millipore Sigma (Burlington, MA). NucBlue DAPI solution was from Molecular Probes (Eugene, OR). 50:50 poly(lactic-co-glycolic acid) (PLGA) (10,000 - 15,000 MW) was from PolySciTech (West Lafayette, IN). Di-2-pyridylketone-4,4-dimethyl-3-thiosemicarbazone (Dp44mT), acetone, ethanol, coumarin-6 (C6), polyvinyl alcohol (PVA) (31,000 - 50,000 MW), dimethyl sulfoxide (DMSO), ribonuclease A (RNase A), propidium iodide (PI), poly-L-lysine, and Fluoroshield mounting solution were from Sigma-Aldrich (St. Louis, MO).

3.3.2. Free Form of Dp44mT

Given the low water solubility of Dp44mT, we prepared a working stock of the free form of Dp44mT in DMSO at 1 mg/mL (≈ 3.5 mM). We then prepared our final desired experimental concentration by diluting our Dp44mT working stock in cell culture medium, DMEM.

3.3.3. Cell Culture

Cells were incubated in proper culture medium supplemented with nutrients and antibiotics at 37°C in a humid incubator with uniform supply of carbon dioxide (5%). Specifically, human glioma cell lines (U251 and U87), human colorectal cell lines (HT29) and human breast cancer cells (MCF7) were cultured in DMEM supplemented with 10% FBS and 2% 100X antibiotic/antimycotic solution. Human astrocytes were cultured in complete Astrocyte Growth Medium. Bovine brain microvascular endothelial cells (BBMVECs) were cultured in complete BBMVEC Growth Medium.

3.3.4. Cellular Viability Measurements and IC_{50}

Cells were seeded into 96-well plates at $1x10^4$ cells per well (glioma), $2x10^4$ cells per well (BBMVEC), $5x10^4$ cells per well (breast and colorectal cancers), or $1x10^5$ cells per well (astrocytes). Cells were allowed to grow until they were confluent (approximately 24 - 48 hrs). Cells were then treated with increasing concentrations of one of following: free Dp44mT, Dp44mT-NPs, or PLGA NPs. After 48 hrs, the treated media was gently removed for MTT development. Following the manufacturer's instruction, 10 μL of MTT reagent diluted in 100 μL of media was added to each well and incubated for 2 - 4 hrs at 37º C. Live cells enzymatically turn this reagent into Formazan crystals that, after incubation and removal of MTT-containing media, were dissolved in DMSO (200 μL per well). The resultant color change was then quantified by UV/vis

spectrophotometry at a 570 nm and 630nm (background) wavelengths. For analysis, the background 630nm signal was first subtracted from the true 570nm signal. The resultant absorbance values were normalized against the signal from the 0 nM control wells, providing the percentage of viable cells. Using these viability measurements, IC_{50} (i.e., drug concentration at which viability is 50%) was calculated for each cell line using **Equation (3.1)**:

$$Y = Vmin + \left(\frac{(Vmax - Vmin)}{1 + \left(\frac{x}{IC50}\right)^{-(n)}} \right). \quad \textbf{(3.1)}$$

In this equation, Y represents the measured percent cellular viability, V_{min} and V_{max} represent the lowest and the highest measured percent cellular viabilities, respectively, x represents the concentration of drug, and n represents the Hill slope (corresponding to the slope of the steepest point of the dose-dependent curve). This equation is further used to calculate best-fit IC_{50} curves for collected cytotoxicity data, represented as a solid line on the corresponding graphs. For all experiments, at least three replicates were used to calculate the average and standard error of the mean (SEM).

3.3.5. Assessment of Apoptotic Cell Population

To determine the percentage of the cells undergoing apoptosis, the cellular DNA was examined by flow cytometry using a sub-G1 assay. U251 glioma cells were first treated for 48 hrs with 100 nM of free Dp44mT or Dp44mT-NPs (calculated based on Dp44mT encapsulation efficiency). Cells were then washed

with 1X DPBS to remove residual media and drug, harvested, and fixed with 75% ice cold ethanol (EtOH). Finally, cells were stained with RNase A and PI for 30 min, to mark the DNA content of these cells. Flow cytometry (FC500, Beckman Coulter, Fullerton, CA) was then used to detect and analyze the apoptotic cellular populations containing fragmented DNA (called "sub-G1").

3.3.6. Cellular Uptake of Nanoparticles via Flow Cytometry

To determine the percentage of uptaken Dp44mT-NPs, U251 cells were treated with C6-loaded PLGA NPs (C6-NPs) prepared with a ratio of 0.01 mg C6:1 mg PLGA. Cells were seeded into 12-well culture plates at a density of $1.25x10^4$ - $2.5x10^4$ cells per well. After allowing the cells to reach confluency (for approximately 24 hrs), cultures were dosed with C6-NPs at a concentration of 10 μg C6/mL (calculated based on C6 encapsulation efficiency). NPs were allowed to incubate on the cells for 0 - 6 hrs, after which the NP-containing media was removed, and the cells were washed twice with 1X DPBS to remove any non-internalized or membrane-bound NPs. The cells were then trypsinized and collected for flow cytometry analysis using an ACEA NovoCyte machine and a NovoExpress software (Accela, Prague, Czech Republic). For analysis, we subtracted the cellular auto-fluorescence detected in 0 hr untreated control cells (as our 0% threshold) and normalized all data to our stain control cells spiked with C6-NPs right before the flow cytometry measurement (as our 100% threshold). The mean percentage of uptaken C6-NPs was plotted against time. Resulting data is represented by mean ± SEM, $n > 3$.

3.3.7. Cellular Uptake of Nanoparticles via Confocal Microscopy

For NP uptake assessment using confocal microscopy, glass coverslips were coated with poly-L-lysine overnight to aid in cell attachment. U251 glioma cells were then cultured on the coverslips ($8x10^4$ cells/mL) for 24 hrs or until at least 60% confluent. Once ready, cells were treated with C6-NPs at a concentration of 10 µg C6/mL (based on the measured C6 encapsulation efficiency), for 0 - 4 hrs in an incubator, mirroring the flow cytometry uptake experiments described above. After incubation, non-internalized NPs were washed with 1X DPBS and cells were fixed with a mixture of ice-cold fixation solution (80% methanol + 20% acetone) at -20°C for at least 30 min. The fixed cells were then stained with DiI (for 45 min) and DAPI (for 20 min) solutions at room temperature in the dark, with multiple washes with 1X DPBS between solutions to remove excess dye. Finally, any remaining solution was removed allowing the coverslips to dry out before adding mounting solution and sealing the glass coverslips onto glass slides. The coverslips were lastly sealed with nail polish and allowed to dry overnight (in the dark) before performing confocal imaging using a 63X oil immersion objective on an LSM 800 Inverted Confocal Microscope (Carl Zeiss Microscopy, Oberkochen, Germany).

For epifluorescence time-lapse imaging, the cells were not fixed but instead imaged live after initial exposure to C6-NPs. In brief, cells were cultured ($1.5x10^5$ cells/mL) for 24 hrs in glass-bottom petri dishes for optimal imaging at high resolution. Once ready, cells were imaged before the addition of C6-NPs and then

every 15 min over the course of 2 hrs after treatment with C6-NPs (10 μg C6/mL) 4 hrs in an incubator, mirroring the flow cytometry uptake experiments described above. Confocal images were collected every 30 min to remove background fluorescence. All images were collected using a 63X oil immersion objective on an LSM 800 Inverted Confocal Microscope (Carl Zeiss Microscopy, Oberkochen, Germany).

3.3.8. IC_{50} Calculations and Statistical Analysis

GraphPad Prism 8 was used to perform IC_{50} calculations and student's t-test to compare experimental groups and to evaluate statistical significance. For all collected data, statistical significance is represented by $*p < 0.05$, $**p < 0.01$, and $***p < 0.001$.

3.4. Results and Discussion

3.4.1. Cytotoxicity of Dp44mT in Glioma Cells

In order to assess the effectiveness of Dp44mT-NPs in defeating malignant cells *in vitro*, we investigated the cytotoxicity of these NPs in two brain glioma cell lines, U87 and U251, as a cancer model. For these experiments, we focused on $^{+}$Dp44mT-NP formula from **Table 2.1** (with 50:50 PLGA and 0.15:1 drug to PLGA ratio) as this formulation provided relatively high loading capacity and encapsulation efficiency as well as slightly faster release compared to the 75:25 PLGA NPs. U251 and U87 cells were treated with increasing amounts of Dp44mT-NPs for 48 hrs and then tested for viability using a MTT assay. Blank

PLGA NPs were tested as control NPs. Since the toxicity of Dp44mT has not been tested in glioma cells before, here we performed these experiments for free Dp44mT as well. As demonstrated in **Figure 3.1A-B**, exposure to increasing amounts of Dp44mT-NPs led to a significant drop in viability of U87 and U251 cells at very low concentrations of < 150 nM, indicating a high-level of cytotoxicity of this formulation against these malignant cells. Indeed, IC_{50} values for these Dp44mT-NPs was ~ 85 nM in U251 and ~ 100 nM in U87 cells (**Table 3.1**), while the blank PLGA NPs did not show a significant effect on the viability of these cells. Notably, free Dp44mT showed an even higher level of cytotoxicity in both examined cells lines, with IC_{50} values of ~ 10 nM for U251 and ~ 5 nM for U87 cells. This difference in IC_{50} values between the free and encapsulated Dp44mT may be attributed to the difference in the mechanism of uptake of Dp44mT in these two forms; while Dp44mT is a lipophilic molecule and thus, may readily cross the lipid bilayer, PLGA NPs are most likely uptaken by receptor-mediated endocytosis [97, 98]. The IC_{50} values for free Dp44mT obtained from these experiments are within the previously reported range of 5 - 400 nM for the free Dp44mT in other types of malignant cells [45]. More importantly, the IC_{50} values of Dp44mT, both in free and encapsulated form, were significantly lower than that of other common anti-cancer drugs, such as Doxorubicin (DOX) and Temozolomide (TMZ) used for eliminating U251 cells ($IC_{50,\,DOX} \approx 5.7$ μM, $IC_{50,\,TMZ} \approx 33.0$ μM) and U87 cells ($IC_{50,\,DOX} \approx 2.2$ μM, $IC_{50,\,TMZ} \approx 23.0$ μM) [76, 99], demonstrating the Dp44mT's excellent anti-tumor activity in these two cancer cell lines.

In cancer therapy, success is often determined by not only the ability to kill malignant cells but also the ability to spare healthy cells. In order to test the safety of Dp44mT-NPs, we studied the toxicity effect of these NPs in human astrocytes as the control healthy cells, as these brain support cells are the ones that, when cancerous, lead to the formation of glioma tumors. Similar to the glioma cells, astrocytes were treated with PLGA NPs, free Dp44mT, or Dp44mT-NPs and evaluated for cell viability after 48 hrs via MTT assay. As **Figure 3.1C** illustrates, the viability of these healthy cells was not significantly affected by Dp44mT, in either free or encapsulated form, within the concentrations that were toxic towards their malignant counterparts (i.e., < 150 nM). It should be noted that more pronounced effects of Dp44mT-NPs on viability of astrocytes (reducing the viability to ~ 60%) was observed only at much higher concentrations (> 2 μM) of Dp44mT, indicating an inherent selectivity of this formulation against malignant cells. These results do not only demonstrate that Dp44mT has an excellent anti-tumor activity in glioma cells –for the first time– but they also highlight the inherent selectivity of this compound towards these neoplastic cells. More importantly, findings of these experiments show that encapsulation of Dp44mT in PLGA NPs did not alter the anti-tumor activity of this chelator in malignant cells.

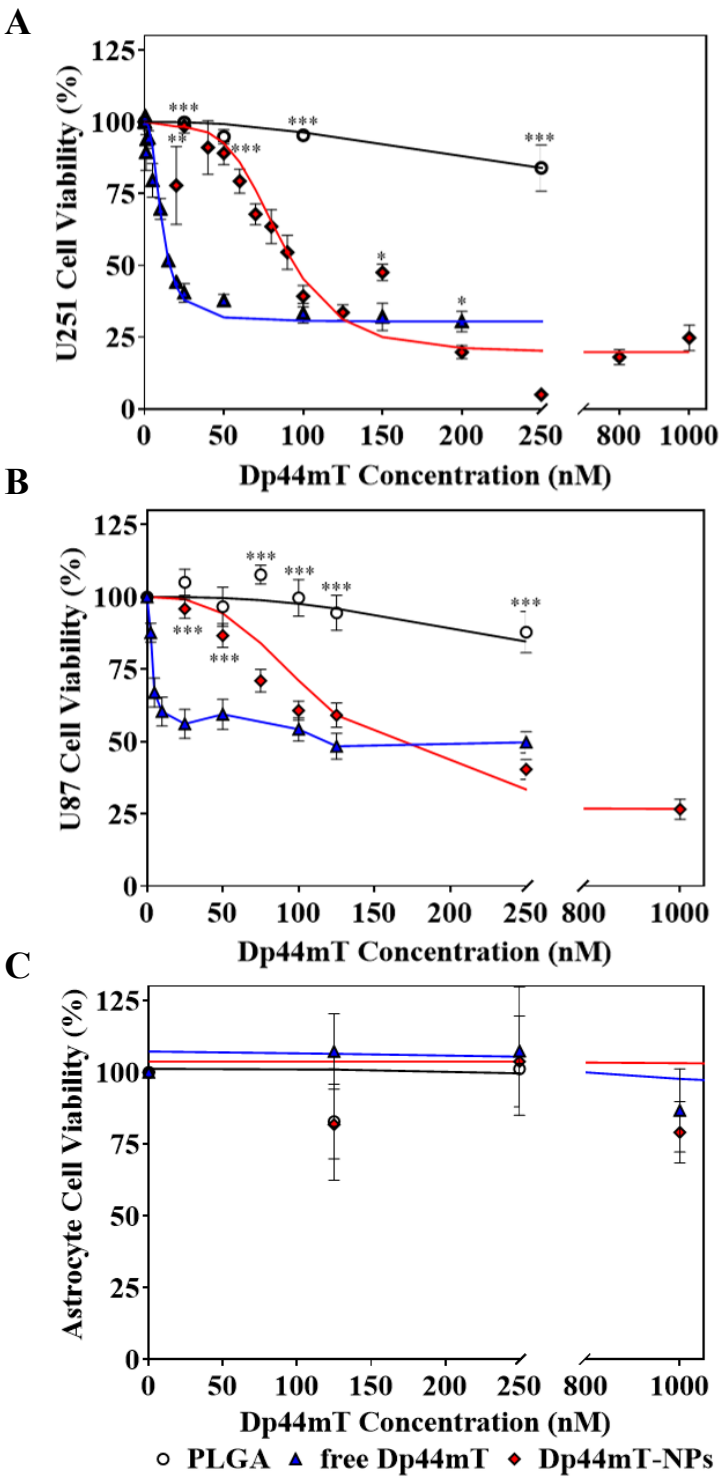

Figure 3.1. Dose-dependent cytotoxicity of free Dp44mT and Dp44mT-NPs in (A) U251 and (B) U87 glioma cells, as well as (C) astrocytes after 48 hrs treatment.

Table 3.1. *IC_{50}* values of Dp44mT and Dp44mT-NPs in glioma and astrocyte cell lines.

	Free Dp44mT	**Dp44mT-NP**
U87	~ 5 nM	~ 93 nM
U251	~ 10 nM	~ 85 nM
Astrocytes	> 32 μM	> 32μM

Prior studies on anti-tumor activity of Dp44mT in malignant cells have shown that this compound induces apoptosis in a number of cancerous cells including neuroepithelioma, lung carcinoma, breast cancer, and leukemic cells [45, 51]. To determine if Dp44mT has a similar effect on glioma cells, we measured the population of U251 glioma cells undergoing apoptosis after 48 hr exposure to free Dp44mT or Dp44mT-NPs, at 100 nM Dp44mT concentration, using a sub-G1 assay. Shown in **Figure 3.2**, flow cytometry analysis of these cells, stained with PI to track apoptotic cells with fragmented DNA, revealed that Dp44mT treatment led to a marked increase in the apoptotic cell populations in U251 cells from ~ 5% in the control (i.e., untreated) group to ~ 22% for free Dp44mT and ~ 26% for Dp44mT-NPs. Similar experiments in U87 cells showed a comparable trend. These data suggest that Dp44mT does induce apoptosis in these glioma cells in agreement with those reported in non-glioma cancer cell types [45, 51]. These results do not only demonstrate that Dp44mT has an excellent anti-tumor activity in glioma cells –for the first time– but they also highlight the inherent selectivity of this compound towards these neoplastic cells. More importantly,

findings of these experiments show that encapsulation of Dp44mT in PLGA NPs did not alter the anti-tumor activity of this chelator in malignant cells.

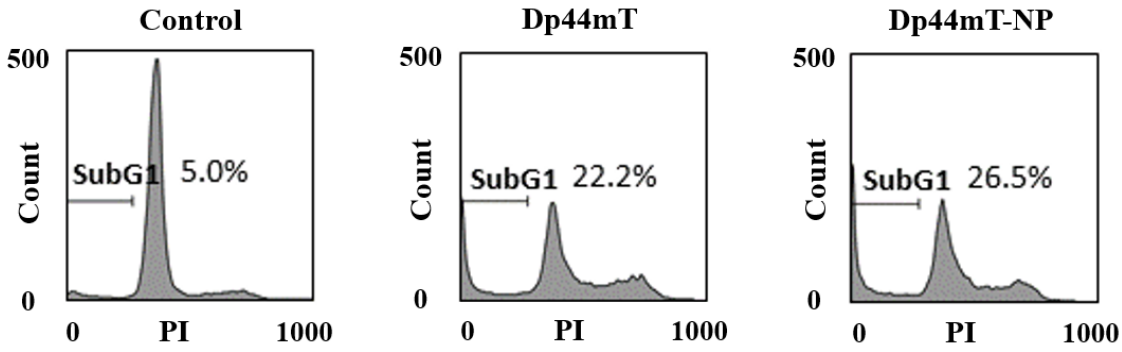

Figure 3.2. Sub-G1 apoptotic population, measured by flow cytometry, in U251 cells after 48 hrs exposure to 100 nM free Dp44mT or Dp44mT-NPs compared to untreated control cells.

To test our theory that the IC_{50} variation between the Dp44mT and Dp44mT-NP treatments is the result of a difference in time-dependent uptake mechanism, we next varied the incubation time of either free Dp44mT or Dp44mT-NPs on U251 glioma cells over the span of 24 and 72 hrs, as compared to the 48 hr incubation results reported in **Figure 3.1A**. From **Figure 3.3A**, we can see that U251 glioma toxicity was reduced in a dose-dependent manner when the cells were exposed to either the free Dp44mT or the Dp44mT-NPs. While the free Dp44mT quickly reduced viability, treatment with Dp44mT-NPs was much slower but eventually surpassed that of free Dp44mT at 200 nM dosage, although the difference was not significant. Interestingly, this trend was similarly observed for 48 hr incubation **(Figure 3.3B)** and 72 hr incubation (**Figure 3.3C**); however,

as incubation time increased, the highest dose of Dp44mT-NPs did significantly reduce glioma viability compared to the equivalent amount of free Dp44mT.

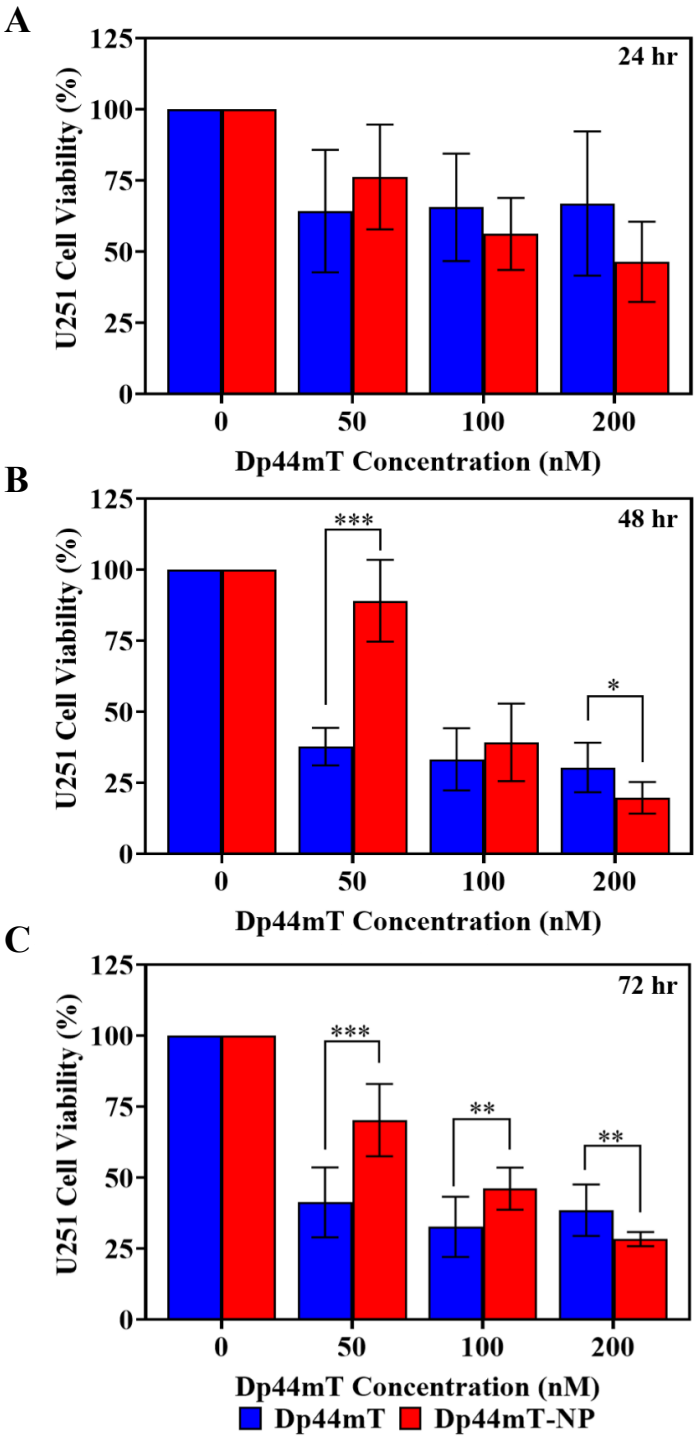

Figure 3.3. Dose-dependent cytotoxicity of U251 glioma cells treated with free Dp44mT or Dp44mT-NPs for (A) 24 hrs, (B) 48 hrs, or (C) 72 hrs.

As depicted in **Figure 3.4** and summarized in **Table 3.2**, increasing incubation time led to a decrease in the IC_{50} values of Dp44mT-NPs and an increase in those of free Dp44mT, indicating that longer incubation times enhanced the overall effectiveness of Dp44mT-NPs but had an opposite effect in free Dp44mT. These results show that there is a time delay factor that must be taken into account when applying nanoparticulate treatments, as these NPs are uptaken into cells by a slower, time-dependent mechanism. Together, these data demonstrated that Dp44mT-NPs were highly toxic towards aggressive glioma cells and their effect on cell viability became more pronounced with longer exposure times.

Table 3.2. IC_{50} of Dp44mT and Dp44mT-NPs due to varied incubation time in U251 glioma cells.

	Free Dp44mT	**Dp44mT-NP**
24 hr	< 1 nM	~ 100 nM
48 hr	~ 10 nM	~ 85 nM
72 hr	~ 20 nM	~ 63 nM

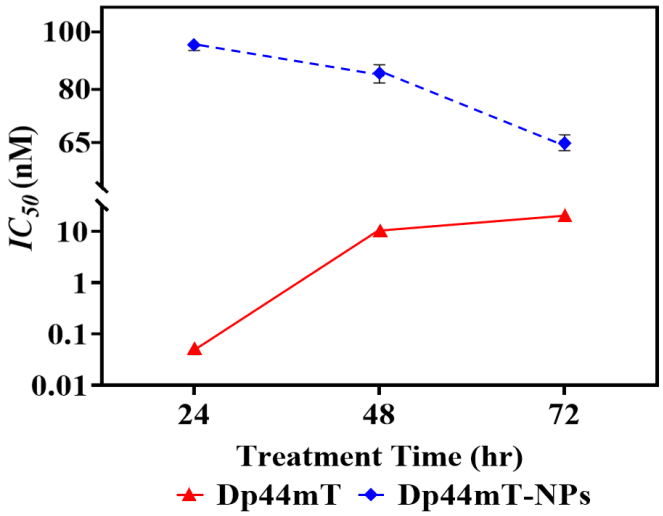

Figure 3.4. Comparison of Dp44mT vs. Dp44mT IC_{50} over time, calculated from dose-dependent viability after treatment with free Dp44mT or Dp44mT-NPs in U251 glioma cells.

3.4.2. Cellular Uptake of C6-loaded Nanoparticles by Glioma Cells

To further evaluate the performance of PLGA NPs as an efficient delivery vehicle for Dp44mT, we studied the U251 glioma uptake of C6-loaded PLGA NPs (C6-NPs), as C6 is a naturally fluorescent compound that is often employed as a model hydrophobic drug to monitor *in vitro* or *in vivo* distribution of nano-carriers [92]. To check the reliability of this labeling approach for tracking NPs, we first tested the release of C6 from NPs co-loaded with Dp44mT and C6 (i.e., Dp44mT/C6-NPs) and demonstrated that only a small fraction (< 5%) of the encapsulated C6 was released during the first few hours [100]. After confirming that C6 could serve as an effective marker for these NPs, we dosed U251 cells with C6-NPs for increasing amounts of time and tracked the amount of NP uptake using flow cytometry. As depicted in **Figure 3.5**, ~ 11% of the C6-NPs were uptaken within 1 hr and their uptake reached a maximum of ~ 14% after about 2

hrs. For U87 glioma cells and astrocytes, a similar but higher trend of uptake was observed, with ~ 33% of the C6-NPs were uptaken within 1 hr and a maximum uptake of ~ 45% after about 2 hrs.

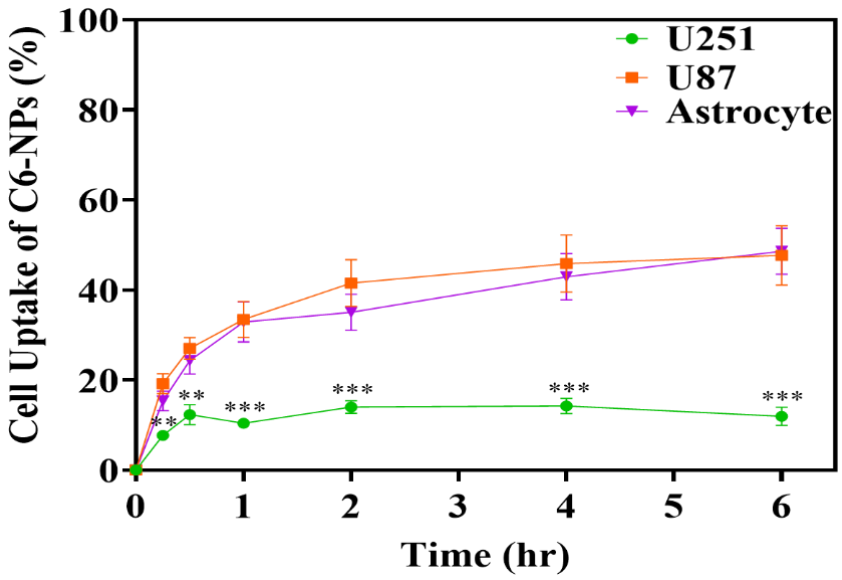

Figure 3.5. Percentage of C6-NPs uptaken by glioma cells and astrocytes as a function of time, measured by flow cytometry.

This uptake trend was further visualized through fluorescence confocal microscopy (**Figure 3.6A**) in which U251 glioma cells were stained to identify cellular membrane (DiI - red), nucleus (DAPI - blue), and NPs (C6 - green). Along with epifluorescence time lapse microscopy (**Figure 3.6B**), our results indicate that these C6-NPs are rapidly uptaken into the cellular cytoplasm, with uptake saturation occurring after several hours. Again, similar fluorescence microscopy results were observed for the U87 glioma cells and astrocytes [100]. We initially attributed increased NP uptake by U87 glioma, as compared to U251 glioma, to the slightly faster replication rate of these cells. However, as astrocytes

were also observed to have increase NP uptake but are known to have a much slower (42 hr) replication rate, this cannot be the case. Rather increased uptake is probably the result of a difference in the endocytosis receptors being expressed on the surface of each of these cell lines. This uptake trend is indeed similar to other reports from hydrophobic drug-loaded PLGA NPs in literature [99, 101]. The relatively rapid uptake of Dp44mT-NPs further demonstrates the therapeutic potential of this nano-formulation for cancer therapy. Of course, future improvements upon this formulation, particularly decorating these PLGA NPs with targeting ligands, are expected to further enhance the cellular uptake of Dp44mT-NPs.

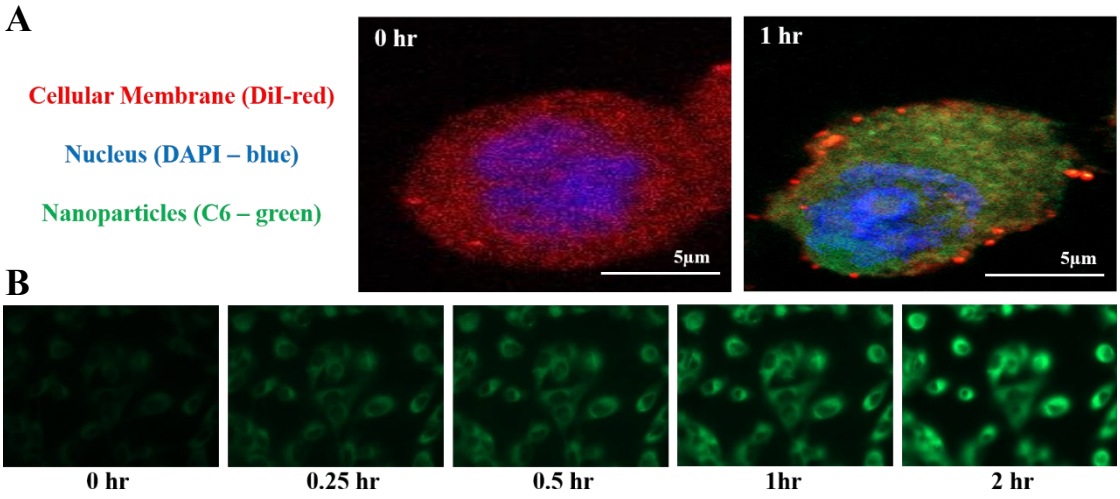

Figure 3.6. Representative localization, via (A) confocal and (B) epi-fluorescence microscopy, of C6-NPs uptaken by U251 glioma cells over time.

3.4.3. Cytotoxicity of Dp44mT-loaded Nanoparticles in Other Cancer Cells

Based on the effectiveness of this Dp44mT-NP formulation against glioma cells, we began to explore the possible use of this platform as a ubiquitous cancer chemotherapeutic. As Dp44mT chelates a compound that is universally required for cellular growth and the PLGA NP core contains no cell-specific moieties, we concluded that this platform should also be generally effective against other types of cancer. Thus, we employed our Dp44mT-NPs *in vitro* against two other cancers, namely MCF7 breast cancer and HT29 colorectal cancer cells. These cell lines were selected as: (1) biologically both of these cancer lines are metastatic and have an epithelial origin like glioma; (2) both of these cancers have relatively high mortality rates with only moderate long-term survival rates, as summarized in **Figure 1.1**; and lastly (3) previous research using free Dp44mT has already been shown to be effective against these cell lines, allowing for better comparison to our platform [45, 51, 102, 103]. Together, these characteristics make MCF7 and HT29 good targets to test our formulation.

Mirroring the U87 and U251 glioma experiments in **Figure 3.1**, here we again focused on the $^{+}$Dp44mT-NP formula from **Table 2.1** (with 50:50 PLGA and 0.15:1 drug to PLGA ratio). MCF7 breast cancer and HT29 colorectal cancer cells were treated with increasing amounts of Dp44mT-NPs for 48 hrs and then tested for viability using an MTT assay. Blank PLGA NPs were tested as a vehicle control and free Dp44mT was tested for comparative toxicity purposes. As demonstrated in **Figure 3.7A-B**, exposure to increasing amounts of Dp44mT-NPs did result in decreased viability, to 80% for MCF7 and 57% for HT29 cells. Both

lines required high concentrations (> 10 μM) of Dp44mT-NPs in order to trigger significant decreases in cell viability. As summarized in **Table 3.3**, the resultant IC_{50} for treatment with Dp44mT-NPs was found to be ~ 11.5 μM in MCF7 cells and ~ 14.5 μM in HT29 cells after 48 hrs treatment. In comparison, free Dp44mT in these cell lines resulted in IC_{50} values of ~ 800 nM for MCF7 and ~ 5.4 μM for HT29 cells. Therefore, while this platform was found to be extremely effective in glioma, it had only moderate effectiveness towards these other two cancer lines. However, it should be noted that the observed cellular toxicity towards our platform was still comparable to dosages reported for other chemotherapeutics.

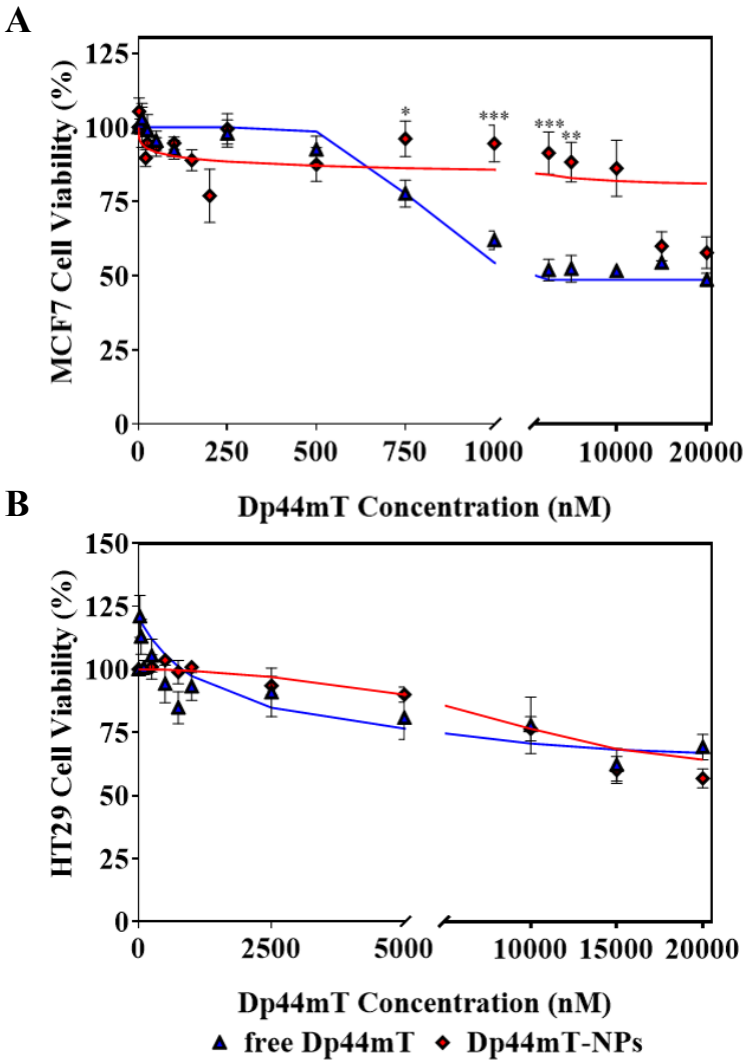

Figure 3.7. Dose-dependent cytotoxicity of free Dp44mT and Dp44mT-NPs in (A) MCF7 breast and (B) HT29 colorectal cancers after 48 hrs treatment with free Dp44mT or Dp44mT-NPs.

We theorized that sensitivity to Dp44mT-NPs and free Dp44mT, compared to glioma cells, may be attributed to distinct characteristics of these cell lines; MCF7 and HT29 cells have slower replication rate (~ 40 hrs) than glioma cells (~ 22 - 24 hrs), and unlike glioma cells, they need adequate cell-cell contact to sustain growth. In fact, other studies have reported lower IC_{50} values of 4 - 60 nM for

free Dp44mT in MCF7 cells after 72 hrs of treatment [45, 51, 102], suggesting that longer Dp44mT incubation times could enhance its toxicity in these cells, similar to our results in glioma cells (**Figure 3.3).** Therefore, we repeated the longer 72 hr incubation on these cell lines. From **Figure 3.8A-B**, we can see that prolonged exposure to our Dp44mT-NP formulation did result in a significant decrease in cell viability, to ~ 25%. The resultant IC_{50} values (**Table 3.3**) were also greatly reduced, compared to the 48 hr incubation, to ~ 1.6 μM for MCF7 cells and ~ 1.4 μM for HT29 cells. These values are now similar to what was reported in literature, suggesting that the dosage time frame as well as the concentration must be optimized to gain the best therapeutic outcomes. Overall, the relatively high dosage requirement of these cells indicates that this specific formulation may not be as widely effective as first predicted, at least not without additional cancer-specific targeting.

Table 3.3. IC_{50} of Dp44mT and Dp44mT-NPs in HT29 colorectal and MCF7 breast cancer cells due to varied incubation time.

	MCF7		**HT29**	
	Free Dp44mT	**Dp44mT-NP**	**Free Dp44mT**	**Dp44mT-NP**
48 hr	~ 800 nM	~ 11.5 μM	~ 5.4 μM	~ 14.5 μM
72 hr	~ 25 nM	~ 1.6 μM	~ 60 nM	~ 1.4 μM

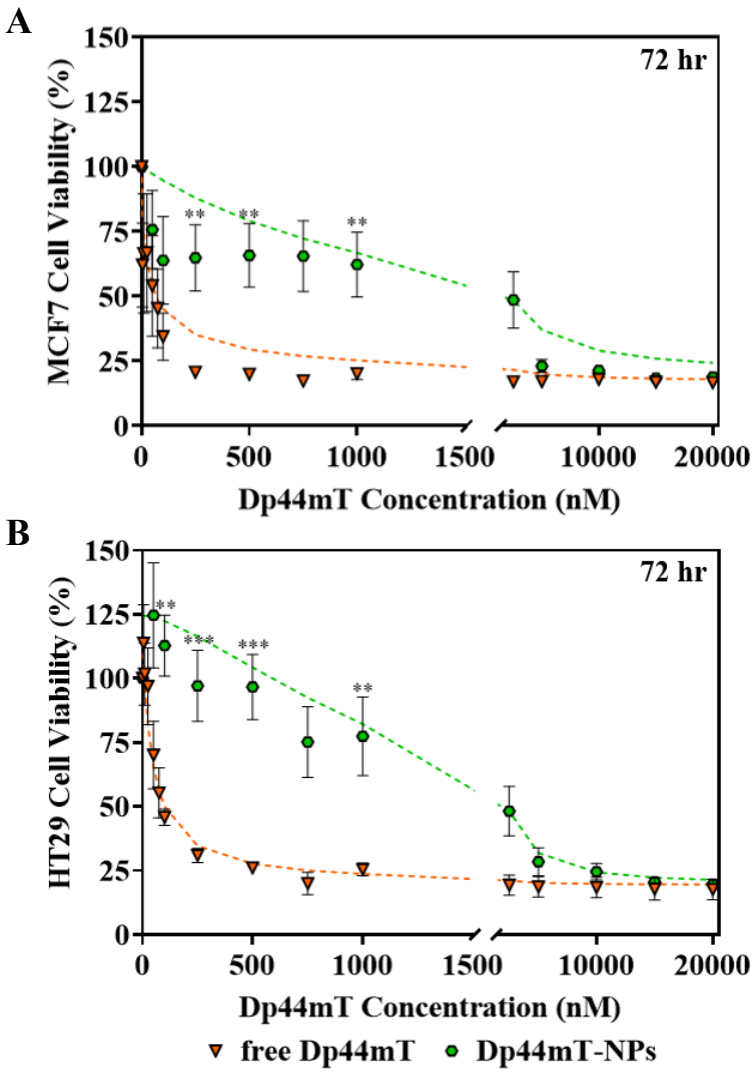

Figure 3.8. Reduced cytotoxicity of free Dp44mT and Dp44mT-NPs in (A) MCF7 breast and (B) HT29 colorectal cancers after 72 hrs treatment with free Dp44mT or Dp44mT-NPs.

3.5. Conclusion

This study presents the initial *in vitro* assessment of our novel anti-cancer nano-formulation. Specifically, it demonstrates, for the first time, the potent anti-tumor activity of Dp44mT in glioma cells. The cytotoxicity studies showed that Dp44mT was highly effective in killing U251 and U87 glioma cells at very low concentrations (IC_{50} < 20 nM). Dp44mT encapsulated in PLGA NPs were found

to be similarly toxic to glioma cells (IC_{50} < 150 nM), confirming that encapsulation of Dp44mT in PLGA NPs did not alter the anti-tumor activity of this chelator in glioma cells. Most importantly, our experiments revealed that, at concentrations toxic to malignant cells, Dp44mT d id not induce significant cell death in healthy astrocytes, suggesting an inherent selectivity towards neoplastic cells. We then expanded the application of our Dp44mT-NP platform to other cancers, specifically MCF7 breast cancer and HT29 colorectal cancer. Cytotoxicity levels in these cell lines (IC_{50} > 10 μM), while significantly higher than in glioma, were still on par with doses of other commonly used chemotherapeutics. Further, for all cancer cell lines, Dp44mT-NP cytotoxicity can be improved with extended exposure time, which is not the case for unencapsulated Dp44mT. Together, these findings demonstrate that Dp44mT has a high-level cytotoxicity against brain glioma cells and that PLGA NPs provide a suitable carrier for the delivery of this hydrophobic compound to malignant cells. The application of Dp44mT-NPs is not limited to brain glioma cells as these NPs may be applied to other types of tumors. In addition, the present nano-formulation may be further optimized for targeting tumor cells through attachment of targeting ligands.

CHAPTER IV

PEGYLATION AND TARGETING OF DP44MT-LOADED NANOPARTICLES FOR IMPROVED THERAPEUTIC EFFECTIVENESS *IN VITRO*

4.1. Abstract

This chapter describes the preparation and optimization of PEGylated Dp44mT-loaded PLGA nanoparticles towards tumor-targeted delivery of Dp44mT to cancer cells *in vivo.* Using nanoprecipitation, we fabricated Dp44mT-NPs, the surface of which was completely covered with a dense layer of PEG. The resultant particles (referred to as Dp44mT-PEG-NPs) were characterized for shape, size, surface potential, colloidal stability, encapsulation efficiency, and loading capacity. We then assessed the efficacy of these Dp44mT-PEG-NPs by applying them to malignant cells (brain, breast, and colorectal cancer) *in vitro*. In addition, we used an *in vitro* model of the Blood-Brain Barrier to track the ability of these PEG-NPs to be transported into the brain. Finally, we applied two distinct methods to conjugate a glioma-specific targeting peptide from Interleukin-13 (IL13), IL13p, to the surface of these Dp44mT-PEG-NPs and assessed the effectiveness of these targeted NPs against glioma cells. This chapter provides insight into the effect of PEGylation on the toxicity of the present Dp44mT-loaded NPs and demonstrates the great therapeutic potential of Dp44mT-PEG-NPs against different malignant cells, with particularly promising results for future targeted cancer-specific chemotherapies.

4.2. Introduction

Two major challenges to effective cancer treatment include poor chemotherapeutic half-life and distribution in the vasculature, as well as undesirable side effects of these toxic therapeutics to healthy tissues. In the previous study (**Chapter 3**), we have shown that our Dp44mT-NPs formulation is highly effective against several different cancer cell lines (U87 & U251 glioma, MCF7 breast, and HT29 colorectal cancer cells) *in vitro* with minimal toxicity in healthy cells [100]. In this chapter, as a step towards future *in vivo* application of our Dp44mT-NPs, we evaluate the effect of adding surface poly(ethylene glycol) (PEG) on NP efficacy towards the examined cancer cell lines. Attachment of hydrophilic PEG chains creates a steric, hydrophilic barrier between the polymer surface and the aqueous environment which carrier's colloidal stability [73, 74]. Enhanced stability leads to increased NP solubility, circulation time, and biodistribution [80, 104], which should enhance the delivery and effectiveness of these NPs. Additionally, the presence of a PEG layer acts as a "stealth layer" that prevents protein adsorption [61, 63, 74] thereby helping the nanoparticle escape detection and degradation by the immune system [63, 74, 75].

We aim to further improve the therapeutic potential of our NP formulation through the attachment of a targeting ligand. Using glioma as a malignant cell model, targeting would afford the selective delivery of our Dp44mT-loaded nano-formulation to glioma cells while sparing healthy cells. Previous research has utilized decoy receptor, Interleukin-13 Receptor alpha 2 (IL13Rα2), for glioma-targeted therapies, as this receptor is overexpressed on 80% of high-grade gliomas, including glioblastoma multiforme [105-109]. Therefore, a peptide from the IL13 protein (referred to as

"IL13p") was chosen as the glioma targeting ligand, since this protein binds to IL13Rα2 with high affinity (K_d = 2.5 ± 0.9 nM) [110] and has been found to increase NP uptake and penetration into glioma cells [111]. Additionally, IL13-targeted nanocarriers have been shown to successfully cross the Blood-Brain Barrier (BBB) [105, 111-113], which will be an essential component of future *in vivo* studies.

To this end, we modified our PLGA NP formulation to add a layer of PEG chains onto the surface of these NPs. Upon preparation of PEGylated NPs (Dp44mT-PEG-NPs) using nanoprecipitation, we characterized the resultant NPs for size, morphology, surface potential, colloidal stability, encapsulation efficiency, and loading capacity, to confirm relative similarity to our previously reported unPEGylated Dp44mT-NPs. After fabrication, we assessed the cytotoxicity of our Dp44mT-PEG-NPs in U251 and U87 glioma cells, as well as MCF7 breast cancer and HT29 colorectal cancer cells, to determine the impact of PEGylation on the cytotoxicity of these NPs. We then decorated these NPs with a glioma targeting ligand, IL13p. For best conjugation results and future dual targeting, we explored two common techniques (**Figure 4.10**): EDC/NHS which attaches the targeting ligand directly to the carboxyl group of PLGA [111, 114, 115], or maleimide-thiol click chemistry in which a small percentage of the PEG chains contained a maleimide end group that served as an anchor for attachment of IL13p [112, 113]. These targeted NPs (referred to as "IL13p-PEG-NPs") were then also tested against glioma cells *in vitro*, to determine if cancer-specific targeting results in enhanced cytotoxic effects, thereby augmenting the chemotherapeutic properties of this nano-carrier platform.

4.3. Experimental Materials and Methods

4.3.1. Materials

Glioma cell lines (U251, U87) were a gift from Dr. James Connor's Lab (Department of Neurosurgery, Penn State University). The breast cancer cell line (MCF7) and colorectal cancer cell line (HT29) were a gift from Dr. Chandra Mohan's Lab (Department of Biomedical Engineering, University of Houston). MTT Cell Viability kit was from Biotium (Fremont, CA). Human Astrocytes, Astrocyte Growth Medium, Bovine Brain Microvascular Endothelial Cells (BBMVECs), BBMVEC media, and Attachment Factor were from Cell Applications (San Diego, CA). Sephadex G15 was purchased from GE Healthcare (Chicago, IL). Dulbecco's modified Eagle's medium (DMEM), Dulbecco's phosphate buffered saline (DPBS), fetal bovine serum (FBS), trypsin, and Antibiotic/Antimycotic solution were from Gibco® BRL (Carlsbad, CA). Centrifuge filter tubes (10,000 MWCO) were from Millipore Sigma (Burlington, MA). Polypropylene columns were purchased from Pierce Thermo Fisher (Waltham, MA). 50:50 methoxy poly(ethylene glycol)-b-poly(lactic-co-glycolic acid) (mPEG-PLGA; 2,000-15,000 MW), and 50:50 maleimide poly(ethylene glycol)-b-poly(lactic-co-glycolic acid) (mal-PEG-PLGA; 5,000-20,000 MW) were from PolySciTech (West Lafayette, IN). Di-2-pyridylketone-4,4-dimethyl-3-thiosemicarbazone (Dp44mT), acetone, ethanol, coumarin-6 (C6), (31,000-50,000 MW), dimethyl sulfoxide (DMSO), EDC (N-(3-Dimethylaminopropyl)-N′-ethylcarbodiimide hydrochloride, MES (2-(N-Morpholino)ethanesulfonic acid), NHS (N-Hydroxysuccinimide), EDTA (ethylenediaminetetraacetic acid),

hydroxylamine hydrochloride, 2-IH (2-iminothiolane hydrochloride, Traut's Reagent), and hydrocortisone were from Sigma-Aldrich (St. Louis, MO). IL13 peptide (NH_2-VDKLL LHLKK LFREG QFNRN FESII ICRDR TC-COOH) was made by Shanghai Royobiotech (Shanghai, China). DTNB (5,5'-Dithiobis(2-nitrobenzoic acid), Ellman's Reagent), L-Cysteine hydrochloride monohydrate, sulphuric acid, 12-well trans-well plate (12 mm insert, 0.4 μm polyester membrane) were purchased from VWR (Radnor, PA).

4.3.2. Fabrication of Dp44mT-loaded PEGylated Nanoparticles via Nanoprecipitation

Using the nanoprecipitation method previously described *(see Section 2.3.2. Fabrication of Dp44mT-loaded Nanoparticles via Nanoprecipitation)*, we modified the formulation of the organic phase so that the resultant nanoparticles would contain an inner core of PLGA shielded by an outer layer of PEG chains. This formulation also included 10% maleimide-PEG which will be used for maleimide click chemistry to allow for the attachment of our desired targeting molecules. For the fabrication of 0.15 mg/mL Dp44mT-PEG-NPs, 4.5 mg of mPEG-PLGA, 0.5 mg of malPEG-PLGA, and 0.75 mg of Dp44mT were co-dissolved in 1 mL of acetone. An increased amount of Dp44mT is used in this formulation to maintain the 0.15 mg drug: 1 mg polymer ratio that has been previously optimized (see **Chapter 2**). This organic phase solution was injected into 3 mL of deionized (D.I.) water at a flow rate of 60 mL/hr under magnetic stirring. The solution was gently stirred for about 45 - 60 min at room temperature in a fume hood to evaporate the organic solvent. The resultant NPs were concentrated via

slightly reduced centrifugation (3,000 rpm for 30 min) to prevent excessive compacting on the filter. The nanoparticles were then washed two-to-three times by addition of 1 mL of D.I. water followed by centrifugal filtration to remove unloaded drug. Lastly the NPs were resuspended to a final concentration of 5 mg/mL PLGA and 0.75 mg/mL of Dp44mT (referred to as 0.15 mg/mL Dp44mT-PEG-NPs) in water. These NPs were stored in 4°C until usage.

4.3.3. Peptide Conjugation via Maleimide-Thiol Click Chemistry

Using a modified version of the protocol originally provided by Madhankumar *et al*. [112, 113], we first attempted to conjugate IL13p to PEGylated NPs via maleimide-thiol click chemistry. For appropriate amide conversion, the IL13p, calculated at a 1:1 or 1:2 molar ratio as compared to the 0.5 mg mal-PEG-PLGA, was combined at 1:40 ratio with 2-IH dissolved in 4 mM EDTA-1XPBS, pH 8. This solution was degassed using nitrogen (N_2) gas to prevent oxygen reaction and then stirred for 2 hr in the dark at room temperature. The converted peptide was then separated from the basic 2-IH solution using a gel permeation/size exclusion chromatography (GPC) column containing sephadex-G15 and a running buffer of 4 mM EDTA-1X PBS, pH 6.5. Fifteen fractions (1 mL each) were collected from the column and tested for the presence of IL13p using Ellman's Reagent (*see 4.3.5. Quantification of Peptide Conjugation).* The fractions containing the most IL13p were then combined with the PEG-NPs and then gently mixed at room temperature in the dark for 2 - 4 hrs. After conjugation, the resultant IL13p-PEG-NPs were washed 3X with 1 mL water and centrifuged in 10,000 MWCO tubes (3,000 rpm, 30 min) to remove any unbound peptide. The NPs and the

wash wastes were again analyzed via Ellman's reagent, to confirm IL13p conjugation to the PEG-NPs.

4.3.4. Peptide Bioconjugation via EDC/NHS

Using a modified protocol provided by ThermoFisher Scientific [111, 114, 115], we also attempted to conjugate IL13p to PEGylated NPs via the EDC/NHS technique. For conjugation using this method, the PEGylated nanoparticle formulation was slightly adjusted to remove the 0.5 mg mal-PEG-PLGA, which was replaced with 0.5 mg of 50:50 PLGA (must contain a carboxyl group at the end of the polymer chain for reaction to work). The PEG-NPs were combined with a final concentration of 400 mM EDC and 100 mM NHS, both of which were separately dissolved in MES buffer, pH 6.0. The solution was gently stirred for 30 min to allow for carboxyl conversion. After modification, the nanoparticles were centrifuged (3,000 rpm, 30 min, 10,000 MWCO tube) and washed with 3 mL 1X DPBS, pH 7.4 to completely remove EDC and NHS while also adjusting the pH of the NP solution to biological levels for optimal conjugation. The nanoparticles were then resuspended with 1X DPBS, pH 7.4 before being combined with IL13p, calculated at a 1:1 or 1:2 molar ratio as compared to the 0.5 mg PLGA, for 4 hr in the dark at room temperature under gentle stirring. After conjugation, the reaction was quenched with a final volume of 10 mM hydroxylamine HCl. The resultant IL13p-PEG-NPs were then washed three times with 1 mL of water (3,000 rpm, 30 min, 10,000 MWCO filter tube) to remove any unbound peptide. Resulting data is represented by mean ± SEM, $n > 1$.

4.3.5. Quantification of Peptide Conjugation

To assess the success of our peptide conjugation, we measured the amount of IL13p conjugated (i.e., bound) to the PEG-NP samples and the amount unbound in the centrifugal wash waste. For this, each sample was exposed to an equal volume of Ellman's Buffer, which is comprised of 100 uL DTNB suspended in 5 mL of sodium sulfate dibasic (Na_2HPO_4) buffer, and incubated at room temperature for 15 min. When in the presence of cysteines, of which there are two on the IL13p, the Ellman's Reagent will turn yellow. The amount of peptide was then measured by UV/vis spectrophotometry (SpectraMax M5 Molecular Devices, Molecular Devices, Sunnyvale, CA) and quantified against a standard curve of known cysteine monohydrate HCl concentrations.

4.3.6. Preparation of *In Vitro* Transwell Blood-Brain Barrier Co-Culture Model

To prepare our *in vitro* BBB co-culture model (**Figure 4.7**), the transwell insert was first inverted and coated with 250 uL of attachment factor and incubated at 37°C for 30 min. The attachment factor was then removed and astrocytes (2.24 $x10^5$ cells/insert) were seeded onto the underside of the membrane polyester in complete Astrocyte Growth Media (AGM). The inserts were placed in the 37°C cell incubator for 6 - 8 hrs to allow the astrocytes to attach to the membrane. After attachment, the insert was flipped right-side up and placed in the transwell plate. The bottom chamber was then filled with 1.5 mL of AGM for continued astrocyte growth for the next 24 hrs. On the following day, BBMVECs were cultured on the top-side of the membrane at 1.22 $x10^5$

cells/insert in 0.5 mL of complete BBMVEC media. The entire co-culture system was then incubated at 37°C for 3 days until all cells reached confluency. On the third day, the media in the top chamber was replaced with 0.5 mL of Astrocyte Conditioned Media (ACM)* containing 180 nM hydrocortisone, to promote tight junction formation. The media in the bottom chamber was replaced with 1.5 mL of fresh AGM. The cells were again allowed to grow at under these conditions at 37°C for an additional 9 days, with the media being exchanged every 3 days. *ACM was prepared using a published protocol [116], in which used AGM was collected from a confluent astrocyte culture, filtered 0.22 μm filter, and then mixed 50:50 with fresh BBMVEC media. After 12 days of incubation, the Trans-endothelial electric resistance (TEER) was measured, per instrument manufacturer instructions, to confirm tight junction integrity.

4.3.7. Nanoparticle Transport Across *In Vitro* Blood-Brain Barrier Model

Once the co-culture was ready, the desired concentration of PEG-NPs (0.1, 0.5, or 1 mg/mL) was diluted in media from the top chamber. The co-culture plate was then returned to the 37°C incubator for 8 hrs to allow NP transport. After 8 hrs, all media (0.5 mL from top chamber and 1.5 mL from the bottom chamber) was collected separately. Each sample was washed twice with DI water by ultracentrifugation (15,000 rpm for 70 min each) and then re-suspended in 1 mL of DI water. The NP concentration in each sample was measured using Malvern LM10 NanoSight (threshold=10) and analyzed using Nanosight NTA 3.2 software.

The NP transport percentage was calculated using **Equation 4.1**:

$$Nanoparticle\ Transport\ (\%) = \left(\frac{NPf}{NPi}\right) \times 100\%. \quad (\mathbf{4.1})$$

In this equation, NP_f represents the final number of PEG-NPs in the bottom chamber (measured at time = 8 hrs of incubation) and NP_i represents the initial number of PEG-NPs added to the top chamber (measured at time = 0 hrs). Resulting data is represented by mean ± SD, n > 3.

4.4. Results and Discussion

4.4.1. Characterization of Dp44mT-loaded PEGylated Nanoparticles

Attachment of PEG to the surface of NPs has been shown to increase their solubility, prolong their circulation, and improve their biodistribution by preventing protein adsorption and opsonization of these NPs [59, 80]. Therefore, as a step towards preparing Dp44mT-NPs for future *in vivo* studies, we modified our PLGA NP formulation by adding a layer of PEG polymer chains onto their surface. The nanoprecipitation method was again used to fabricate these PEG-NPs encapsulating Dp44mT (**Figure 4.1**). Briefly, mPEG-PLGA, mal-PEG-PLGA, and Dp44mT were co-dissolved in acetone and the resulting mixture was injected into an aqueous solution under magnetic stirring. Here, mal-PEG-PLGA was added to the recipe for the future attachment of targeting ligands, which will be discussed later. The acetone was then evaporated under gentle stirring and the particles were collected and washed with water by centrifugal filtration. All NP formulations were then characterized for morphology,

size, surface potential, colloidal stability, encapsulation efficiency, and loading capacity, as summarized in **Table 4.1**.

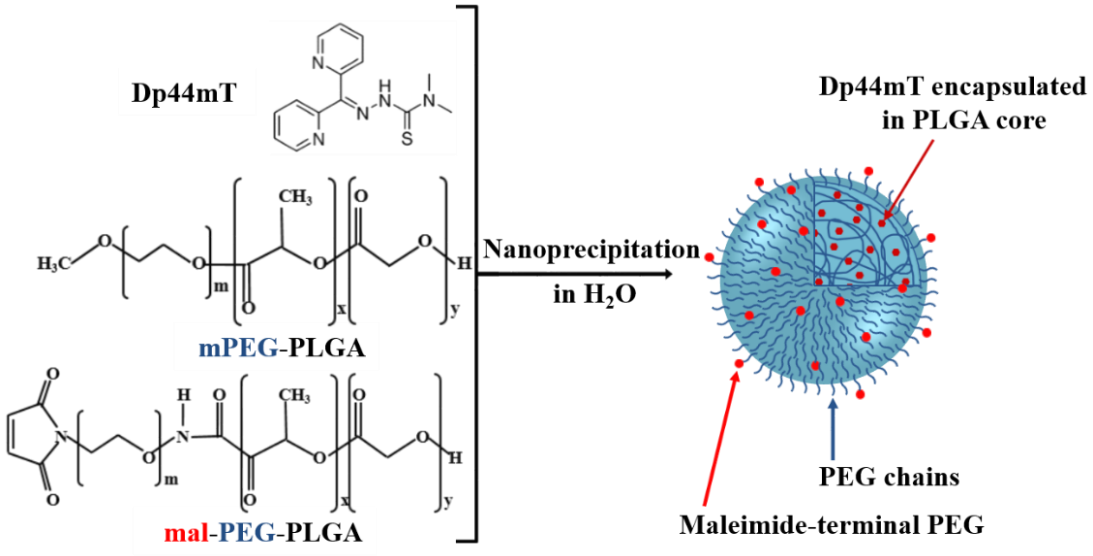

Figure 4.1. Schematic of nanoprecipitated Dp44mT-loaded PEG-NPs, consisting of Dp44mT entrapped in a PLGA core, with an outer PEG shell containing maleimide groups for conjugation.

Table 4.1. PEG-NP formulations, formed via nanoprecipitation, examined in this study with their corresponding size distribution, polydispersity index (PDI), drug encapsulation efficiency, and drug loading capacity.

	Organic Phase				Particle Size [nm]	PDI	Encapsulation Efficiency [%]	Loading Capacity [%]
	Drug:PLGA [mg/mL]	PLGA [mg/mL]	mPEG [mg/mL]	mal-PEG [mg/mL]				
(100%) PEG-NP	-	-	4.5	0.5	97±17	0.25±0.08	-	-
+ Dp44mT-(100%) PEG-NP	0.15:1 (0.75:5)	-	4.5	0.5	103 ±15	0.25±0.04	55±9	7.5±1.2
Dp44mT-(100%) PEG-NP	0.0375:1 (0.15:5)	-	4.5	0.5	97±20	0.24±0.01	69±15	2.0±0.4
C6-(100%) PEG-NP	0.01:1 (0.05:5)	-	4.5	0.5	94±7	0.24±0.02	99±1	0.98
(20%) PEG-NP	-	4.0	1.0*	0.5*	101±10	0.21±0.06	-	-
Dp44mT-(20%) PEG-NP	0.0375:1 (0.15:5)	4.0	1.0*	0.5*	97±7	0.16±0.05	56±3	1.7±0.1
† Dp44mT-(20%) PEG-NP	0.15:1 (0.75:5)	4.0	1.0*	0.5*	95±13	0.27±0.20	59±7	8.1±0.8

+,† The NP formulation used for the cytotoxicity experiments.

*If the PEG-NPs were used for mal-PEG click conjugation, they contained 10% mal-PEG + 10% mPEG for a total 20% PEGylation. If the PEG-NPs were used for EDC/NHS conjugation, they did not contain mal-PEG and instead consisted of a total of 20% mPEG-PLGA.

SEM confirmed that the PEG-NPs were spherical and relatively homogenous in size **(Figure 4.2A)**. As represented in **Figure 4.2B**, the size distribution of these PEG-NPs, measured by DLS, was narrow with a diameter of 97 ± 17 nm and a PDI of < 0.25. This size range is optimal for our future studies, as previous research has shown that NPs with a diameter of approximately 80 - 120 nm have a higher tendency to accumulate in hypervascular tumors, including brain tumors, compared to significantly smaller or larger particles [22, 78, 79]. In **Figure 4.2C**, colloidal stability assessed under physiological conditions over the course of a week confirmed the relative stability of these PEGylated NPs in both water and complete media over the course of a week, which was further supported with average negative surface potentials of approximately -55 mV. The presence of PEG on the surface of the NPs is known to minimize the interfacial free energy which increases the steric repulsion between the NPs and *in vivo* circulation time [61, 117].

Next, we evaluated the encapsulation efficiency of Dp44mT in these particles. The Dp44mT-loaded PEG-NPs had an encapsulation efficiency of ~ 55 ± 9%, which was found to be similar to the encapsulation efficiency of Dp44mT in PLGA NPs previously reported [87, 89, 100]. Reducing the drug-to-polymer ratio (D:P) increased encapsulation efficiency ~ 69 ± 15%. Based on the encapsulation efficiency values, we calculated the loading capacity of these NPs, as this is the drug loading value used for clinical applications. While the encapsulation efficiency was lower for the 0.15:1 formula, the loading capacity was at least three-fold higher (7.5% to 2.0% respectively). These values mirror those calculated for the unPEGylated Dp44mT-NPs, indicating that

this modified nanocarrier remained a good vehicle for the encapsulation and delivery of Dp44mT.

Together, the physical characteristics of these PEG-NPs were similar to the unPEGylated Dp44mT-NPs reported in **Chapter 2**. It should be noted that the addition of a PEG layer did significantly reduce the rate of drug release from these NPs [118], as compared to the bare NPs. This effect is in agreement with previous findings by Xu *et al*. that higher density of PEG on drug-loaded PLGA NPs led to a more sustained drug release from the NPs [119]. As such, this characteristic must be taken into account and modulated along with polymer type (LA:GA) and drug-to-polymer ratio (D:P) to gain the optimal sustained drug release for ideal therapeutic conditions [118].

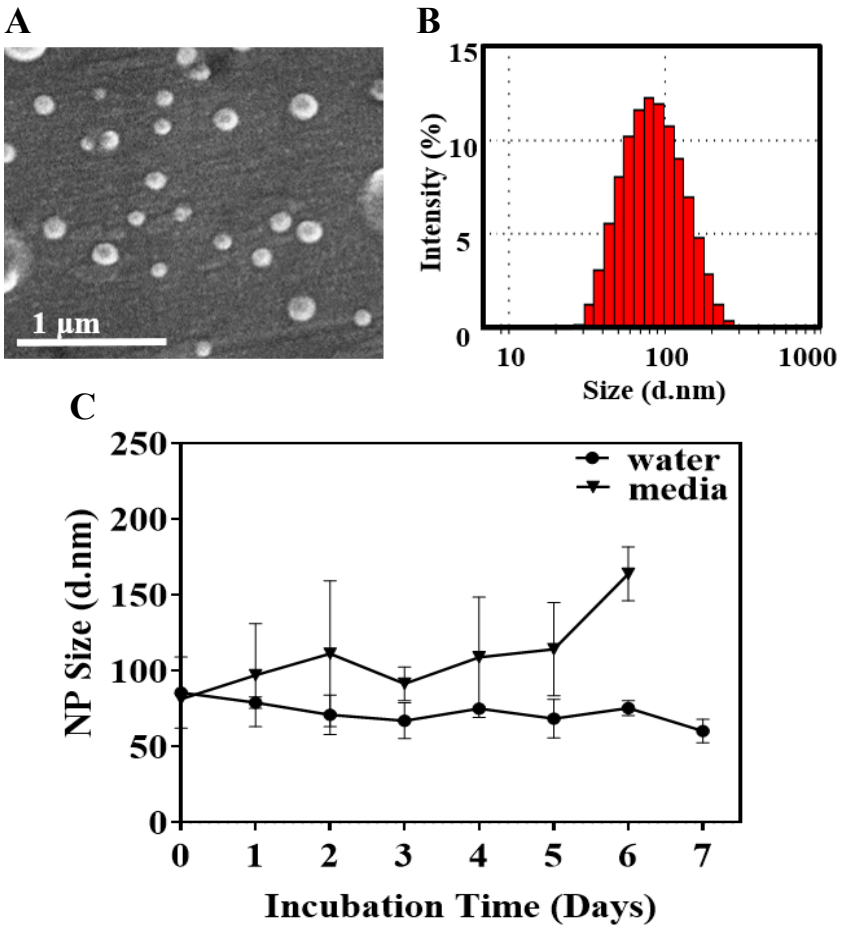

Figure 4.2. Characterization of PEGylated NPs, prepared by nanoprecipitation, by (A) SEM, (B) representative DLS size distribution, and (C) colloidal stability of PEG-NPs in physiological solutions over time.

4.4.2. Cytotoxicity of Dp44mT-loaded PEGylated Nanoparticles in Glioma Cells

After fabrication and characterization, we investigated the impact of PEGylation on the effectiveness of these Dp44mT-PEG-NPs in defeating glioma cells *in vitro*. For these experiments, we focused on $^{+}$Dp44mT-(100%)PEG-NP formula from **Table 4.1** (with 50:50 PLGA and 0.15:1 drug to PLGA ratio) as this formulation provided relatively high Dp44mT loading capacity and encapsulation efficiency. We repeated the previously performed cytotoxicity

assay, wherein U251 and U87 cells were treated with increasing amounts of Dp44mT-PEG-NPs for 48 hrs and then tested for viability using an MTT assay. Blank PEG-NPs were tested as control NPs. As demonstrated in **Figure 4.3A-B**, exposure to increasing amounts of Dp44mT-PEG-NPs led to an observable decrease in U87 and U251 cell viability concentrations of < 250 nM. Specifically, the IC_{50} value for these Dp44mT-PEG-NPs was ~ 135 nM in U251 and ~ 210 nM in U87 cells (**Table 4.2**), while the blank PLGA NPs did not show a significant effect on the viability of these cells.

Table 4.2. IC_{50} values of free, unPEGylated, and PEGylated Dp44mT-loaded NPs in glioma cells.

	Free Dp44mT	**Dp44mT-NP**	**Dp44mT-PEG-NP**
U87	~ 5 nM	~ 93 nM	~ 210 nM
U251	~ 10 nM	~ 85 nM	~ 135 nM

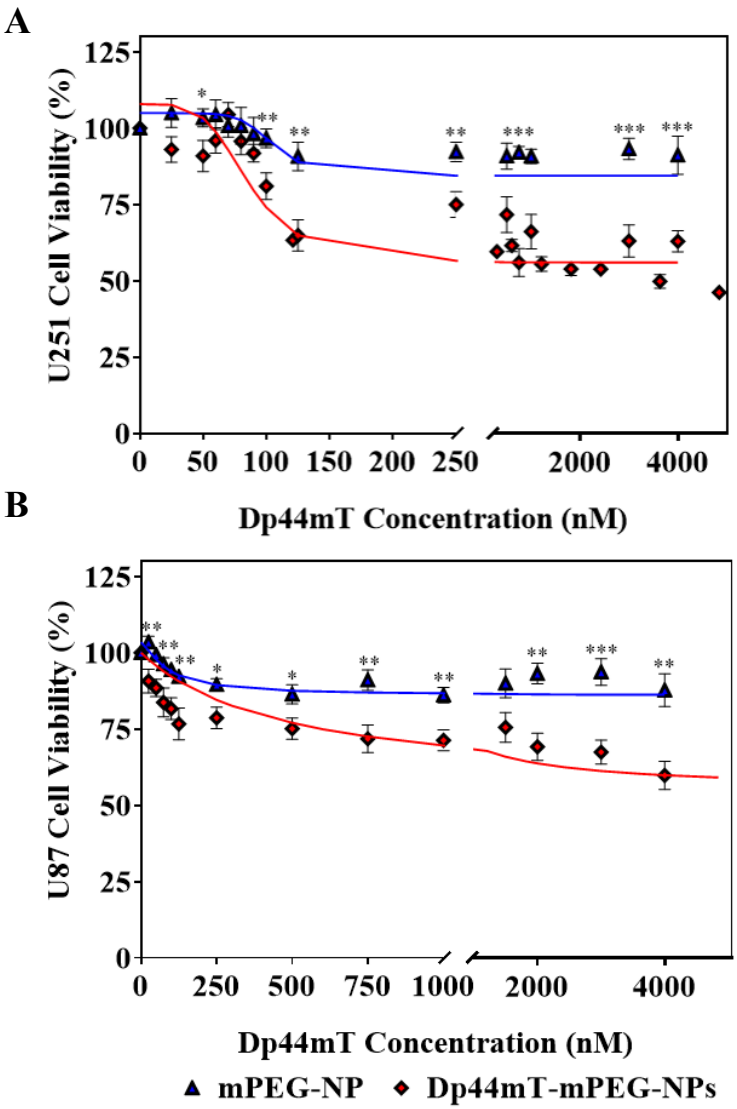

Figure 4.3. Dose-dependent cytotoxicity of PEG-NPs and Dp44mT-PEG-NPs in (A) U251 and (B) U87 glioma cells after 48 hrs treatment with PEG-NPs or Dp44mT-PEG-NPs.

As demonstrated in **Figure 4.4A**, low doses of Dp44mT-PEG-NPs had a similar effect on cell viability to non-PEGylated NPs. However, as dosage increased, PEGylation started to show a pronounced impact on cytotoxicity, particularly at doses higher than 100 nM. As a result, the addition of PEG layer to the surface of Dp44mT-NPs increased the IC_{50} values in U251 cells from

85 nM to 135 nM (**Table 4.2**).While the PEG layer created a steric barrier that prevents protein adsorption onto NPs, its hydrophilicity and neutral charge has also been reported to reduce the NP internalization [120]. Therefore, the presence of PEG on these NPs likely hindered their cellular uptake to some extent and, as a result, dampened their cytotoxicity. We observed a similar trend in U87 glioma cells, leading to an increase in the IC_{50} values from 100 nM to 210 nM. It is noteworthy that, despite the reduced level of toxicity due to PEGylation, these Dp44mT-NPs remained highly toxic towards glioma tumor cells with outstanding IC_{50} values.

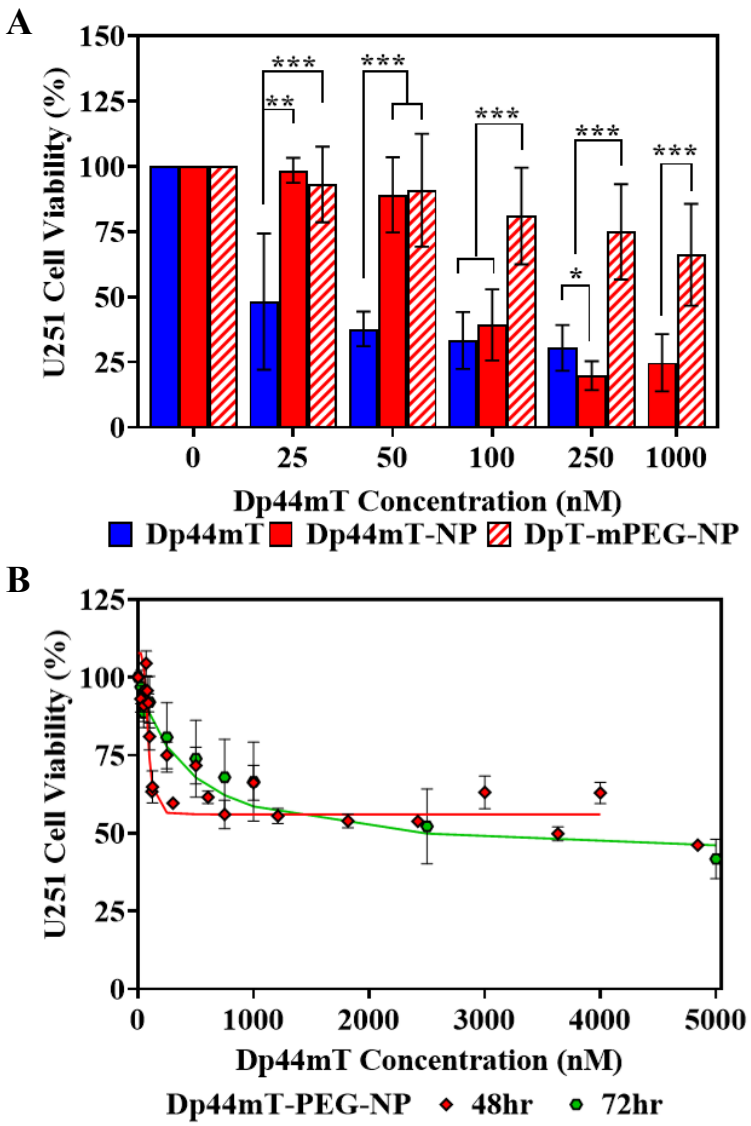

Figure 4.4. Comparative dose-dependent cytotoxicity as a result of (A) PEGylation of Dp44mT-NPs incubated in U251 cells after 48 hrs treatment, or (B) increased Dp44mT-PEG-NP incubation time (48 hrs vs 72 hrs).

For both glioma cell lines, we also noticed that the effectiveness of these particles quickly plateaued at ~ 50% similar to the unPEGylated Dp44mT-NPs (**Figure 3.2**). Due to the increased toxicity observed after 72 hr Dp44mT-NP treatment in glioma cells (**Figure 3.4**), we again applied our PEGylated NPs with increased incubation times.

From **Figure 4.4B,** preliminary results indicate that extended dosage time results in a cytotoxicity plateau of approx. 35 - 40% and an IC_{50} of 400 nM in U251 glioma cells. Interestingly, the extended incubation time did not result in a lower IC_{50} value but the cytotoxicity plateau was lower. This data suggests that increased exposure time for this PEGylated formulation does not result in a lowered required dosage but can help to remove more of the remaining cancer cell population. Over all, these results demonstrate that, while not as immediately effective as the unPEGylated formulation of our NPs, these Dp44mT-PEG-NPs still contain excellent anti-tumor activity in these two glioma cell lines and have the future potential for targeted delivery.

In the previous study, we confirmed that our unPEGylated Dp44mT-NP formulation appeared to have minimal toxicity in healthy astrocytes, supporting the assertion that Fe chelators have an apparent selectivity for neoplastic cells. Now that we have modified our NPs for improved *in vivo* application, we wanted to confirm that this new formulation poses little toxicity to healthy cells. Therefore, we evaluated the cytotoxicity of our Dp44mT-PEG-NPs in healthy astrocytes and Bovine Brain Microvascular Endothelial Cells (BBMVECs), the cells of the BBB that will be the first barrier to transport into the brain parenchyma. Mirroring the cytotoxicity experiments in cancer cells, astrocytes and BBMVECs were treated with either blank PEG-NPs or Dp44mT-PEG-NPs and evaluated for cell viability after 48 hrs via MTT assay. As illustrated in **Figure 4.5A-B**, the viability of these healthy cells was slightly reduced upon exposure to > 1 μM of Dp44mT-PEG-NPs. However, overall viability did not drop below 70% indicating that these NPs are still relatively non-toxic to healthy cells. Together, while the effect is dampened compared to cytotoxicity results from Dp44mT-

NPs, this data demonstrates that our new Dp44mT-PEG-NP formulation is still toxic to glioma cells with minimal effect to healthy cells.

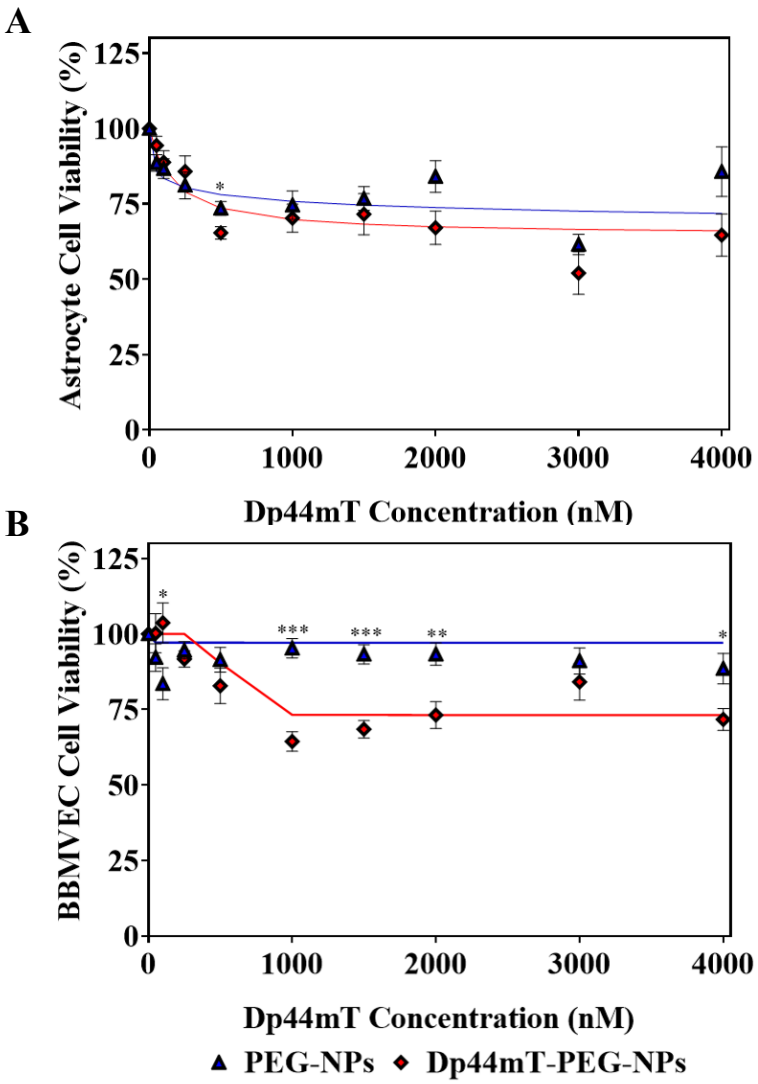

Figure 4.5. Dose-dependent cytotoxicity of PEG-NPs and Dp44mT-PEG-NPs in healthy (A) astrocytes and (B) BBMVECs after 48 hrs treatment with PEG-NPs or Dp44mT-PEG-NPs.

4.4.3. Cellular Uptake of C6-loaded PEGylated Nanoparticles by Glioma Cells

To test the performance of PEG-NPs as an effective delivery vehicle for future *in vivo* chemotherapy, we next evaluated the uptake of these NPs by glioma cells and astrocytes *in vitro*. The cells were treated with PEG-NPs loaded with fluorescent Coumarin-6 (C6), and uptake of these C6-PEG-NPs was then tracked over the course of 6 hrs by flow cytometry and confocal microscopy. As illustrated in **Figure 4.6A-B**, C6-PEG-NPs were rapidly uptaken in the first few hours by all cell types, though more so by the healthy astrocytes (~ 45%) as compared to the cancerous glioma cells (~ 30%).

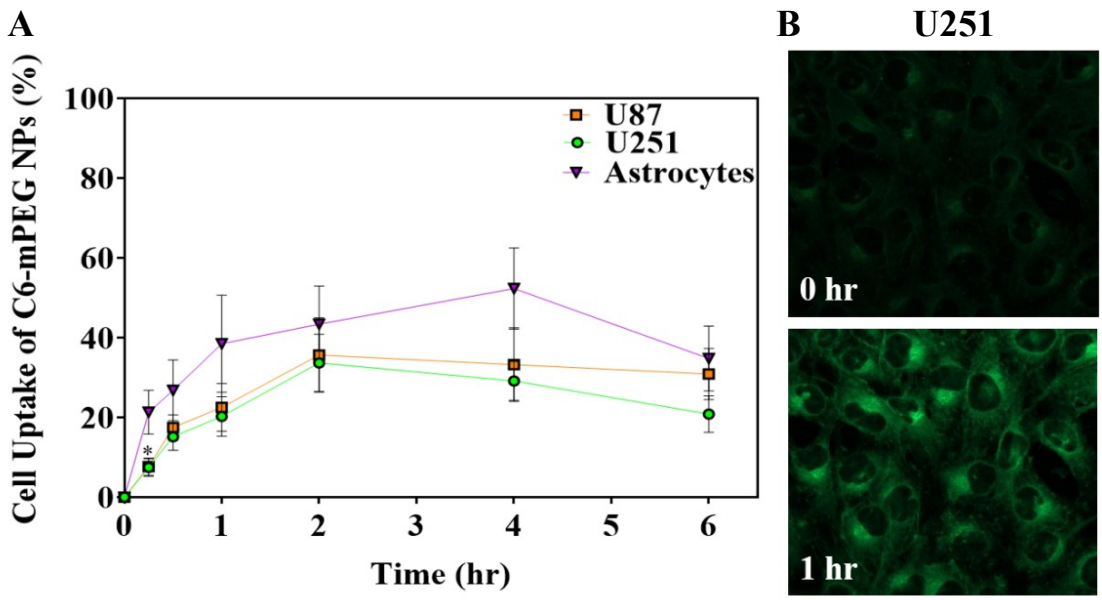

Figure 4.6. Uptake of C6-loaded PEG-NPs by glioma cells and astrocytes as a function of time, measured by (A) flow cytometry and (B) confocal fluorescence microscopy.

These flow cytometry results were then compared, in **Figure 4.7**, to unPEGylated C6-NP uptake previously reported in **Chapter 3**. Based on the dampened cytotoxicity

results observed with our Dp44mT-PEG-NPs and previous reports as to the effect of a PEG layer on NP internalization, we predicted that here we would also observe reduced NP uptake. While this was the case for U87 glioma, the opposite trend was observed for U251. This suggests that these cells might express more of the endocytosis receptor required for PEGylated NP uptake. Interestingly, astrocytes had no observable uptake bias between the two different types of NPs, which can be attributed to the fact that astrocytes act as neuronal support cells and their main function is influx and efflux of components from the environment. Together, these results suggest that, while reduced cytotoxicity is likely the result of decreased or slower NP uptake, there could be a cancer-specific endocytosis mechanism that can be exploited for more targeted delivery to these cancerous cells.

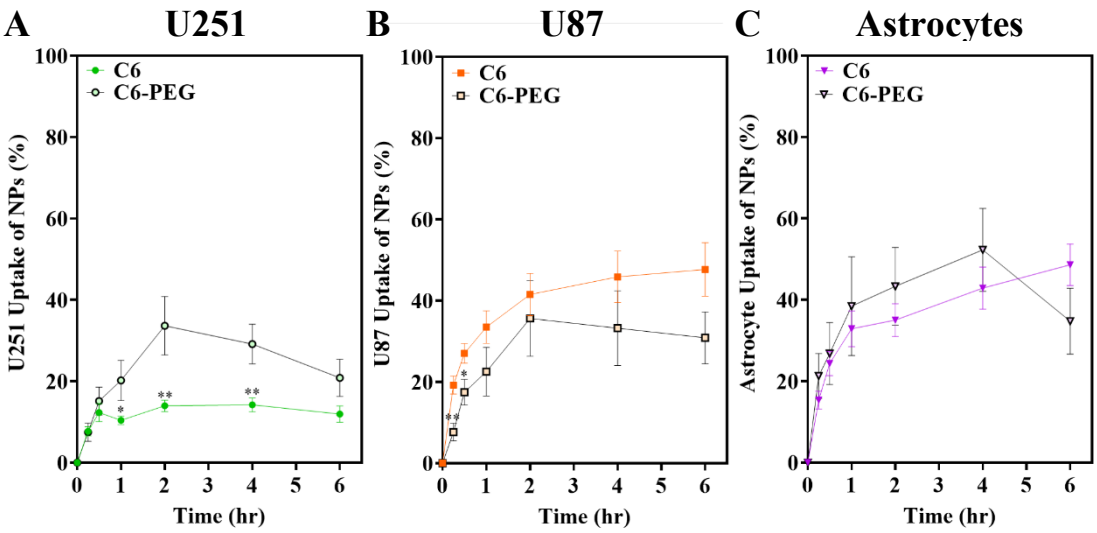

Figure 4.7. Comparative uptake of C6-loaded NPs, with and without PEGylation, as a function of time in (A) U251 cells, (B) U87 cells, and (C) astrocytes.

4.4.4. Cytotoxicity of Dp44mT-PEG-NPs in Other Cancer Cells

To further assess the applicability of Dp44mT-PEG-NPs against other types of cancer, we again assessed their efficacy in MCF7 breast and HT29 colorectal cancer cell lines. While 48 hr treatment with unPEGylated Dp44mT-NPs resulted in IC_{50} values > 10 μM in both cell lines, PEGylation further reduced the toxicity of these NPs to IC_{50} > 20 μM in these cells (**Table 4.3**). From **Figure 4.8A-B**, it is clear that the PEGylated NPs barely had an impact on these cancer cells. Application of blank PEG-NPs enabled continued cancer cell growth, while application of Dp44mT-PEG-NPs maintained the cancer cell populations (e.g., there was not noticeable decrease in the cell viability but at the same time there was also no new cell growth). Due to the effect of increased incubation time previously observed on cytotoxicity in these cancer cell lines (**Figure 3.7**), we predict that increased incubation times would again improve the cytotoxicity of this Dp44mT-PEG-NP formulation against MCF7 and HT29 cancer cells. These results suggest that, while 48 hr incubation is standard for *in vitro* drug toxicity studies, this time frame should be re-evaluated as the NP treatments applied to all of the cancers examined here required more time to be effective. This effectiveness is most likely the result of the uptake mechanism and the controlled drug release inherent in this polymeric platform, which should be modulated for best *in vivo* results.

Table 4.3. *IC_{50}* values of free, unPEGylated, and PEGylated Dp44mT-loaded NPs in MCF7 breast cancer and HT29 colorectal cancer cells.

	Free Dp44mT	Dp44mT-NP	Dp44mT-PEG-NP
MCF7	~ 800 nM	~ 11.5 μM	> 20 μM
HT29	~ 5.4 μM	~ 14.5 μM	> 20 μM

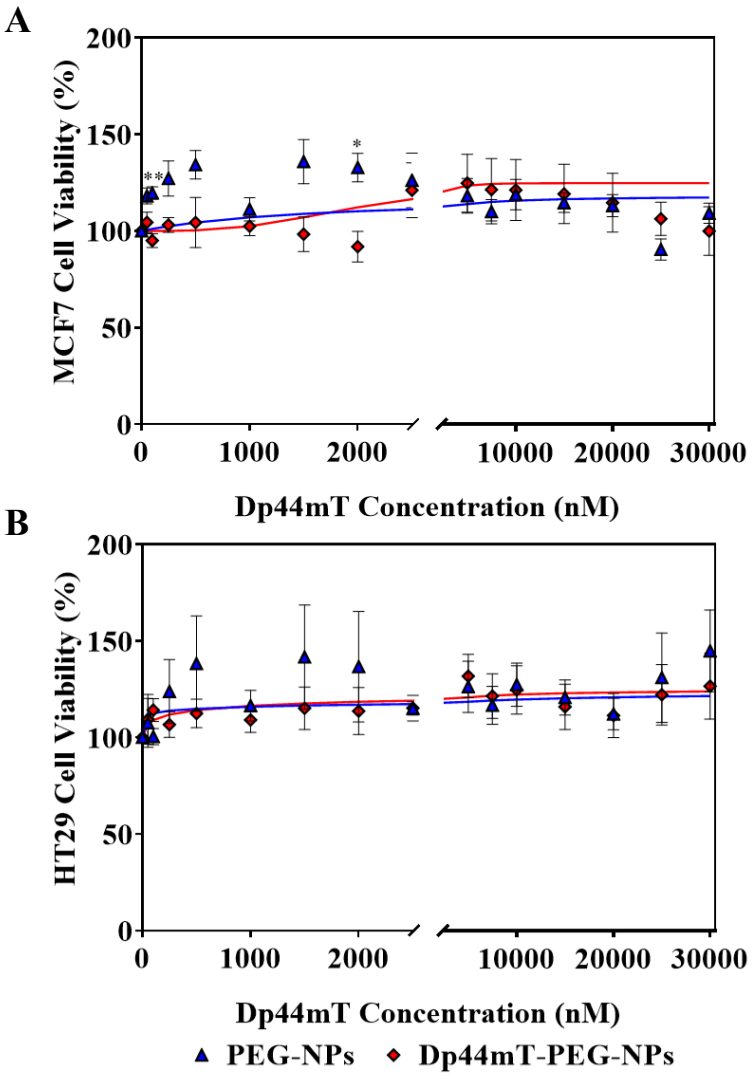

Figure 4.8. Dose-dependent cytotoxicity of PEG-NPs and Dp44mT-PEG-NPs in (A) MCF7 breast and (B) HT29 colorectal cells after 48 hrs treatment with PEG-NPs or Dp44mT-PEG-NPs.

4.4.5. Effect of PEG Density on Nanoparticle Cytotoxicity

Given the reduced cytotoxicity of PEGylated Dp44mT-NPs in malignant cells, we hypothesized that the presence of PEG chains affects the cellular interactions of NPs and hence, their uptake. To test this hypothesis, we prepared Dp44mT-PEG-NPs with varying percentages of PEG and evaluated their cytotoxicity in U251 glioma cells. Specifically, we fabricated Dp44mT-NPs with 10, 20, and 30% PEG and compared their cytotoxicity levels to those previously collected for non-PEGylated Dp44mT-NPs (**Figure 3.1**) and 100% PEGylated Dp44mT-NPs (**Figure 4.3** and identified as $^{+}$Dp44mT-(100%)PEG-NP in **Table 4.1).** As illustrated in **Figure 4.9**, there was no significant difference between the toxicity of NPs with 10 - 20% PEGylation and what was observed for the 100% PEGylated NPs, especially at higher doses. Interestingly, these results did not appear to have a concentration-dependent trend. For instance, the cell viability for NPs with the lowest examined PEG percentage (10%) was similar to that for NPs with 100% PEGylation. Prior studies have shown that, while the addition of PEG decreases NP uptake [120], a minimum of 5 - 20% PEG is required to prevent protein adsorption to the NP surface [121]. Thus, we chose a 20% surface PEGylation (identified by †Dp44mT-(20%)PEG-NP in **Table 4.1**) for these Dp44mT-NPs, as this should provide an optimal balance between the desired colloidal stability and the lower toxicity due to reduced cellular uptake. The modification of the PEG layer on the NP surface will also allow us to perform different bioconjugation techniques for optimal targeting to specific cancer cells.

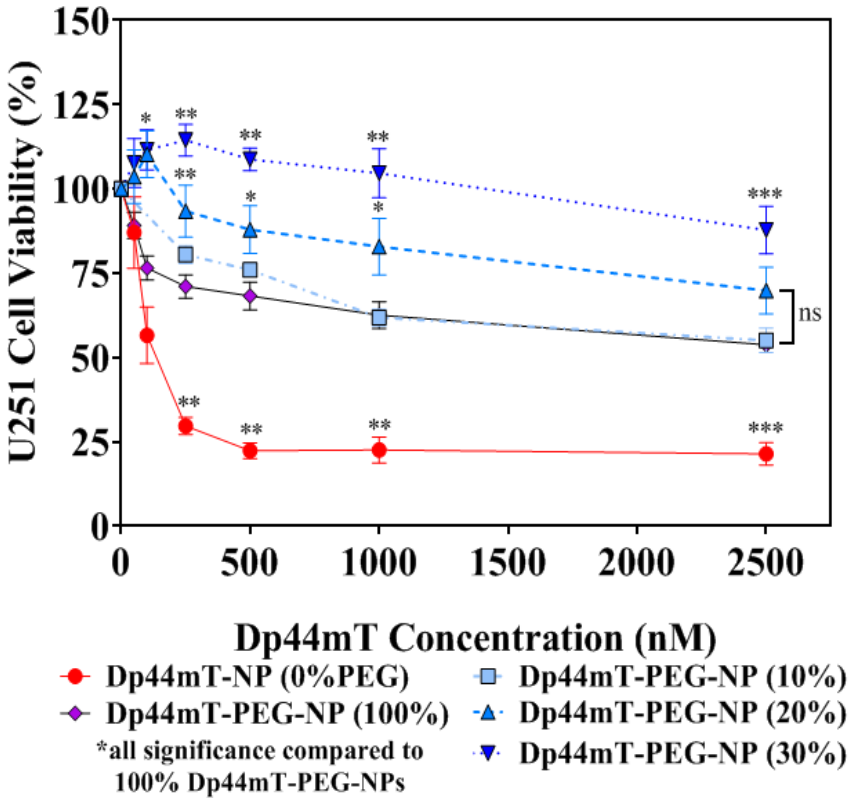

Figure 4.9. Dose-dependent cytotoxicity of Dp44mT-PEG-NPs with varying PEG density in U251 glioma cells after 48 hrs treatment.

4.4.6. Transport of PEGylated Nanoparticles across an *In Vitro* Blood Brain Barrier Model

After optimizing the PEG density on the surface of our PEG-NPs, we next wanted to examine the delivery of our 20% PEG-NP formulation across endothelial layer, as a model for transport of NPs from vasculature into tissue. As such, we studied the movement of our PEG-NPs across an *in vitro* transwell BBB co-culture model containing BBMVECs and astrocytes (**Figure 4.10A**) After establishing our *in vitro* BBB co-culture model (*as described in 4.3.6 Preparation of In Vitro Transwell Blood-Brain Barrier Co-Culture Model*), we confirmed the integrity of the endothelial tight junctions through measurement of the trans-epithelial electrical resistance (TEER), with

an average of ≥ 130 Ω-cm^2. We then added increasing concentrations of our 20% PEG-NP formulation to the top transwell chamber and then collected samples from the bottom chamber after 8 hrs of incubation. The collected samples were then analyzed for NP concentration using Nanosight. The percentage of PEG-NPs transported was then calculated using **Equation 4.1**.

From our preliminary data in **Figure 4.10C**, we observed that the highest percentage of PEG-NPs transported was ~ 5%, which equates to ~ 3.2x10^8 NPs moving across the endothelial layer. Interestingly, increasing the concentration of PEG-NPs added to the top chamber did not result in a significant change to the number of NPs transported across the BBB (**Figure 4.10B**). This is not the trend observed for PEG-NP transport across a bare membrane, which is driven solely by diffusion rather than transcytosis; in this case, increasing the polymer concentration in the top chamber resulted in an expected increase in the number of NPs collected from the bottom chamber. Therefore, the overall percentage of PEG-NPs transported actually decreased with increasing polymer concentration. These results, together with our C6-PEG-NP uptake results from **Figure 4.6,** suggest there is a threshold of NP saturation. For therapeutic application, this data suggests that increased NP dosage will not necessarily improve chemotherapeutic delivery.

Our results are comparable to those collected from a previous pilot study, which tracked the permeability of the *in vitro* transwell BBB using untargeted and targeted densely PEGylated NPs [118]. During these experiments, the transport of untargeted PEG-NPs was approximately 1.3 ± 0.1%. The addition of an IL13-targeting protein to the surface of these PEG-NPs increased transport to ~ 1.8%, which is a 42.5% increase

in transport. Similar transport was observed for NPs targeted with Transferrin (Tf), the gold standard in BBB targeting molecules, resulted in 2.0 ± 0.2% transport. Currently, the observed transport for our unconjugated partially PEGylated polymeric NPs is within the range reported for unconjugated liposomes (0.1 - 3.2%). Conjugating Tf to those liposomes increased transport significantly, to 1.2 - 5.6% [122, 123]. This is further evidence that coating our NP formulation with a targeting ligand is the best way to achieve improved endothelial transcytosis and enhanced NP uptake within the tissue.

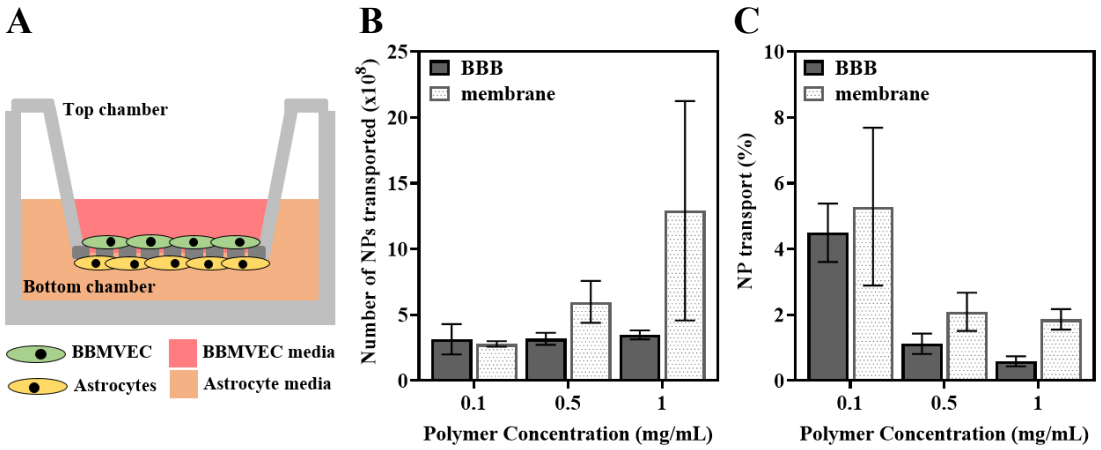

Figure 4.10. Effect of polymer concentration, across an (A) *in vitro* co-culture trans-well model of the Blood-Brain Barrier, on the (B) number of NPs and (C) percentage of NPs transported.

4.4.7. Targeting Dp44mT-PEG-NPs with IL13 peptide

We have now optimized our Dp44mT-PEG-NP for improved survival in an *in vivo* system and have shown the effect of these particles on various cancer cells *in vitro*. Our next objective is to increase therapeutic potential and decrease toxic side effects to healthy tissues by coating our PEGylated NPs with a cancer-specific targeting ligand, which will facilitate delivery to only the cancer cells of our choice. For this, we used

glioma as our malignant cell model; accordingly, we chemically attached a small peptide, IL13p, to the surface of our PEG-NPs, since this peptide should bind to the decoy IL13Rα2 that has been shown to be overexpressed on glioma cell surfaces [105-107]. To achieve this, we investigated two common methods for bioconjugation (**Figure 4.11**) and optimized both procedures for the attachment of our peptide. First, EDC/NHS chemically modifies the carboxyl group on PLGA, allowing for direct linkage to the amine groups on the IL13p. Second, maleimide-thiol click chemistry chemically modifies the amine group on the peptide, allowing for thiol attachment to the maleimide group found on a small percentage of the PEG chains added during NP fabrication [112, 113].

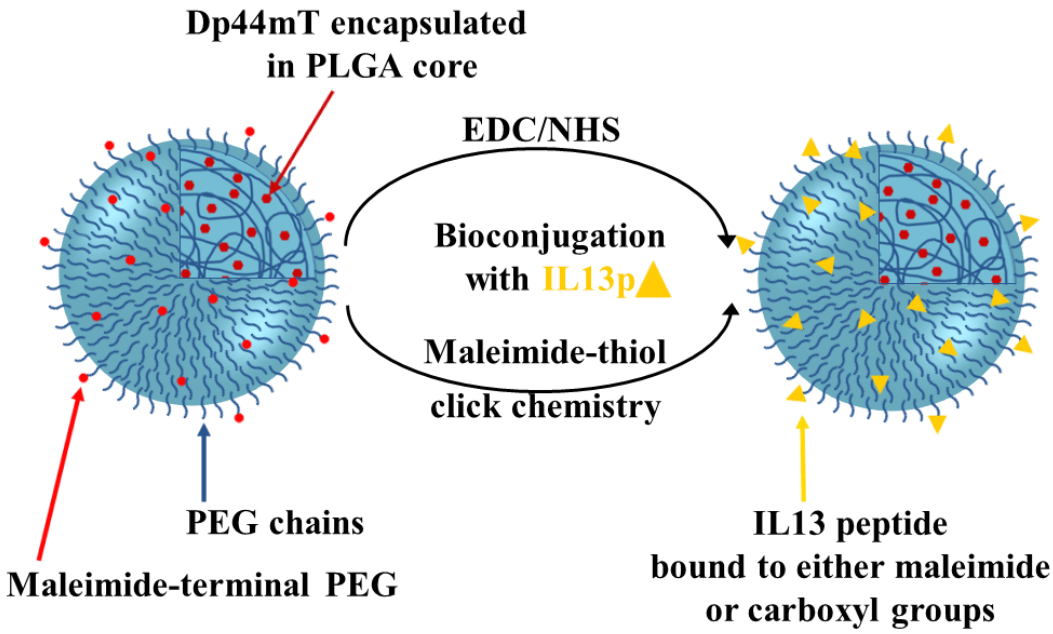

Figure 4.11. Schematic of IL13p conjugation to PEG-NPs for NP targeting to glioma. Conjugation is achieved either by EDC/NHS or maleimide-thiol click chemistry.

Previous pilot studies in our lab were able to successfully conjugate the full IL13 protein to the surface of a similar PEG-NP using maleimide-thiol click chemistry [118]. Preliminary work with those targeted particles indicated that the presence of the targeting ligand did improve NP cytotoxicity, uptake, and even transcytosis across an *in vitro* BBB model. Now, with our optimized PEG-NP and our smaller peptide, we find that the EDC/NHS method is much more efficient for attaching a targeting ligand to the NP surface. Preliminary cytotoxicity results with these streamlined IL13p-conjugated Dp44mT-PEG-NPs (named Dp44mT-IL13p-PEG-NPs) indicate that the addition of the targeting peptide can decrease cell viability by 15 - 20% as compared to the untargeted Dp44mT-PEG-NPs (**Figure 4.12**). These results were especially apparent in the U87 glioma cells, indicating that these cells may be more susceptible to this targeting peptide than U251 glioma cells. The observed cytotoxicity resulted in an IC_{50} of ~ 500 nM in U87 cells and ~ 1.2 μM in U251 cells. While these values are currently not lower than the IC_{50} values reported for untargeted Dp44mT-PEG-NPs in **Table 4.2**, it should be noted that the therapeutic threshold of the untargeted NPs was 55% for both cell lines. Here, the therapeutic threshold was as low as 40% for targeted Dp44mT-IL13p-PEG-NPs in U87 glioma cells. These preliminary results suggest that targeting can help improve the effectiveness of this nano-formulation in glioma cells.

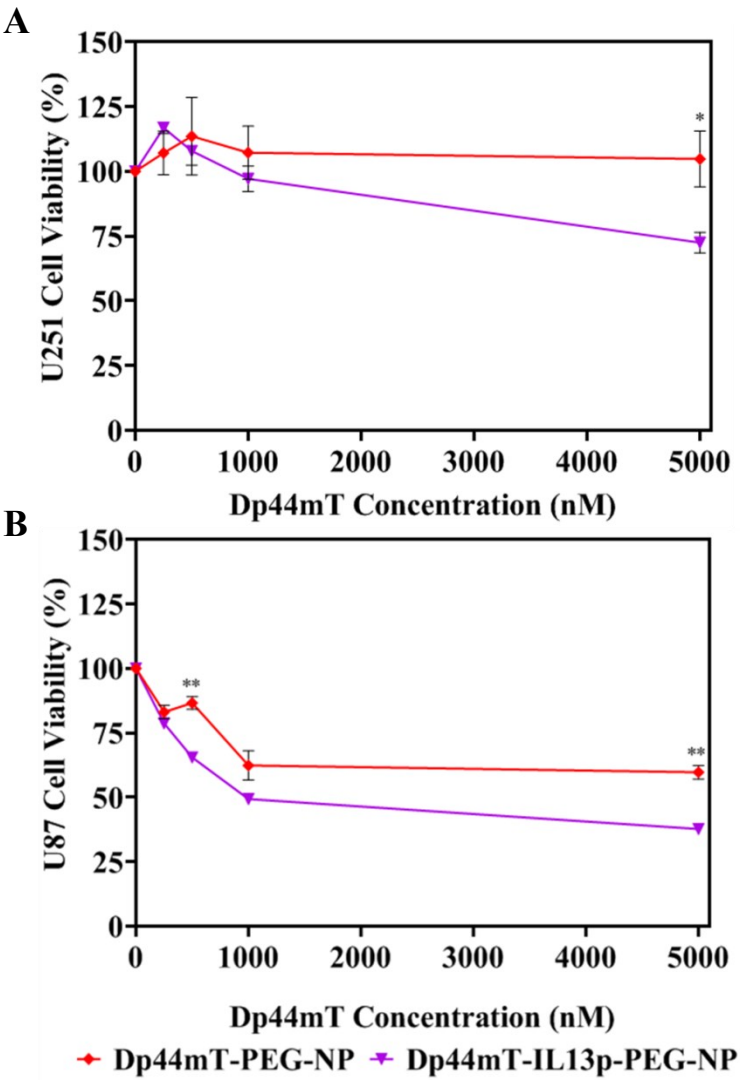

Figure 4.12. Dose-dependent cytotoxicity of Dp44mT-PEG-NPs and Dp44mT-IL13p-PEG-NPs in (A) U251 and (B) U87 glioma cells after 48 hrs treatment.

4.5. Conclusion

This chapter presents the effect of adding surface PEGylation and targeting ligands to our Dp44mT-NPs, as a step towards enhanced tumor toxicity *in vivo*. Using nanoprecipitation, we fabricated PLGA NPs coated with a surface layer of PEG for improved biodistribution and stability. Our PEG-NPs were homogeneous in size (97 ± 17 nm) and shape, had negative surface potential (-55 mV), and showed good colloidal

stability in physiological solutions, similar to our previously reported PLGA NPs. The PEG-NPs were also able to efficiently encapsulate Dp44mT, with a moderate encapsulation efficiency of ~ 69 ± 15%, which equates to 2.0 - 7.5% loading capacity. The cytotoxicity studies showed that these Dp44mT-PEG-NPs were toxic to U251 and U87 glioma cells (IC_{50} < 250 nM), though not to the degree as what was observed with the unPEGylated Dp44mT-NPs. Toxicity was enhanced by reducing the PEG coating to the minimal 20%. This platform was then expanded to MCF7 breast cancer and HT29 colorectal cancer cells. There was very little toxicity apparent in these cell lines (IC_{50} > 20 μM) but toxicity can most likely be enhanced with PEG density optimization, increased exposure time, and cancer-specific targeting. Afterwards, we conjugated these NPs with a novel ligand, IL13p, to enable targeted delivery to malignant glioma cells. Preliminary results indicate that Dp44mT-loaded IL13p-PEG-NPs showed a higher level of cytotoxicity in glioma cells (U251, U87) compared to Dp44mT-PEG-NPs, presumably due to the increased cellular uptake of these IL13p-PEG-NPs. Overall, this IL13p-conjugated nanoparticle formula offers an attractive strategy to enable the targeted delivery of this chelator to brain cancer cells. This nanoparticle platform may be further applied for the encapsulation of other hydrophobic anti-cancer drugs or the attachment of other targeting ligands for the treatment of other types of tumors.

CHAPTER V
CONCLUSION & FUTURE DIRECTIONS

5.1. Conclusion

This dissertation presents the development and *in vitro* assessment of a novel anti-cancer nano-formulation, as a new strategy for the application of this chelator towards cancer. In the first part of this dissertation, we discussed the preparation, optimization, and characterization of PLGA NPs encapsulating anti-tumor Dp44mT using two common fabrication methods of nanoprecipitation and single emulsion. We demonstrated that PLGA NPs provide a suitable carrier for the encapsulation of Dp44mT for the future application against cancer cells.

In the second part of this dissertation, we evaluated the therapeutic effectiveness of this nano-formulation against malignant cells *in vitro*, in comparison to application of free Dp44mT. We demonstrated that application of free and encapsulated Dp44mT effectively kills glioma cells, while selectively bypassing healthy cells. Similar application to other cancer cells, specifically HT29 colorectal and MCF7 breast cancer cells, further demonstrated the applicability of this nano-formulation as a future chemotherapeutic against cancer.

In the last part of this dissertation, we discussed the surface modification of our nano-formulation towards future application *in vivo*. We demonstrated that the addition of PEG and glioma-targeting ligand, IL13p, can enhance the efficacy of these NPs. This IL13p-decorated Dp44mT-PEG-NP formulation offers an

attractive strategy to enable the targeted delivery of Dp44mT chelator to brain cancer cells. We anticipate that the continued modification of this nanoparticle formulation will enhance its efficiency for the treatment of malignant cells.

5.2. Future Directions

5.2.1. Interleukin-13α2 Receptor Expression on Glioma Cell Surface

First, since we are using glioma as a malignant cell model and have targeted our nano-formulation with a peptide designed to bind to a glioma-specific receptor, IL13Rα2, it is important to confirm and quantify the cell surface expression of our target receptor in our glioma cell lines. From our preliminary Dp44mT-loaded IL13p-PEG-NP cytotoxicity results (Figure 4.11), it appears that U87 glioma cells have a more significant reaction to these targeted nanoparticles, as compared to U251 glioma cells. Since receptor binding should lead to NP internalization and improved toxicity, the dampened cytotoxic effect we are observing could be the result of reduced levels of IL13Rα2 on the surface of U251 glioma cells. Results from these experiments would indicate (1) if our cells are actually expressing this target receptor, as has been suggested in literature; and (2) whether the difference in cytotoxicity observed between the U87 and U251 cell lines is due to a difference in receptor expression. As such, a Western blot should be performed to quantify the level of receptor being expressed by cells. Alternatively, flow cytometry could be performed to determine whether a specific subset of our glioma cells is highly expressing this receptor. Results from these experiments will determine if continued use of IL13p as a targeting ligand is ideal or if other ligands, like Tf, should be considered.

5.2.2. Targeting PEGylated Nanoparticles to Other Cancers

At the same time, we have also shown the potential of this nano-formulation to be used as a universal chemotherapeutic platform by assessing the cytotoxicity of these Dp44mT-NPs in breast cancer and colorectal cancer cells. Therefore, we should continue with this line of inquiry by targeting our nano-formulation against these other types of cancer. For the targeting ligand, there are two paths we can take: generalized cancer targeting or cancer-cell specific targeting. For the first option, we could utilize a more general targeting moiety, which could include EGFR (epidermal growth factor receptor), Tf, or folate receptor (FOLR2), as these targets have been implicated in the growth and metastasis of a variety of cancers. Results from these experiments would demonstrate the general applicability of our drug delivery platform against malignant cells. The second option is to target the cancers individually, as we have previously done with glioma. For these experiments, a more specific target should be used. CXCR4 and VEGF have been found to be upregulated in colorectal cancers while the estrogen (ER) and progesterone receptors (hPR-A/B) would make promising targets for breast cancer-specific delivery. These cell-specific targeting experiments would not only prove that applicability of our nano-formulation against these cancers, but would also support our assertion that this platform can be easily modified for more universal applications.

5.2.3. Apoptotic Mechanisms of Dp44mT in Glioma

Due to particular interest in Dp44mT as an anti-cancer drug in glioma, we should more closely examine the specific apoptotic mechanisms being used by Dp44mT, in its

free form, to kill glioma cells. Other than iron chelation and ROS production, previous studies have proposed Dp44mT functions through several intracellular signaling pathways, of which NDRG1 and CDK-2 are just two of the proteins that have been implicated. For these experiments, proteomic analysis of cell lysate after incubation with Dp44mT can give use some insight as to which proteins levels are changing. Isolation of changing protein levels can help narrow down the major pathways associated with Dp44mT action. Understanding the specific mechanisms of action for Dp44mT in our target cancer cells could give us better insight as to why our platform was so effective in one cancer cell line compared to another. This information could also be used to improve the efficacy of our platform, possibly through conjugation of additional targeting ligands or perhaps co-encapsulation with another drug for dual release.

5.2.4. Nanoparticle Uptake and Transcytosis *In Vitro*

The next set of experiments that should be explored in the future focus on the transport and endocytosis of this nano-formulation. In **Chapter 3 and 4**, we reported the uptake of both bare and PEGylated NPs by glioma cells and healthy astrocytes. While there is a general consensus in literature that these NPs were uptaken via receptor-mediated endocytosis [124], the specific mechanism and receptor being employed is unclear. For this area of research, endocytosis inhibitors can be applied during uptake experiments to tease out the specific mechanism that is being used by each nano-formulation. For these experiments, which are currently in progress, glioma cells were dosed for 1 hr with C6-NPs *(as previously described in 3.3.6. Cellular Uptake of C6-*

Nanoparticles via Flow Cytometry) at the same time as endocytosis inhibitor, either Chloropromazine HCl (CPH) or Filipin. The cells were then processed and analyzed for C6-NP uptake via flow cytometry. Preliminary results suggest that, for both U251 and U87 glioma, uptake of our unPEGylated (bare) NPs is driven primarily by clathrin-mediated endocytosis (**Figure 5.1A**) rather than caveolae-mediated endocytosis (**Figure 5.1B**). Experiments examining the other uptake mechanisms, including pinocytosis and clathrin-independent endocytosis, are also currently being explored. Continued experiments examining PEG-NP and IL13p-PEG-NP uptake will indicate which receptors are the best targets for future NP optimization.

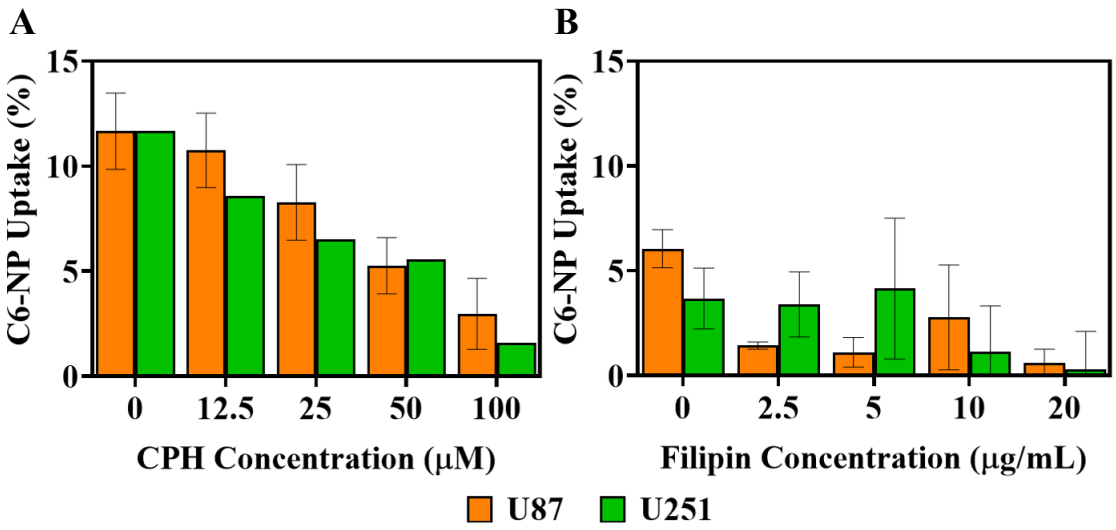

Figure 5.1. Uptake of C6-loaded nanoparticles by glioma cells in the presence of (A) clathrin-mediated endocytosis inhibitor, CPH, and (B) caveolae-mediated endocytosis inhibitor, Filipin.

Further, it has been shown in literature that IL13-targeted liposomes were able to cross the BBB for delivery to the brain, though the mechanism is not completely understood. Therefore, we should again employ inhibition experiments, like those

discussed in **Figure 5.1**, to assess the transcytosis of our glioma-targeted NPs. For this, we can apply our IL13p-PEG-NPs to our *in vitro* BBB model, as was previously used in **Figure 4.9A.** We would then be able to track NP transport, for comparison to our untargeted PEG-NPs. The addition of transcytosis inhibitors would then determine the receptor and uptake mechanism being leveraged by IL13 targeting for endothelial transcytosis.

5.2.5. Nanoparticle Biodistribution and Toxicity *In Vivo*

The following set of experiments should examine the *in vivo* biodistribution and tumor-targeted delivery of our nano-formulations. This nano-carrier has been optimized for in vivo application and now needs to be tested against the stresses of an *in vivo* system. Therefore, these NPs should be applied a mouse model and the subsequent biodistribution should be tracked to determine where these NPs naturally accumulate and the circulation half-life of this formulation. For this, we can replace the encapsulated Dp44mT with a near-infrared fluorescent dye (e.g., DiR) which can be tracked in real time using a specialized non-invasive *In Vivo* Imaging System (IVIS). This experiment should be performed first on our bare PLGA NPs, optimized for size, before continuing with the PEGylated NPs and finally the IL13p-targeted PEG-NP formulations, so we can carefully determine the effect of each layer of our nano-formulation.

Continuing with the *in vivo* studies, we are especially interested in nanoparticle delivery to brain cancer *in situ*, hence our previous use of a glioma-specific targeting ligand. Based on the combined results of the proposed *in vitro* transport studies and *in vivo* biodistribution studies using IL13p-targeted PEG-NPs, we should apply this

glioma-targeted nano-formulation towards treatment of brain tumors in a glioma mouse model to truly assess the delivery and effectiveness of our final nano-formulation. Similar studies in literature have applied Dp44mT, in its free form, directly to various tumor types which were often implanted into the mouse flank. While this method does assess relative drug toxicity *in vivo*, it completely bypasses the need to cross the BBB, which is the main obstacle to effective delivery of chemotherapeutics to the brain. As we are the first to encapsulate this drug in a nano-carrier and demonstrate its effectiveness against malignant cells, we should next prove the ability of this nano-carrier to also adequately cross the BBB for successful delivery directly to primary brain tumors.

REFERENCES

[1] A. C. Society, "Cancer Facts & Figures 2019," ed, 2019, p. 71.

[2] M. Heron, "Deaths: Leading Causes for 2017," in "National Vital Statistics Reports," Hyattsville, MD2019, vol. 68.

[3] U. S. Department of Health and Human Services. (June 2019). *U.S. Cancer Statistics: Data Visualizations*.

[4] *World Cancer Report 2014* (World Cancer Reports). Lyon, France: International Agency for Research on Cancer, 2014, p. 630.

[5] A. Jemal, R. Siegel, E. Ward, Y. Hao, J. Xu, and M. Thun, "Cancer statistics," *Ca Cancer J Clin,* vol. 59, no. 4, 2009.

[6] B. Weigelt, J. L. Peterse, and L. J. van't Veer, "Breast cancer metastasis: Markers and models," *Nature Reviews Cancer,* vol. 5, no. 8, pp. 591-602, 2005.

[7] R. Siegel, C. DeSantis, K. Virgo, K. Stein, A. Mariotto, T. Smith, D. Cooper, T. Gansler, C. Lerro, and S. Fedewa, "Cancer treatment and survivorship statistics, 2012," *CA: a cancer journal for clinicians,* vol. 62, no. 4, pp. 220-241, 2012.

[8] B. M. Wolpin and R. J. Mayer, "Systemic treatment of colorectal cancer," *Gastroenterology,* vol. 134, no. 5, pp. 1296-1310. e1, 2008.

[9] P. Y. Wen and S. Kesari, "Malignant gliomas in adults," *N Engl J Med,* vol. 359, no. 5, pp. 492-507, 2008.

[10] X. Zhang, W. Zhang, W. D. Cao, G. Cheng, and Y. Q. Zhang, "Glioblastoma multiforme: Molecular characterization and current treatment strategy (Review)," *Exp Ther Med,* vol. 3, no. 1, pp. 9-14, 2012.

[11] H. Ohgaki, P. Dessen, B. Jourde, S. Horstmann, T. Nishikawa, P.-L. Di Patre, C. Burkhard, D. Schüler, N. M. Probst-Hensch, P. C. Maiorka, N. Baeza, P. Pisani, Y. Yonekawa, M. G. Yasargil, U. M. Lütolf, and P. Kleihues, "Genetic Pathways to Glioblastoma," *A Population-Based Study,* vol. 64, no. 19, pp. 6892-6899, 2004.

[12] R. Stupp, W. P. Mason, M. J. van den Bent, M. Weller, B. Fisher, M. J. B. Taphoorn, K. Belanger, A. A. Brandes, C. Marosi, U. Bogdahn, J. Curschmann, R. C. Janzer, S. K. Ludwin, T. Gorlia, A. Allgeier, D. Lacombe, J. G. Cairncross, E. Eisenhauer, and R. O. Mirimanoff, "Radiotherapy plus Concomitant and Adjuvant Temozolomide for Glioblastoma," *New England Journal of Medicine,* vol. 352, no. 10, pp. 987-996, 2005.

[13] D. N. Louis, H. Ohgaki, O. D. Wiestler, W. K. Cavenee, P. C. Burger, A. Jouvet, B. W. Scheithauer, and P. Kleihues, "The 2007 WHO Classification of Tumours of the Central Nervous System," *Acta Neuropathologica,* vol. 114, no. 2, pp. 97-109, 2007.

[14] R. O. Weller, "Brain tumours in man," *Food and Chemical Toxicology,* vol. 24, no. 2, pp. 91 - 98, 1986.

[15] M. Lacroix, D. Abi-Said, D. R. Fourney, Z. L. Gokaslan, W. Shi, F. DeMonte, F. F. Lang, I. E. McCutcheon, S. J. Hassenbusch, E. Holland, K. Hess, C. Michael, D. Miller, and R. Sawaya, "A multivariate analysis of 416 patients

with glioblastoma multiforme: prognosis, extent of resection, and survival," *J Neurosurg,* vol. 95, no. 2, pp. 190-8, 2001.

[16] M. D. Walker, S. B. Green, D. P. Byar, E. Alexander, Jr., U. Batzdorf, W. H. Brooks, W. E. Hunt, C. S. MacCarty, M. S. Mahaley, Jr., J. Mealey, Jr., G. Owens, J. Ransohoff, 2nd, J. T. Robertson, W. R. Shapiro, K. R. Smith, Jr., C. B. Wilson, and T. A. Strike, "Randomized comparisons of radiotherapy and nitrosoureas for the treatment of malignant glioma after surgery," *N Engl J Med,* vol. 303, no. 23, pp. 1323-9, 1980.

[17] J. F. Holland and R. E. Pollock, *Holland-Frei cancer medicine 8*. PMPH-USA, 2010.

[18] N. C. Institute. (2019). *Radiation Therapy to Treat Cancer*. Available: https://www.cancer.gov/about-cancer/treatment/types/radiation-therapy

[19] J. M. Brown and A. J. Giaccia, "The unique physiology of solid tumors: opportunities (and problems) for cancer therapy," *Cancer research,* vol. 58, no. 7, pp. 1408-1416, 1998.

[20] N. C. Institute. (2015). *Chemotherapy to Treat Cancer* Available: https://www.cancer.gov/about-cancer/treatment/types/chemotherapy

[21] M. S. Lesniak and H. Brem, "Targeted therapy for brain tumours," *Nature reviews Drug discovery,* vol. 3, no. 6, pp. 499-508, 2004.

[22] E. Blanco, H. Shen, and M. Ferrari, "Principles of nanoparticle design for overcoming biological barriers to drug delivery," *Nature Biotechnology,* vol. 33, no. 9, pp. 941-951, 2015.

[23] Q. Wu, Z. Yang, Y. Nie, Y. Shi, and D. Fan, "Multi-drug resistance in cancer chemotherapeutics: mechanisms and lab approaches," *Cancer letters,* vol. 347, no. 2, pp. 159-166, 2014.

[24] N. Y. Presbyterian. (2020). *What is Precision Medicine?* Available: https://healthmatters.nyp.org/precision-medicine/

[25] S. V. Torti and F. M. Torti, "Iron and cancer: more ore to be mined," *Nature Reviews Cancer,* vol. 13, p. 342, 2013.

[26] Z. Liu and R. Hider, "Design of iron chelators with therapeutic application," *Coordination Chemistry Reviews,* vol. 232, pp. 151-171, 2002.

[27] J. J. Knox, S. J. Hotte, C. Kollmannsberger, E. Winquist, B. Fisher, and E. A. Eisenhauer, "Phase II study of Triapine® in patients with metastatic renal cell carcinoma: a trial of the National Cancer Institute of Canada Clinical Trials Group (NCIC IND.161)," *Investigational New Drugs,* vol. 25, no. 5, pp. 471-477, 2007.

[28] P. M. B. Pahl and L. D. Horwitz, "Cell permeable iron chelators as potential cancer chemotherapeutic agents," *Cancer Investigation,* vol. 23, no. 8, pp. 683-691, 2005.

[29] C. Santini, M. Pellei, V. Gandin, M. Porchia, F. Tisato, and C. Marzano, "Advances in copper complexes as anticancer agents," *Chem Rev,* vol. 114, no. 1, pp. 815-62, 2014.

[30] A. E. L. Douglas X. West, Subhash B. Padhye, Rajeev C. Chikate, Pramila B. Sonawane, Avinash S. Kumbhar, Ratnamala G. Yerande, "Thiosemicarbazone

complexes of copper(II): structural and biological studies," *Coordination Chemistry Reviews,* vol. 123, no. 1, pp. 49 - 71, 1993.

[31] H. Beraldo and D. Gambino, "The wide pharmacological versatility of semicarbazones, thiosemicarba-zones and their metal complexes," *Mini Rev Med Chem,* vol. 4, no. 1, pp. 31-9, 2004.

[32] Y. Yu, J. Wong, D. Lovejoy, D. Kalinowski, and D. Richardson, "Chelators at the Cancer Coalface: Desferrioxamine to Triapine and Beyond," *Clinical cancer research : an official journal of the American Association for Cancer Research,* vol. 12, pp. 6876-83, 2007.

[33] N. F. Olivieri and G. M. Brittenham, "Iron-chelating therapy and the treatment of thalassemia," *Blood,* vol. 89, no. 3, pp. 739-61, 1997.

[34] T. Yamasaki, S. Terai, and I. Sakaida, "Deferoxamine for Advanced Hepatocellular Carcinoma," *New England Journal of Medicine,* vol. 365, no. 6, pp. 576-578, 2011.

[35] D. L. Becton and B. Roberts, "Antileukemic effects of deferoxamine on human myeloid leukemia cell lines," *Cancer Res,* vol. 49, no. 17, pp. 4809-12, 1989.

[36] H. C. John B. Lloyd, Catherine Rice-Evans, "Evidence that desferrioxamine cannot enter cells by passive diffusion," *Biochemical Pharmacology,* vol. 41, no. 9, pp. 1361 - 1363, 1991.

[37] M. A. Howland, "Risks of parenteral deferoxamine for acute iron poisoning," *J Toxicol Clin Toxicol,* vol. 34, no. 5, pp. 491-7, 1996.

[38] D. B. Lovejoy, P. J. Jansson, U. T. Brunk, J. Wong, P. Ponka, and D. R. Richardson, "Antitumor Activity of Metal-Chelating Compound Dp44mT Is

Mediated by Formation of a Redox-Active Copper Complex That Accumulates in Lysosomes," *Cancer Research,* vol. 71, no. 17, pp. 5871-5880, 2011.

[39] V. Melotte, X. Qu, M. Ongenaert, W. van Criekinge, A. P. de Bruine, H. S. Baldwin, and M. van Engeland, "The N-myc downstream regulated gene (NDRG) family: diverse functions, multiple applications," *Faseb j,* vol. 24, no. 11, pp. 4153-66, 2010.

[40] Z. Chen, D. Zhang, F. Yue, M. Zheng, Z. Kovacevic, and D. R. Richardson, "The iron chelators Dp44mT and DFO inhibit TGF-beta-induced epithelial-mesenchymal transition via up-regulation of N-Myc downstream-regulated gene 1 (NDRG1)," *J Biol Chem,* vol. 287, no. 21, pp. 17016-28, 2012.

[41] Y. Yu, Y. S. Rahmanto, and D. Richardson, "Bp44mT: an orally active iron chelator of the thiosemicarbazone class with potent anti-tumour efficacy," *British Journal of Pharmacology,* vol. 165, no. 1, pp. 148-166, 2012.

[42] J. A. Crim and H. G. Petering, "The antitumor activity of Cu(II)KTS, the copper (II) chelate of 3-ethoxy-2-oxobutyraldehyde bis(thiosemicarbazone)," *Cancer Res,* vol. 27, no. 7, pp. 1278-85, 1967.

[43] M. R. Taylor, E. J. Gabe, J. P. Glusker, J. A. Minkin, and A. Patterson, "The Crystal Structures of Compounds with Antitumor Activity. 2-Keto-3-ethoxybutyraldehyde Bis (thiosemicarbazone) and Its Cupric Complex1," *Journal of the American Chemical Society,* vol. 88, no. 8, pp. 1845-1846, 1966.

[44] P. J. Jansson, P. C. Sharpe, P. V. Bernhardt, and D. R. Richardson, "Novel thiosemicarbazones of the ApT and DpT series and their copper complexes:

identification of pronounced redox activity and characterization of their antitumor activity," *J Med Chem,* vol. 53, no. 15, pp. 5759-69, 2010.

[45] M. Whitnall, J. Howard, P. Ponka, and D. R. Richardson, "A class of iron chelators with a wide spectrum of potent antitumor activity that overcomes resistance to chemotherapeutics," *Proceedings of the National Academy of Sciences of the United States of America,* vol. 103, no. 40, pp. 14901-14906, 2006.

[46] N. T. V. Le and D. R. Richardson, "Iron chelators with high antiproliferative activity up-regulate the expression of a growth inhibitory and metastasis suppressor gene: a link between iron metabolism and proliferation," *Blood,* vol. 104, no. 9, pp. 2967-2975, 2004.

[47] D. S. Kalinowski and D. R. Richardson, "The evolution of iron chelators for the treatment of iron overload disease and cancer," *Pharmacol Rev,* vol. 57, no. 4, pp. 547-83, 2005.

[48] S. Wadler, D. Makower, C. Clairmont, P. Lambert, K. Fehn, and M. Sznol, "Phase I and pharmacokinetic study of the ribonucleotide reductase inhibitor, 3-aminopyridine-2-carboxaldehyde thiosemicarbazone, administered by 96-hour intravenous continuous infusion," *J Clin Oncol,* vol. 22, no. 9, pp. 1553-63, 2004.

[49] J. Shao, B. Zhou, A. J. Di Bilio, L. Zhu, T. Wang, C. Qi, J. Shih, and Y. Yen, "A Ferrous-Triapine complex mediates formation of reactive oxygen species that inactivate human ribonucleotide reductase," *Mol Cancer Ther,* vol. 5, no. 3, pp. 586-92, 2006.

[50] B. Ma, B. C. Goh, E. H. Tan, K. C. Lam, R. Soo, S. S. Leong, L. Z. Wang, F. Mo, A. T. C. Chan, B. Zee, and T. Mok, "A multicenter phase II trial of 3-aminopyridine-2-carboxaldehyde thiosemicarbazone (3-AP, Triapine®) and gemcitabine in advanced non-small-cell lung cancer with pharmacokinetic evaluation using peripheral blood mononuclear cells," *Investigational New Drugs,* vol. 26, no. 2, pp. 169-173, 2008.

[51] J. Yuan, D. B. Lovejoy, and D. R. Richardson, "Novel di-2-pyridyl-derived iron chelators with marked and selective antitumor activity: in vitro and in vivo assessment," *Blood,* vol. 104, no. 5, pp. 1450-1458, 2004.

[52] V. A. Rao, S. R. Klein, K. K. Agama, E. Toyoda, N. Adachi, Y. Pommier, and E. B. Shacter, "The Iron Chelator Dp44mT Causes DNA Damage and Selective Inhibition of Topoisomerase IIα in Breast Cancer Cells," *Cancer Research,* vol. 69, no. 3, pp. 948-957, 2009.

[53] Z. Kovacevic, S. Chikhani, D. B. Lovejoy, and D. R. Richardson, "Novel thiosemicarbazone iron chelators induce up-regulation and phosphorylation of the metastasis suppressor N-myc down-stream regulated gene 1: a new strategy for the treatment of pancreatic cancer," *Mol Pharmacol,* vol. 80, no. 4, pp. 598-609, 2011.

[54] E. Noulsri, D. R. Richardson, S. Lerdwana, S. Fucharoen, T. Yamagishi, D. S. Kalinowski, and K. Pattanapanyasat, "Antitumor activity and mechanism of action of the iron chelator, Dp44mT, against leukemic cells," *American Journal of Hematology,* vol. 84, no. 3, pp. 170-176, 2009.

[55] K. M. Dixon, G. Y. L. Lui, Z. Kovacevic, D. Zhang, M. Yao, Z. Chen, Q. Dong, S. J. Assinder, and D. R. Richardson, "Dp44mT targets the AKT, TGF-β and ERK pathways via the metastasis suppressor NDRG1 in normal prostate epithelial cells and prostate cancer cells," *British Journal of Cancer,* vol. 108, no. 2, pp. 409-419, 2013.

[56] D. Richardson, P. Sharpe, D. Lovejoy, D. Senaratne, D. Kalinowski, M. Islam, and P. Bernhardt, "Dipyridyl Thiosemicarbazone Chelators with Potent and Selective Antitumor Activity Form Iron Complexes with Redox Activity," *Journal of medicinal chemistry,* vol. 49, pp. 6510-21, 2006.

[57] C. R. Martin, "Welcome to nanomedicine," vol. 1, no. 1, June 16, 2006. Available: https://www.futuremedicine.com/doi/full/10.2217/17435889.1.1.5

[58] C. R. Martin, "Welcome to nanomedicine," 2006.

[59] S. E. McNeil, S. E. McNeil, Ed. *Characterization of Nanoparticles Intended for Drug Delivery* (Methods in Molecular Biology, no. 697). Springer, New York: Humana Press, 2011.

[60] S. Bhatia, "Nanoparticles types, classification, characterization, fabrication methods and drug delivery applications," in *Natural polymer drug delivery systems*: Springer, 2016, pp. 33-93.

[61] S. Naahidi, M. Jafari, F. Edalat, K. Raymond, A. Khademhosseini, and P. Chen, "Biocompatibility of engineered nanoparticles for drug delivery," *Journal of Controlled Release,* vol. 166, no. 2, pp. 182 - 194, 2013.

[62] S. Palvai and S. Basu, "Biocompatible vitamin D3 nanoparticles in drug delivery," pp. 413-428, 2015.

[63] H. K. Makadia and S. J. Siegel, "Poly Lactic-co-Glycolic Acid (PLGA) as Biodegradable Controlled Drug Delivery Carrier," *Polymers,* vol. 3, no. 3, pp. 1377-1397, 2011.

[64] R. A. Jain, "The manufacturing techniques of various drug loaded biodegradable poly(lactide-co-glycolide) (PLGA) devices," *Biomaterials,* vol. 21, no. 23, pp. 2475-2490, 2000.

[65] C. Wischke and S. P. Schwendeman, "Principles of encapsulating hydrophobic drugs in PLA/PLGA microparticles," *International Journal of pharmaceutics,* vol. 364, no. 2, pp. 298-327, 2008.

[66] K. E. Uhrich, S. M. Cannizzaro, R. S. Langer, and K. M. Shakesheff, "Polymeric systems for controlled drug release," *Chemical reviews,* vol. 99, no. 11, pp. 3181-3198, 1999.

[67] X. S. Wu and N. Wang, "Synthesis, characterization, biodegradation, and drug delivery application of biodegradable lactic/glycolic acid polymers. Part II: biodegradation," *Journal of Biomaterials Science, Polymer Edition,* vol. 12, no. 1, pp. 21-34, 2001.

[68] R. Jalil and J. Nixon, "Biodegradable poly (lactic acid) and poly (lactide-co-glycolide) microcapsules: problems associated with preparative techniques and release properties," *Journal of microencapsulation,* vol. 7, no. 3, pp. 297-325, 1990.

[69] X. S. Wu, "Synthesis and properties of biodegradable lactic/glycolic acid polymers," *Encyclopedic handbook of biomaterials and bioengineering,* vol. 2, pp. 1015-1054, 1995.

[70] D. H. Lewis, "Controlled release of bioactive agents from lactide/glycolide polymers," *Drugs and the pharmaceutical sciences,* vol. 45, pp. 1-41, 1990.

[71] H. Heinz, C. Pramanik, O. Heinz, Y. Ding, R. K. Mishra, D. Marchon, R. J. Flatt, I. Estrela-Lopis, J. Llop, and S. Moya, "Nanoparticle decoration with surfactants: molecular interactions, assembly, and applications," *Surface Science Reports,* vol. 72, no. 1, pp. 1-58, 2017.

[72] A. Abuchowski, T. Van Es, N. Palczuk, and F. Davis, "Alteration of immunological properties of bovine serum albumin by covalent attachment of polyethylene glycol," *Journal of Biological Chemistry,* vol. 252, no. 11, pp. 3578-3581, 1977.

[73] M. Tobío, R. Gref, A. Sánchez, R. Langer, and M. J. Alonso, "Stealth PLA-PEG Nanoparticles as Protein Carriers for Nasal Administration," *Pharmaceutical Research,* vol. 15, no. 2, pp. 270-275, 1998.

[74] P. L. Ahl, S. K. Bhatia, P. Meers, P. Roberts, R. Stevens, R. Dause, W. R. Perkins, and A. S. Janoff, "Enhancement of the in vivo circulation lifetime of l-α-distearoylphosphatidylcholine liposomes: importance of liposomal aggregation versus complement opsonization," *Biochimica et Biophysica Acta (BBA)-Biomembranes,* vol. 1329, no. 2, pp. 370-382, 1997.

[75] F. Danhier, E. Ansorena, J. M. Silva, R. Coco, A. Le Breton, and V. Preat, "PLGA-based nanoparticles: An overview of biomedical applications," *Journal of Controlled Release,* vol. 161, no. 2, pp. 505-522, 2012.

[76] S. Acharya and S. K. Sahoo, "PLGA nanoparticles containing various anticancer agents and tumour delivery by EPR effect," *Advanced Drug Delivery Reviews,* vol. 63, no. 3, pp. 170-183, 2011.

[77] S. H. Medina and M. E. H. El-Sayed, "Dendrimers as Carriers for Delivery of Chemotherapeutic Agents," *Chemical Reviews,* vol. 109, no. 7, pp. 3141-3157, 2009.

[78] F. Alexis, E. Pridgen, L. K. Molnar, and O. C. Farokhzad, "Factors affecting the clearance and biodistribution of polymeric nanoparticles," *Molecular Pharmaceutics,* vol. 5, no. 4, pp. 505-515, 2008.

[79] M. J. Ernsting, M. Murakami, A. Roy, and S. D. Li, "Factors controlling the pharmacokinetics, biodistribution and intratumoral penetration of nanoparticles," *Journal of Controlled Release,* vol. 172, no. 3, pp. 782-794, 2013.

[80] A. Mahapatro and D. K. Singh, "Biodegradable nanoparticles are excellent vehicle for site directed in-vivo delivery of drugs and vaccines," *Journal of Nanobiotechnology,* vol. 9, p. 11, 2011.

[81] S. H. Medina, G. Tiruchinapally, M. V. Chevliakov, Y. Y. Durmaz, R. N. Stender, W. D. Ensminger, D. S. Shewach, and M. E. H. ElSayed, "Targeting Hepatic Cancer Cells with PEGylated Dendrimers Displaying N-Acetylgalactosamine and SP94 Peptide Ligands," *Advanced Healthcare Materials,* vol. 2, no. 10, pp. 1337-1350, 2013.

[82] M. S. Cartiera, E. C. Ferreira, C. Caputo, M. E. Egan, M. J. Caplan, and W. M. Saltzman, "Partial Correction of Cystic Fibrosis Defects with PLGA

Nanoparticles Encapsulating Curcumin," *Molecular Pharmaceutics,* vol. 7, no. 1, pp. 86-93, 2010.

[83] J. M. Chan, L. F. Zhang, K. P. Yuet, G. Liao, J. W. Rhee, R. Langer, and O. C. Farokhzad, "PLGA-lecithin-PEG core-shell nanoparticles for controlled drug delivery," *Biomaterials,* vol. 30, no. 8, pp. 1627-1634, 2009.

[84] F. Danhier, N. Lecouturier, B. Vroman, C. Jerome, J. Marchand-Brynaert, O. Feron, and V. Preat, "Paclitaxel-loaded PEGylated PLGA-based nanoparticles: In vitro and in vivo evaluation," *Journal of Controlled Release,* vol. 133, no. 1, pp. 11-17, 2009.

[85] R. L. McCall and R. W. Sirianni, "PLGA nanoparticles formed by single-or double-emulsion with vitamin E-TPGS," *JoVE (Journal of Visualized Experiments),* no. 82, p. e51015, 2013.

[86] T. Govender, S. Stolnik, M. C. Garnett, L. Illum, and S. S. Davis, "PLGA nanoparticles prepared by nanoprecipitation: drug loading and release studies of a water soluble drug," *Journal of Controlled Release,* vol. 57, no. 2, pp. 171-185, 1999.

[87] Y. J. Kang, C. F. Kuo, and S. Majd, "Nanoparticle-Based Delivery of an Anti-Proliferative Metal Chelator to Tumor Cells," *2017 39th Annual International Conference of the Ieee Engineering in Medicine and Biology Society,* pp. 309-312, 2017.

[88] J. Stariat, P. Kovarikova, J. Klimes, D. B. Lovejoy, D. S. Kalinowski, and D. R. Richardson, "HPLC methods for determination of two novel thiosemicarbazone anti-cancer drugs (N4mT and Dp44mT) in plasma and their

application to in vitro plasma stability of these agents," *Journal of Chromatography B-Analytical Technologies in the Biomedical and Life Sciences,* vol. 877, no. 3, pp. 316-322, 2009.

[89] C. K. Holley, S. Alkhalifah, and S. Majd, "Fabrication and Optimization of Dp44mT-Loaded Nanoparticles," *2018 40th Annual International Conference of the IEEE,* no. Proceedings of Annual International Conference of the Ieee Engineering in Medicine and Biology Society, pp. 5733-5736, 2018.

[90] J. Molpeceres, M. Guzman, M. R. Aberturas, M. Chacon, and L. Berges, "Application of central composite designs to the preparation of polycaprolactone nanoparticles by solvent displacement," *Journal of Pharmaceutical Sciences,* vol. 85, no. 2, pp. 206-213, 1996.

[91] W. Tao, X. W. Zeng, T. Liu, Z. Y. Wang, Q. Q. Xiong, C. P. Ouyang, L. Q. Huang, and L. Mei, "Docetaxel-loaded nanoparticles based on star-shaped mannitol-core PLGA-TPGS diblock copolymer for breast cancer therapy," *Acta Biomaterialia,* vol. 9, no. 11, pp. 8910-8920, 2013.

[92] S. S. Bhattacharyya, S. Paul, A. De, D. Das, A. Samadder, N. Boujedaini, and A. R. Khuda-Bukhsh, "Poly (lactide-co-glycolide) acid nanoencapsulation of a synthetic coumarin: Cytotoxicity and bio-distribution in mice, in cancer cell line and interaction with calf thymus DNA as target," *Toxicology and Applied Pharmacology,* vol. 253, no. 3, pp. 270-281, 2011.

[93] J. Panyam, M. A. Dali, S. K. Sahoo, W. X. Ma, S. S. Chakravarthi, G. L. Amidon, R. J. Levy, and V. Labhasetwar, "Polymer degradation and in vitro release of a model protein from poly(D,L-lactide-co-glycolide) nano- and

microparticles," *Journal of Controlled Release,* vol. 92, no. 1-2, pp. 173-187, 2003.

[94] C. Berkland, E. Pollauf, C. Raman, R. Silverman, K. Kim, and D. W. Pack, "Macromolecule release from monodisperse PLG microspheres: Control of release rates and investigation of release mechanism," *Journal of Pharmaceutical Sciences,* vol. 96, no. 5, pp. 1176-1191, 2007.

[95] G. Acharya, C. S. Shin, K. Vedantham, M. McDermott, T. Rish, K. Hansen, Y. R. Fu, and K. Park, "A study of drug release from homogeneous PLGA microstructures," *Journal of Controlled Release,* vol. 146, no. 2, pp. 201-206, 2010.

[96] S. K. Pandey, D. K. Patel, A. K. Maurya, R. Thakur, D. P. Mishra, M. Vinayak, C. Haldar, and P. Maiti, "Controlled release of drug and better bioavailability using poly (lactic acid-co-glycolic acid) nanoparticles," *International journal of biological macromolecules,* vol. 89, pp. 99-110, 2016.

[97] G. Sahay, D. Y. Alakhova, and A. V. Kabanov, "Endocytosis of nanomedicines," *Journal of Controlled Release,* vol. 145, no. 3, pp. 182-195, 2010.

[98] J. Panyam and V. Labhasetwar, "Dynamics of endocytosis and exocytosis of poly(D,L-lactide-co-glycolide) nanoparticles in vascular smooth muscle cells," *Pharmaceutical Research,* vol. 20, no. 2, pp. 212-220, 2003.

[99] K. Y. Win and S. S. Feng, "Effects of particle size and surface coating on cellular uptake of polymeric nanoparticles for oral delivery of anticancer drugs," *Biomaterials,* vol. 26, no. 15, pp. 2713-2722, 2005.

[100] C. K. Holley, Y. J. Kang, C.-F. Kuo, M. R. Abidian, and S. Majd, "Development and in vitro assessment of an anti-tumor nano-formulation," *Colloids and Surfaces B: Biointerfaces,* vol. 184, p. 110481, 2019.

[101] Y. K. Zhao, S. S. Tang, J. M. Guo, M. Alahdal, S. X. Cao, Z. C. Yang, F. F. Zhang, Y. M. Shen, M. J. Sun, R. Mo, L. Zong, and L. Jin, "Targeted delivery of doxorubicin by nano-loaded mesenchymal stem cells for lung melanoma metastases therapy," *Scientific Reports,* vol. 7, p. 12, 2017.

[102] E. Potuckova, H. Jansova, M. Machacek, A. Vavrova, P. Haskova, L. Tichotova, V. Richardson, D. S. Kalinowski, D. R. Richardson, and T. Simunek, "Quantitative analysis of the anti-proliferative activity of combinations of selected iron-chelating agents and clinically used anti-neoplastic drugs," *PloS one,* vol. 9, no. 2, 2014.

[103] A. Gaál, G. Orgován, Z. Polgári, A. Réti, V. G. Mihucz, S. Bősze, N. Szoboszlai, and C. Streli, "Complex forming competition and in-vitro toxicity studies on the applicability of di-2-pyridylketone-4, 4,-dimethyl-3-thiosemicarbazone (Dp44mT) as a metal chelator," *Journal of inorganic biochemistry,* vol. 130, pp. 52-58, 2014.

[104] S. E. McNeil, "Characterization of Nanoparticles Intended for Drug Delivery," 2018.

[105] S. R. Husain and R. K. Puri, "Interleukin-13 receptor-directed cytotoxin for malignant glioma therapy: from bench to bedside," *Journal of neuro-oncology,* vol. 65, no. 1, pp. 37-48, 2003.

[106] N. A. Gandhi, B. L. Bennett, N. M. Graham, G. Pirozzi, N. Stahl, and G. D. Yancopoulos, "Targeting key proximal drivers of type 2 inflammation in disease," *Nature reviews Drug discovery,* vol. 15, no. 1, pp. 35-50, 2016.

[107] M. Kawakami, P. Leland, K. Kawakami, and R. K. Puri, "Mutation and functional analysis of IL-13 receptors in human malignant glioma cells," *Oncology Research Featuring Preclinical and Clinical Cancer Therapeutics,* vol. 12, no. 11-12, pp. 459-467, 2001.

[108] B. H. Joshi, G. E. Plautz, and R. K. Puri, "Interleukin-13 receptor α chain: a novel tumor-associated transmembrane protein in primary explants of human malignant gliomas," *Cancer research,* vol. 60, no. 5, pp. 1168-1172, 2000.

[109] K. S. Kahlon, C. Brown, L. J. Cooper, A. Raubitschek, S. J. Forman, and M. C. Jensen, "Specific recognition and killing of glioblastoma multiforme by interleukin 13-zetakine redirected cytolytic T cells," *Cancer research,* vol. 64, no. 24, pp. 9160-9166, 2004.

[110] A.-L. Andrews, J. W. Holloway, S. M. Puddicombe, S. T. Holgate, and D. E. Davies, "Kinetic analysis of the interleukin-13 receptor complex," *Journal of Biological Chemistry,* vol. 277, no. 48, pp. 46073-46078, 2002.

[111] H. Gao, Z. Yang, S. Zhang, S. Cao, S. Shen, Z. Pang, and X. Jiang, "Ligand modified nanoparticles increases cell uptake, alters endocytosis and elevates glioma distribution and internalization," *Scientific reports,* vol. 3, p. 2534, 2013.

[112] A. B. Madhankumar, B. Slagle-Webb, X. S. Wang, Q. X. Yang, D. A. Antonetti, P. A. Miller, J. M. Sheehan, and J. R. Connor, "Efficacy of

interleukin-13 receptor-targeted liposomal doxorubicin in the intracranial brain tumor model," *Molecular Cancer Therapeutics,* vol. 8, no. 3, pp. 648-654, 2009.

[113] A. Madhankumar, B. Slagle-Webb, A. Mintz, J. M. Sheehan, and J. R. Connor, "Interleukin-13 receptor–targeted nanovesicles are a potential therapy for glioblastoma multiforme," *Molecular cancer therapeutics,* vol. 5, no. 12, pp. 3162-3169, 2006.

[114] G-Biosciences. *2-Step Coupling with EDC & NHS*. Available: https://info.gbiosciences.com/blog/2-step-protein-coupling-edc-nhs

[115] P. T. Scientific. (2017). *Procedure for two-step Coupling of Proteins Using EDC and NHS or Sulfo-NHS*. Available: https://www.thermofisher.com/document-connect/document-connect.html?url=https%3A%2F%2Fassets.thermofisher.com%2FTFS-Assets%2FLSG%2Fmanuals%2FMAN0017099_2162629_PierceEDC_UG.pdf&title=VXNlciBHdWlkZTogUGllcmNlIEVEQywgTm8tV2VpZ2ggRm9ybWF0

[116] L. Rubin, D. Hall, S. Porter, K. Barbu, C. Cannon, H. Horner, M. Janatpour, C. Liaw, K. Manning, and J. Morales, "A cell culture model of the blood-brain barrier," *The Journal of cell biology,* vol. 115, no. 6, pp. 1725-1735, 1991.

[117] C. Yu, B. He, M. H. Xiong, H. Zhang, L. Yuan, L. Ma, W. B. Dai, J. Wang, X. L. Wang, X. Q. Wang, and Q. Zhang, "The effect of hydrophilic and hydrophobic structure of amphiphilic polymeric micelles on their transport in epithelial MDCK cells," *Biomaterials,* vol. 34, no. 26, pp. 6284-6298, 2013.

[118] Y. J. Kang, C. K. Holley, A. B. Madhankumar, J. R. Connor, and S. Majd, "Targeted Delivery of a Potent Anti-Cancer Chelator to Glioma Tumors," ed, in preparation.

[119] Q. Xu, L. M. Ensign, N. J. Boylan, A. Schön, X. Gong, J.-C. Yang, N. W. Lamb, S. Cai, T. Yu, and E. Freire, "Impact of surface polyethylene glycol (PEG) density on biodegradable nanoparticle transport in mucus ex vivo and distribution in vivo," *ACS nano,* vol. 9, no. 9, pp. 9217-9227, 2015.

[120] S. Essa, J. M. Rabanel, and P. Hildgen, "Characterization of rhodamine loaded PEG-g-PLA nanoparticles (NPs): Effect of poly(ethylene glycol) grafting density," *International Journal of Pharmaceutics,* vol. 411, no. 1, pp. 178-187, 2011.

[121] R. Gref, M. Lück, P. Quellec, M. Marchand, E. Dellacherie, S. Harnisch, T. M. Blunk, and R. H. Müller, "'Stealth' corona-core nanoparticles surface modified by polyethylene glycol (PEG): Influences of the corona (PEG chain length and surface density) and of the core composition on phagocytic uptake and plasma protein adsorption," *Colloids and Surfaces B: Biointerfaces,* vol. 18, pp. 301-313, 2000.

[122] A. Sharma and U. S. Sharma, "Liposomes in drug delivery: progress and limitations," *International journal of pharmaceutics,* vol. 154, no. 2, pp. 123-140, 1997.

[123] A. Al-Shehri, M. E. Favretto, P. V. Ioannou, I. A. Romero, P.-O. Couraud, B. B. Weksler, T. L. Parker, and P. Kallinteri, "Permeability of PEGylated immunoarsonoliposomes through in vitro blood brain barrier-medulloblastoma

co-culture models for brain tumor therapy," *Pharmaceutical research,* vol. 32, no. 3, pp. 1072-1083, 2015.

[124] A. M. Merlot, N. Pantarat, S. V. Menezes, S. Sahni, D. R. Richardson, and D. S. Kalinowski, "Cellular Uptake of the Antitumor Agent Dp44mT Occurs via a Carrier/Receptor-Mediated Mechanism," *Molecular Pharmacology,* vol. 84, no. 6, pp. 911-924, 2013.